ANTAL KERPELY DOCTORAL SCHOOL OF MATERIALS SCIENCE & TECHNOLOGY

IMPROVEMING THE HARDNESS AND WEAR RESISTANCE OF CAST IRON SURFACE BY LASER MELT BEAM INJECTION METHOD (LMI) WITH MECHANICAL ALLOYED POWDER

A PhD dissertation submitted in the defence process for the degree of
Doctor of Philosophy in the subject of Material Science and Technology
By

Ali Hussein Hasan AL-AZZAWI

Supervisors:

Dr. Péter Baumli, Associate Professor

Dr. Gábor Mucsi, Associate Professor

Head of the doctoral school
Prof. Dr. Zoltán Gácsi

Institute of Metallurgy, Metal Forming and Nanotechnology
Faculty of Material Science and Engineering
University of Miskolc
Hungary, 2019

ACKNOWLEDGEMENT

My success in this doctoral school was made possible by the combined effort of many people.

First and foremost, I would like to thank my supervisor Dr. Péter Baumli. His continuous encouragement and focused guidance toward innovative research had given me the excuse and spirit to complete this PhD course within a framed time limit. His support and patience had provided me with sufficient guidance to solve various scientific problems through my works. It would have been impossible without his advising and mentoring. I learned a lot from his vast experience in research and teaching field. Apart from the PhD works he also possesses me an extensive knowledge and competent experience. He was so helpful and provided me complete guidance to survive in Hungary which is not my home country.

I would also like to thank my co-supervisor Dr. Gábor Mucsi, for his valuable contribution and support in several experimental works, especially in how to prepare research articles. He provided my professional guidance and generous advice at several stages of work. His advice and encouragement have given me the strength and patience to overcome all work pressure.

Many thanks to the Kerpely Antal Doctoral School of the Faculty of Materials Science and Engineering for providing me with a comfortable workspace in the nano-GINOP project "Sustainable operation of the workshop of excellence for the research and development of crystalline and amorphous nano-structured materials”. His valuable contribution and generosity had provided me strength and financial support to complete the course, has given me a wide knowledge and hands on experience in several surface treatment which would be highly helpful in my career.

I am also very grateful to my reviewer Prof. Dr. Tamás Török for his valuable contribution and advice at various points in my research work. I gained a lot of information from his vast chemistry knowledge and scientific curiosity. His

constant support and trust in my work capabilities had given me self-confidence and encouragement to publish several journal papers. His inspiration and positive opinions about my work throughout this PhD course helped me to achieve the desired results since the very beginning.

I would also like to thank Dr. Anna Sytcheva and Dr. Daniel Koncz-Horvathfor their assistance in conducting the investigation related to scanning electron microscopy and energy dispersive spectrum for the samples, also for Dr. Adám Rácz, Mrs. Bohács Katalin and Dr. Kristály Ferenc, faculty of Earth Science & Engineering, for their assistance to complete my experiments related to grinding and mechanical alloying of powders, also for Dr. Mária Svéda, Mrs. Anikó Márkus, Mrs. Napsugár Bodnár, for their assistance to complete my research work.

I would like to thank, to the "Bay Zoltan Institute Department of Industrial Laser Technology-Budapest" starting with the director and all employees, especially to Mr. Janos Csizmazia and to Mr. Karai Ambrus, for their assistance related to conducting the laser melt injection beam experiments. I am also grateful to my friend József Szabó, who was on my side from the first day I arrived in Hungary until to this day.

Eventually, these achievements and success would be highly impossible without support, blessings, and understanding of my parents and my dear wife.

CONTENTS

LIST OF FIGURES AND TABLES

LIST OF ABBREVIATION

MA	Mechanical Alloying
LMI	Laser Melt beam Injection
EDS	Energy Dispersive X-ray Spectroscopy
XRD	X-ray Diffraction
SEM	Scanning Electron Microscopy
LPSA	Laser Particle Size Analysis
HPDL	High-power diode lasers
ADI	Austempered Ductile Iron
HAZ	Heat Affected Zone
IMC	Inter-Metallic Compounds
HPDL	High Power Diode Lasers
LCVD	Laser Chemical Vapour Deposition
HE	High Energy
MMC	Metal Matrix Composites
HV	Vickers Hardness
NbC	Niobium Carbide
Si	Silicon
Fe	Iron
Cr	Chromium
B	Boron
TiC	Titanium Carbide
TaC	Tantalum Carbide

1 INTRODUCTION

The study of the technical questions of grinding and fundamental research are especially crucial in a stirred media mill because the applicability of the equipment has not yet been investigated in detail in mechanical alloying in wet media. In this process, elemental powders are collided in a high-speed stirred media mill, suffering a severe plastic deformation and forming a high density of lattice defects and dislocations [1, 2]. These lattice defects and disorders, as well as a momentary increase in temperature of particles trapped between colliding balls, accelerate the diffusion of components, rendering the multi-component powders into homogeneous alloy powders [3]. Nanocrystalline powders usually possess a characteristic microstructure indicating their potential for various applications [4].

The use of high-energy milling in this system (and in other refractory metals or intermetallic systems) is desirable mainly because it can avoid the processing difficulties associated with high melting points, such as the need for thermomechanical heat treatments and natural alternative for the addition of insoluble dispersions. High-energy milling can be used to produce intermetallic compounds by mechanical alloying, reactive milling or conventional milling and results in an amorphous phase that can be further crystallised.

During high-energy milling, powders experience large mechanical deformation, welding, and fracture and there are three main processing variables. The first variable is the milling power, which is defined as the ratio between the weight of the spheres and the weight of the mixture. The energy involved in the milling process is directly proportional to the milling power [5] under specific conditions of milling power. The second variable is the atmosphere/milling environment which can influence the final composition of the alloy or can affect the mechanisms of phase transformation; for example, small amounts of oxygen and nitrogen during milling can result in the formation of oxides and nitrates which can promote amorphisation or mechanical crystallisation. The third variable is processing time. For example, for the same milling power, the effect of processing

time has been found to be very strong in Cr, Si and B alloys [6], with short processing times resulting in the formation of intermetallic compounds and long processing times resulting in an amorphous alloy. Therefore, depending on the above mentioned processing variables, the products of high-energy milling can be compounds, composites, amorphous phases [7], nanocrystalline materials and metastable [8] and supersaturated solid solutions. Interest in Nb-Si was associated with the possibility of development of Nb refractory alloys which can be hardened by the intermetallic phase Nb_5Si_3 [9]. The goal of milling in the current work is to improve the initial surface properties and structure of NbC and Si using green chemistry by mechanical alloying to produce desired characteristics for laser melt injection. It is well understood that after laser powder deposition the strengthening of the coating will be dependent on the carbide dispersion as the matrix will melt. It is, therefore, essential to control the size of such carbides to ensure proper distribution in the melt [10].

Many engineering materials used for applications in which hardness and wear resistance is the primary requirement are multiphase materials [11]. A particular group of multiphase materials is especially relevant to tribological applications: materials composed of a metallic matrix reinforced by dispersion of hard particles often applied to tool steel, cast irons, cobalt-based alloys, hard metal and some metallic matrix composites [12-14]. As a result, the preparation of the wear-resistance materials, especially the hardfacing coating, is an essential topic in the tribological field. Hardfacing coating methods, which use high energy density sources such as the electric arc and laser, have been widely applied commercially to enhance wear and corrosion resistance. It is well known that wear behaviour is not an intrinsic property of the material but depends on the overall conditions of the tribological system: loading conditions, hardness, dimensions, shape, and roughness of the counter-body, sliding speed and environment.

Nevertheless, the designing and selection of materials is an essential step when submitted to a given set of conditions. Increasing attention is given to metal matrix composites consisting of hard and brittle carbide particles embedded in a sturdy metal binder.

Typical applications are the laser melt injection process as protective coatings and in rapid tooling and laser-assisted mould repair [15]. Laser powder deposition is a widely used process in fast tooling applications and as a coating technique [16]. Metal-matrix composite materials may be prepared by directly depositing a previously synthesised composite material or by in-situ synthesis [17].

In the current work, the laser melt beam injection process (LMI) is applied to cast iron to increase surface hardness and abrasive wear resistance using iron coated NbC+Si powders after the mechanical alloying (MA) process for different time periods (5, 15, 30, 60, 120 and 240 min) and investigate the effect of MA time on the microstructure and the hardness values of the reinforcing powder. 15 wt% of the silicon was added to the reinforcing powder to improve the surface tension of the molten pool on the iron surface [18]. Laser melt injection utilises a laser heat source to deposit a thin layer of the desired metal's powder on a moving cast iron substrate. There are several methods to transfer the deposited material onto the substrate, including powder injection and pre-placed powder on the substrate. Cast iron substrates treated by LMI with various hard materials like iron coated NbC powder, iron coated NbC+Si powder or iron coated NbC+Si powders after the MA process, and laser energies are applied at 2500 W with a feed speed of 500 mm/min.

The effect of MA on the physical and mechanochemical properties of iron coated NbC+Si powders and the microstructure of the cast iron samples treated by LMI was studied and investigated using scanning electron microscopy (SEM), energy-dispersive spectroscopy (EDS) and X-ray diffraction (XRD). The particles' size, morphology and structural changes were characterised using laser particle size analysis (LPSA), while the hardness values were measured by the Vickers hardness test, and the wear resistance was measured by a dry sliding friction ball-on-disc wear tester from Taylor Hobson.

Results show that the binding alloy and the hard phase were fine distributed in the hard layer and that the hard material was composed of a FeNb, FeSi, NbSi and FeNbSi phases with a dispersion hardening mechanism. Strong metallurgical bonds were formed between the cast iron and the reinforcement powder particles.

Due to the mutual diffusion of alloying elements, the hardness of cast iron specimens increased by 3 times and the wear resistance increased by 4.6-7.3 times.

2 LITERATURE OVERVIEW

2.1 Mechanical Alloying (MA)

Mechanical alloying (MA) the powder processing technique was first developed by John Benjamin in the mid-1960s to prepare nickel-based oxide dispersive strengthened superalloys for gas turbine applications. Most studies so far have focused on a superficial level involving repeated cold welding, fracturing and rewelding of powder particles in high-energy ball mills [19]. It is possible to create a variety of alloys with equilibrium and non-equilibrium phases starting from their powdered state. The development of MA along with grinding processes is significant both scientifically and industrially because of the growing energy demands and research into meaningful ways to cut down on energy expenses without having to compromise on processing quality. However, the science of MA is being developed by inculcating other fields like mechanochemistry where the combined technique has found takers in technological applications. Three main developmental stages include technical development of grinding essential for operation parameter optimisation, enhancement of mechanochemical transformations and development of grinding aids, all of which contribute economically and ergonomically.

MA is the generic term for the processing of metal powders in high-energy mills (planetary ball mill, stirred media mill or shaker mill). Therefore, depending on the state of the starting powder mix and the processing steps involved, it can describe the process when mixtures of powders (of different compounds, metals or alloys) are milled together. Thus, if powders of pure metals are ground together to produce a solid solution (either equilibrium or supersaturated), intermetallic, or amorphous phase, the process is referred to as mechanical alloying, which is a

simple, effective and productive method for producing different nanocrystalline powders. The primary effect of MA is the comminution of mineral particles, which results in changes in a high number of physicochemical properties of a particular system. During MA, the crystal structure of a mineral usually becomes disordered, and the generation of defects or other metastable forms can be registered [20]. Solid-state MA was developed as an alternative to the cumbersome methods involved in preparing nanoscale materials with a broad range of chemical composition and atomic structures. Lattice defects are produced within a single crystalline powder particle with a reduction of average grain size by a factor of 10^3-10^4. There is a result of creation and self-organisation of cell dislocation networks and the formation of high-angle and low-angle grain boundaries during mechanical deformation [21].

The properties of the nanophase materials become size dependent controlled by grain size distribution, atomic structure and cohesive energy of interphase boundaries. Additionally, there are changes associated with the thermodynamic, mechanical and chemical properties of these materials. Such a transition from dislocation-controlled properties to grain boundary-controlled properties are expected for nanocrystalline materials synthesised by other methods as well [21]. It has been reported that the implementation of high-energy mills like vibratory mills or planetary mills has made spectacular changes possible in the structure and surface properties of solid materials [22, 23]. Mechanical alloying is a new method for producing composite metal powders with controlled microstructures. It is unique in that it is an entirely solid-state process, permitting dispersion of insoluble phases such as refractory oxides and addition of reactive alloying elements such as aluminium and titanium. Inter dispersion of the ingredients occurs by repeated cold welding and fracture of free powder particles. The grain refinement changes logarithmically with time and depends on the mechanical energy input for the work hardening of materials. A condition of steady-state processing is eventually achieved, marked by constant hardness and particle size distribution, although structural refinement continues. However, the process applies to a large number of systems which, due to liquid- or solid-phase

segregation, high melting temperature or very high reactivity, are not amenable to production by conventional techniques.

The actual process of MA starts with the mixing of the powders in the right proportion and loading the powder mix into the mill along with the grinding medium. This mix is then milled for the desired period until a steady state is reached when the composition of every powder particle is the same as the proportion of the elements in the starting powder mix. The milled powder is then consolidated into a bulk shape and heat-treated to obtain the desired microstructure and properties. According to the previous reports [19-24], there are different parameters of mechanical alloying involved in the selection of raw materials, types of mills and process variables:

1. **Raw material**: The raw materials used for MA are the commercially available pure powders that have a particle size in the range of 1-200 μm. However, the main criterion at this point is that the particle size should be smaller compared to the ball size; the powdered particle size reduces exponentially with milling time and typically reaches minimum value within minutes of milling. Raw powders can be categorised broadly into pure metal powders, alloy powders, and refractory material powders. The oxygen content in these raw materials usually ranges from 0.05 to 2 wt%. Typically, high-purity raw materials are preferred for any experimental studies, and the MA method is no different. The purity of the raw material powder is essential as the type of mechanochemical transformations is determined by the number of impurities in the material, hence the use of pure raw materials is highly recommended.
2. **Type of mill:** There are different mills available for producing mechanical alloy powders. Their design, capacity and efficiency, along with the additional components that come with the machines, differentiate the type of mills.
3. **Selection of grinding medium:** Choosing a grinding medium is a complex process involving the selection of the following parameters:
    - **Specific gravity:** The high specific gravity of milling media gives better results due to the high kinetic energy of the balls which in turn imparts

high energy to the milled powder. A general rule is that the milling media should be denser than the powder to be ground.

- **Initial feed size:** Initial feed size should be larger than the powder particle size and grinding balls should be of varied sizes for better attrition.
- **Final particle size:** Final particle size directly depends on the size and distribution of the grinding media. The smaller the grinding media particles, the smaller the final size.
- **Hardness:** The harder the medium, the less powder contamination, and consequently the medium lasts longer. However, if the medium is brittle, the edge of the grinding medium can be chipped off and get incorporated into the milled powder and cause contamination.
- **PH value:** Some strong acids or primary slurries may react with specific metallic media.
- **Discolouration:** Specific media result in colour development, therefore it is not suitable for the production of some materials such as light coloured coatings.
- **Cost:** Media that are two to three times more expensive may last considerably longer. These may look expensive in the short term but will prove worthwhile in the long term.

4. **Milling time:** The milling time is the most critical parameter. Usually, the time is chosen to achieve a steady state between the fracturing and cold welding of the powder particles. The times required vary depending on the type of mill used, the intensity of milling, the ball-to-powder ratio and the temperature of milling. These times have to be decided for each combination of the above parameters and the particular powder system. However, it should be noted that the level of contamination increases and some undesirable phases may form if the powder is milled for times longer than required [24]. It is therefore highly desirable to mill the powder for the required duration and not longer.

2.1.1 Benefits of mechanical alloying

Presently, MA is being used for developing alloys from immiscible liquids or solids, incongruent melting, intermetallics and metastable phases and has emerged as a technology capable of providing unique materials with consistent properties for a wide range of high-performance applications. The MA process has several associated advantages:

1. The homogeneity in fine powder is independent of the initial powder size, which avoids the hazards of fine powders.
2. In particle size of 1μm or less high concentration of alloying elements disperse finely without occluding air.
3. Grinding times are reduced to 1/10 or even less compared to those required in a conventional ball mill.
4. Liquid metal techniques are most convenient and cheaper for developing an alloy, but in cases where it is not possible to get a homogeneous alloy by these techniques, powder metallurgy is adopted instead. The value of MA becomes apparent when attempts to make these conventional routes cannot take a composite. If the two metals form a solid solution, MA can be used to accomplish the same at lower temperatures. If the two minerals are insoluble in the solid state, such as immiscible solids (e.g. Cu-Fe), or in a liquid state, such as immiscible liquids (e.g. Cu-Pb), excellent dispersion of one of the metals in the other can achieved.
5. Mechanical alloying represents a cold alloying process, thus it is suitable for hazardous operations. With proper precautions, even volatile inflammable materials can be handled safely.

2.1.2 Formation of nanoparticles by milling in a stirred media mill

Besides the production of nanoparticles from liquefied materials, solutions or the gas phase, it is possible to produce particles below 100 nm by milling coarser solid particles. Moreover, the production of nanoparticles by bottom-up

procedures (e.g. by precipitation) often leads to agglomeration and formation of aggregates that are required to be deagglomerated later. A practical device producing nanoparticles by grinding coarse particles or by dispersing agglomerates is the stirred media mill.

The problem of producing nanoparticles by milling can quickly be realised by considering the number of particles generated from a few coarse feed particles. For example, find a spherical particle with a size of 1 mm. If it is assumed that spherical fragments of this particle are produced by grinding, extremely high numbers of pieces arise depending on the size of these fragments [25]. The extremely high number of pieces resulting from one particle with a size of 1 mm shows that we have to stress an extremely high number of particles to produce particles in the nanometre size range and also that we have to deal with an extensive solid surface area. Therefore, to grind and disperse particles down to particle sizes below a few hundred nanometres, the following conditions must be fulfilled:

a. Per unit time, an extremely high number of particles must be stressed, i.e. the stress frequency must be very high.
b. The intensity of single stress events must be sufficient to break the particles or destroy the agglomerates.
c. The newly created surface of fragments or primary particles must be stabilised by adsorption of sufficient additives so that Van der Waals attractive forces form no new agglomerates.
d. The theology, particularly the viscosity of the suspension, must be controlled in a way that the suspension can handle, and the grinding effect of the mill is preserved.

One main factor in milling is the frequency of some particles being stressed at each grinding contact, which in turn can be increased by using an appropriate solid concentration. If the solid density is too high, a distinct increase of viscosity and decrease in efficiency can be observed. The intensity of single stress events

(point b) is determined above all by the kinetic energy of the grinding media, which is influenced by the density and size of the grinding media and by the stirrer tip speed. In nano-range grinding, the stress intensities produced are usually sufficient to break the particles and agglomerates. When grinding hard particles with too soft media, in some cases the media particles are more deformed than the product. Increasing the fineness will increase particle strength against breakage, and this can make the particles overcome the stress intensity supplied by the grinding media. Suspension viscosity is not too high or else the kinetic energy of the grinding media becomes small and would not be sufficient enough to cause a significant breaking impact. Another critical parameter is the stabilisation of newly formed nanoparticles. If unchecked, they re-agglomerate, which is a dangerous phenomenon. Control of rheology is essential here because the dispersed nanoparticles and their attractive forces increase more than the inertia forces causing viscosity an increase in viscosity resulting in a change of fluid dispersion behaviour from Newtonian to a non-newtonian.

2.1.3 Formation of nanocrystalline refractory alloy powders by the high-energy mill

Preparation of alloy powders is considered a problematic aspect in processing niobium alloys by powder metallurgy [28, 29]. However, considering all limitations, high melting points and reactivity, high-purity powders can be produced by highly expensive procedures such as the hydride-dehydride or centrifugal atomisation equipped with an electron beam or plasma heat source [28].

Niobium material alloys are considered the next-gen high-temperature materials by replacing Ni superalloys [30]. Many approaches such as solid solution strengthening (W and Mo) and composite strengthening by intermetallic compounds IMC (Nb_3Al, Nb_3Ir, and Nb_5Si_3) or carbide phases (TiC, ZrC, and HfC) were investigated to improve the strength of Nb alloys [31-34]. The low alloys of the Nb–W–Mo–Zr system, exhibiting a combination of high intensity

with low-temperature ductility, present an excellent alloying element content. Generally, Nb–W–Mo system alloys are produced by common metalworking processes such as vacuum-arc melting, forging, hot rolling, cold rolling and long-time recrystallisation annealing [30, 32-37]. These processes have exhibited disadvantages such as the inability to produce complicated shapes, poor material utilisation, and causing of pollution [38].

Mechanical alloying has been used to synthesise various transition element carbide phases [10]. These are used in different heat transfer, wear resistance and thermal stability applications. Some of the areas are plastic moulding, rapid tooling, protective coatings, etc. [39]. In particular for the Cu–NbC system, both composites [40] and cermets [41] have been prepared via mechanical alloying. In the reported work on NbC–Cu metal-matrix composite synthesis, materials with up to 10% NbC in a Cu matrix were produced, but full development of the NbC structure is only achieved after heat treating [40]. In the case of cermets, materials with 65-95% NbC, severe iron contamination was observed in the sample, owing to wear of milling media during grinding [41]. The alloys prepared by milling procedures were found to have reduced particle size of NbC, qualitatively on par with commercially produced composites. They also show a uniform dispersion of particles in the matrix, besides their most significant advantage: inhibiting tungsten carbide grain growth in the hard metal. In NbC produced at low temperatures by solid-gas reactions, heterogeneous WC coarsening was inhibited increasing the hardness [42].

The previously reported results [43, 44] show that by using high-energy milling, it is possible to synthesise in-situ and at room temperature a composite material consisting of niobium carbide nanocrystalline particles dispersed in a nanostructured copper matrix. It was achieved for 5, 10 and 20 vol% NbC by milling elemental Cu, Nb and C powders.

Nanocrystalline powders (NP), exhibiting a large specific surface area and a high defect density (especially in milled powders), have been reported to sinter at much lower temperatures of about 2-3% of melting temperature with a high sintering rate [45-47]. Samples prepared from nanocrystalline powders usually

possess a characteristic microstructure indicating their potential for various applications [45]. High-energy milling is a useful but straightforward process for making ultrafine powders. In this process, elemental powders are collided by high-speed milling media, suffering a severe plastic deformation, and forming a high density of lattice defects and dislocations [1, 2, 48]. These lattice defects and disorders, as well as a momentary increase in temperature of particles trapped between colliding balls, accelerate the diffusion of components, rendering the multi-component powders into homogeneous alloy powders [3]. Thus mechanical alloying process (MA) can produce the ultrafine nanocrystalline refractory alloy powders at room temperature.

2.1.4 Phase transformation in elemental powders processed by high-energy milling

Conventional milling and reactive milling are associated with high-energy milling, which forms a part of mechanical alloying in which where materials and processing variables are mechanically alloyed in contrast with thermally activated processes. The formalisation of each process variable and their correlation is very difficult and is not possible even in the easiest of mechanisms [49]. For example, mechanical alloying occurs with a different range of elemental powders when ball milling was used, but in a conventional mill, it happens only with pure powders.

The present evolving interest in NbC-Si arises from their refractory character, which can be hardened into intermetallic phase Nb_5Si_3 [9]. The use of a ball mill is desirable as it can avoid processing difficulties. Variables like melting points, thermomechanical activation, heat treatments and insolubility in dispersion are all avoided with this technique. High-energy ball mills are also used to produce IMC by mechanical alloying, reactive milling or conventional milling resulting in amorphous phase [50]. Many studies have focused on amorphous phase evolution during ball milling of elemental powders of Nb and Si [6].

Direct formation of Nb_5Si_3 IMC was observed [51], which was the same case as our study at this time. Milling power of 10:1 and short milling times (around 1h) resulted in the formation of intermetallic phases. Mechanical crystallisation of

Nb(Si) mixture was formed after partial amorphisation of the mix, supported by studies [52, 53] and is associated with local temperature rise due to impact between powder and balls [54] and concentration of solid-state transformations [52]. Temperature measurements show little variation during the milling process [55], which is not enough to trigger the reaction between Nb-Si [6]. However, an exothermic mixture of Al_2Zr-Nb_5O_2 results in Al_2O_3-ZrO_2-Nb [56] even though the temperature rise is not enough for reaction initiation. However, a eutectic structure was observed later, which states that for systems like these, only a small increase in local temperature is enough to initiate crystallisation. From the previous studies' results, we can conclude that initial stages of milling at low milling power and short times is characterised by the formation of the supersaturated solid solution and that increasing the milling power or milling time resolved in a nanocrystalline and amorphous mixture. Further increases in milling time and milling power caused a transformation of the nanocrystalline phase and mechanical crystallisation of the amorphous phase and the metastable phase.

2.2 Laser melt beam injection (LMI)

Laser melt beam injection (LMI) technology has been known since the 1980s and has been in use to improve surface characteristics of metal alloys such as steels, aluminium, titanium, nickel and magnesium. Industrial applications such as cutting tools, gas turbines and power plants all need specific alloys with exceptional mechanical and thermal properties to withstand the wear and tear of processing beyond being hard.

Laser treatment of the alloy surface offers a considerable advantage over the conventional methods. Some of these advantages include fast processing, precision of operation and low cost. In addition to the benefits mentioned above, laser surface treatment involves controlled melting through which the hard particles such as TiC can be injected on the surface vicinity during the treatment process. However, niobium segregation, Laves phase, and microfissures could occur in the vicinity of the heat-affected zone (HAZ) after the laser processing,

thus limiting the practical applications of laser-processed surfaces. Consequently, the investigation into laser treatment of alloys and microstructural changes in the treated region becomes essential because the heat-affected zone of the laser beam exhibits significant differences in mechanical properties. However, a slight decrease in fracture toughness was observed [57]. The results of recast layers formed during trepan drilling by laser beam indicate that the assist gas pressure, peak power and the focal position exerted the most considerable influence on the thickness of the recast layer [58, 59].

Optical energy can be considered one of the ideal forms of energy for surface treatment, including surface heating, bending, scrabbling, melting, alloying, cladding, texturing, roughening and the processes of layered manufacturing. Surface treatment by laser offers excellent advantages that are the highly localised with a low distortion ratio, high-quality finish and clean processing. Development of highly automated workstations, along with less expensive, more robust, more reliable and more compact lasers, means surface treatment by lasers is expected to be the general trend in future years [60].

As described above, laser cladding can perform permanent structural repair and refurbishment with a wide range of different alloys which are generally considered by the manufacturing as unattainable to weld by any traditional process. In turn, laser cladding offers many advantages such as a small heat-affected zone, rapid solidification, increased cleanliness, minimum dilution and improved ability to control the depth of the heat-affected zone [61, 62]. In comparison with conventional techniques, the energy input of laser cladding is low, which results in finer microstructures with superior properties and minimal component distortion. Also, the smooth clad surface improved the in-service performance, the deficiency of defects in the clad and the metallurgical bond of the substrate [63].

In recent years, laser surface cladding has developed from a simple layer process into a composite layer process by adding high-melting-point and high-hardness compounds such as carbides, nitrides, borides, oxides and their composite particles into the coatings [64]. Laser cladding was developed as a

method for producing coatings to enhance the surface resistance of materials against wear, corrosion, erosion and high-temperature oxidation. Parallel with other surface modification methods, some unique advantages it can offer are fine microstructure, minimally clad dilution, and perfect fusion bonding. Earlier studies were carried out by injecting carbide particles into the laser molten pool to produce carbide-reinforced composite coatings [65].

The deposition of high-quality laser clad can form with low porosity and few defects. Rapid cooling rates and solidification result in fine solidified clad microstructures offering excellent wear and abrasion properties, as well as the formation of beneficial metastable phases and expanded solid solubility that improves properties. The rapid cooling rates cause an increase in the sensitivity of the clad and heat-affected zone to cracking, and precautions such as preheating may be indispensable [63, 66].

In the clad melt pool, the altitude rate of mixing causes homogenisation of the melt if the speeds are below a specific value, thus the alloys can be formed in-situ from an inexpensive component. Using this process, the alloy systems can be quickly analysed. Therefore, the rather rapid cooling rates in the small melt pool generated finer microstructures than contending methods [60, 62].

As the beam can be delivered precisely, this provides an ability to treat discrete regions of surfaces, thus contributing to reduction in the overall energy input and surface deformation. Moreover, using expensive alloying elements can be reduced since they are used only in shallow areas instead of throughout the mass. Also the clad thickness can be precisely controlled, which contributes to reducing the amount of post-treatment machining demand [67, 67].

Laser beams, owing to their wide range of wavelengths, power and energy parameters, can be manipulated quickly according to our flexibility, enabling us to carry out various treatments. During operation, the ease of the beam shaping provides the possibility to process a wide range of shapes and the opportunity to switch rapidly between different treatment geometries. The process is therefore extremely appropriate for automation, including beam shaping and beam switching. The beam can use mirrors or fibre-optic beam delivery to be directed

into inaccessible locations [63, 66, 68]. Laser processing helps in achieving reduced processing times, lowered labour and maintenance costs, less tool wear and shorter cycle times, all of which contribute to the higher overall efficiency of the process [69].

2.2.1 Advantages of laser surface treatment technology

Laser heat treatment was initially used as a selective surface hardening heat treatment process but later evolved into a technology that can induce metallurgical and mechanical changes in the material [60]. Practical benefits of laser heat treatment include hardness increase, strength increase, reduced friction, wear reduction, increase in fatigue life, surface carbide creation, creation of unique geometrical wear patterns and in some cases, tempering.

Laser heat treatment processes range from the low-power-density operations of transformation hardening, bending, scrabbling and laser chemical vapour deposition (LCVD), which rely on surface heating without surface melting, to operations involving surface melting requiring higher power densities to overcome latent heat effects and larger conduction heat losses. These melting processes include simple surface melting to achieve greater homogenisation or very rapid self-quench processes [62], which is possible in certain alloys [60]. Melting processes also include those where the material is added either by mixing it into the melt pool, as in surface alloying and particle injection, or by fusing on a thin surface melt, as in cladding [63].

With continued technological developments in high-power diode lasers (HPDL), fibre lasers and sophisticated knowledge-based controllers, the laser treatment process shows great industrial potential for use in metallic coating and prototyping applications. Moreover, because laser processing is using clean energy and few contaminating materials, it can be considered one of the environmentally friendly processes, where the optical energy generates very few environmental disorders (e.g. noise, external electrical and magnetic fields) which enables processing to be carried out in quiet surroundings.

2.2.2 Composite coating by laser cladding

Many engineering materials used for applications in which wear resistance is the primary requirement are multiphase materials [69, 70]. A particular group of multiphase materials is especially relevant to tribological applications: materials composed of a metallic matrix reinforced by dispersion of hard particles, often applied to tool steel, cast irons, cobalt-based alloys, hard metals and some metallic matrix composites [12-14]. One main area of interest in the tribological field is the preparation of hardfacing coatings using lasers to enhance the wear and corrosion resistance.

Increasing attention to detail is being given to metal matrix composites with brittle reinforcements like carbides. The excellent wear resistance of tungsten carbide and in particular of WC/W_2C or WC–Co, as hardfacing material is well known, while Co- or Ni-base alloys are mostly used as binders [71, 72]. In most of these cases, the effectiveness strongly depends on the microstructure of the coating which in turn depends on the input energy. For instance, WC vanishes and decomposes at a high temperature when using high-density sources. As an alternative, Iron-based coatings are widely employed due to their excellent mechanical properties and their surface to cost-effectiveness.

The surface composite coating can be produced by the laser cladding method, which is reminiscent of the traditional hardfacing welding. In this process, the laser beam is used as the heat source to melt the hardfacing alloy onto the substrate and the reinforcing particles. Laser cladding provides good metallurgical bonds and minimal dilution, which are hard to achieve by other hardfacing techniques [73].

Laser cladding of composite coating has been developed for its capability of introducing hard particles such as WC [74], TiC [75], SiC [76] and Cr_3C_2 [77] as reinforcements, each of which has very high hardness and excellent wear resistance. Among the hardfacing alloys, nickel-based alloys have been investigate most frequently in recent years owing to their added characteristics of excellent resistance against abrasion and corrosion at higher temperatures [72].

A Cr_3C_2-Ni/(Ni+Cr) composite coating can be fabricated by the laser cladding method [77, 78]. The hardness of the Ni or N-B coating is improved by adding Cr_3C_2 phase into the Ni or Ni-B due to the complete dissolution of the Cr_3C_2 particles in the Ni matrix alloy. The dissolution of Cr_3C_2 can increase the Cr and C concentration in the melted Ni-alloy. This dissolution during the rapid cooling process leads to the formation of Cr_7C_3, $Fe_{23}(C_6, B_6)$ phases, resulting in significant improvement in the hardness of the coating [76]. The hardness and wear resistance increase as the amount of Cr_3C_2 phase on the surface is increased [79]. Partial dissolution of the reinforcing particles can be observed in the case of a WCp/Ni–Cr–B–Si–C composite [80]. Metastable phases like α-W_2C, W_2C and η1-β-M_6C compounds can be formed on the interface of the WC particles. These phases deteriorate the mechanical properties of the composite [74].

The partial dissolution of reinforcing particles has also been observed in a TiC/Ni–Cr–B–Si–C composite on steel. During cooling the dissolved TiC can crystallise on the surface of the undissolved TiC [80]. When using TiC in a Ni-based alloy, an intermetallic phase with Ti cannot be observed [74, 81].

Laser cladding can produce in-situ composite coatings NbC particles reinforced Ni_{45} [82, 83], was the γ solid solution Ni(Fe) the main component of the matrix, while the NbC, $Cr_{23}C6$, Cr_2B, Cr_7C3 and few of Cr_3C_2, was the main content of reinforcement phases, and homogeneous distribution and regular of in-situ NbC particles. The mechanical properties were improved; excellent wear resistance and high hardness were exhibited in the composite coating [77, 82, 83].

The surfaces of steel materials can be modified by laser cladding coatings using a reinforced metal matrix of composite carbide. Ex-situ processing and in-situ processing, are the two methods that can be used to introduce the carbide into the coating [84]. Also, laser cladding can fabricate a composite layer of the NbC reinforced Fe-based, where there are three phases of NbC exist as particles on the surface, networks, dendrites and polyhedrons [85, 86].

At the primary stages of solidification, NbC particles are engulfed by a liquid-solid interface, which causes decreasing in their sizes. During a long growth process, the NbC particles not immersed by the interface the polyhedral NbC

phases was evolved, the final stages of solidification, presented the eutectic substances that formed as dendritic and network NbC phases.

Metal matrix dilution caused decreased NbC content in the coating [85]. Dissolved Nb and NbC content in coating causes an increase in the microhardness, while there is no significant effect of NbC morphology on the coating microhardness [86].

2.2.3 Composite coating by laser melt injection

The composite coating can be achieved by the laser melt beam injection process (LMI) where a laser beam melts the surface of the substrate in the pool with a depth of 1 mm and particles with a size range of 10-100 μm are delivered by an inert carrier gas.

Although it seems to be an advantageous process, there are certain disadvantages to this method; at first, solid particles are not wetted sufficiently by the melted alloy. Good wettability is needed for pushing the particles into the melted alloy with low energy, and perfect wettability is required for spontaneous immersion [87, 88]. The other difficulties associated with the preparation of a composite coating with this method are the large density difference between the melted metal and the reinforcing particles and the chemical reaction on the surface of the particle/metal matrix. These difficulties can be solved when the particles are formed in-situ during the cooling of the melted metal. In-situ a composite coating has been prepared for an Al_2O_3 particle-reinforced carbon steel surface composite coating [89] or for the in-situ production of bulk Fe/TiCp [90].

Ex-situ composite layers are also possible by the LMI method. Ex-situ means the reinforcing particles are prepared independently from the LMI process. Various ex-situ composite layers have been made via the LMI method in the last two decades, SiC particle-reinforced composite coating [91, 92], WC particle-reinforced coating on titanium alloys [93, 94], a WC particle composite with Fe matrix [95, 96] and a TiB_2 particle-reinforced surface composite on steel substrate [97]. In the case of the preparation of an ex-situ WC particle-reinforced Fe surface

composite, it was observed that the WC particles could be dissolved/melted during the LMI process.

From the melted or dissolved WC, a Fe_3W_3C compound layer was observed to form on the top of the surface composite. The same compound layer can be seen on the surface of the undissolved WC particles [95]. It was found conclusively that 10 wt% WC (particle size 80 μm) is sufficient in the WCp/Duplex Stainless Steel system for a significant (approximately 50%) improvement in the wear properties [96].

2.2.4 Mechanism of the transformation process in the cast iron

There are differences in characteristics of cast iron treated by laser beam depending on the type of cast iron. Ferritic grey cast iron consists of ferrite and graphite regions and is challenging to harden by the laser because the diffusion time is too short, hence, all that created is a hard crust around the graphite nodules or flakes. That can still give excellent wear properties despite no change in the overall hardness value being observed. Pearlite cast iron, formed by moderately rapid cooling, contains graphite and pearlite. In this case, the laser transformation hardening is very effective in achieving very high hardness levels, as for irons of 0.8% carbon or more. With cast irons, there is a relatively narrow window between transforming and melting [60].

Laser transformation hardening of spheroidal graphite cast iron may result in preferential melting around the graphite nodules owing to the lowering of the melting point as the carbon diffuses away from the graphite.

2.3 Knowledge gap

Previous reports have demonstrated the production of Nb-Si, Nb-Cr and Nb-Al composite powders via mechanical alloying (MA) and the effect of mechanical alloying properties, i.e. milling time, milling energy and milling atmosphere, on the characteristics of those powders [97-101]. However, the fabrications of composite (NbC-Fe-Si-Al) system alloy powders by the mechanical alloying

process have not been reported so far. Also, there are many previous studies of produced in-situ carbide and ceramic particles reinforced composite coatings by laser cladding [89-97], but there are no reports for using iron coated NbC+Si powders as a reinforcement powder to produce composite coating by the laser melt beam injection process, for forming hard composites and nanocarbide phases uniformly distributed throughout the bulk of the sample, resulting in high microhardness [106-111]. There are also no studies about the effect of the characteristics of the powders fabricated by mechanical alloying on the essence of the laser melt beam injection process (i.e. on the mechanical properties such as hardness and wear resistance) of the materials treated by laser melt injection process.

2.4 Objectives

The primary objective of the current work is to improve the mechanical properties (hardness and wear resistance) of cast iron surfaces by the laser melt beam injection method with a reinforcement powder of iron coated niobium carbide and silicon prepared by mechanical alloying which is a solid-state process that has been successful in producing nanocomposite and nanostructure compounds by mechanochemical reactions [102-105]. The goal of the mechanical alloying is to improve the initial surface properties and structure of iron coated NbC and Si using green chemistry, thus producing the characteristics for laser melt beam injection process. The iron coated niobium carbide was chosen for its ability to synthesise and form of the Fe + NbC + Fe_3C composite with uniformly distributed nanocarbide phases, which results in increased microhardness of the reinforcement powder [106], This carbide exhibits some important characteristics for tribological applications [107]. In addition to high hardness, NbC presents increased toughness and stiffness, extremely high melting temperature and chemical stability [108]. Also, the silicon was added to the powder for its ability to synthesise hard and brittle phase (Nb_5Si_3 and/or Nb_3Si) precipitates dispersed in the Nb matrix and promote grain refinement, as well as impede the dislocation

mobility and increase the deformation resistance of the matrix [84], therefore improving the microhardness of NbC, which would contribute to enhancing the microstructures and mechanical properties of the reinforcement powder [109, 110]. In addition to silicon's property to increase the diffusivity of NbC in Fe at high temperatures [111] as mentioned earlier, that after laser powder deposition the strengthening of the coating will be dependent on the carbide dispersion since the matrix will be melted [10].

The present work is aimed at developing iron coated NbC+Si composite powder for use in applications where effective wear resistance, higher hardness, and long-term thermal stability are simultaneously required. Typical applications are the LMI process, as protective coatings and in rapid tooling and laser-assisted mould repair, where the laser powder deposition is a widely used process in fast tooling applications and as a coating technique [112]. Metal–matrix composite materials may be prepared by directly depositing a previously synthesised composite material or by in-situ syntheses [113].

Based on previous studies [85, 86, 101, 106, 109, 110], in this work mixtures of iron coated NbC and Si powders corresponding to nominal contents 85 wt% of iron coated NbC and 15 wt% of Si were prepared by MA, and these powders were applied during the LMI process to treat the surfaces of cast iron specimens in order to achieve the following aims:

1. To investigate the effect of mechanical alloying time on the microstructure of iron coated NbC+Si powder and what possible phases can be generated during the mechanical alloying process for different milling periods.
2. To study the effect of mechanical alloying time on the specific surface area of iron coated NbC+Si powder particles and the dissolving rate of the powder components in the liquid iron matrix during the LMI process.
3. To investigate the effect of mechanical alloying time on the wettability and diffusivity of iron coated NbC+Si powder in the liquid iron matrix during the LMI process.
4. To study the effect of different mechanical alloying times on iron coated NbC+Si powder used as a reinforcement powder in the LMI process on the hardness and wear resistance values of the cast iron samples.

3 MATERIALS AND METHODS

3.1 Materials

3.1.1 Cast iron (ADI)

The Austempered Ductile Iron (ADI) is a ferrous, cast material with excellent dynamic properties and high strength-to-weight ratio. However, only a few designers are vaguely familiar with the savings regarding close to net shape casting an entirely unfamiliar with this material that can compete favourably with steel and aluminium castings, weldments and forgings. The austempering process is an isothermal heat treatment and a high-performance method that imparts excellent properties to ferrous materials. Developed in 1940, ductile iron (or spheroidal graphite iron) is in extensive use despite being familiar to only a fraction of the design community. Ductile iron, with its distinctive spheroidal graphite morphology, forms an iron that has tensile and impacts properties appropriate for products as varied as pump impellers, steering knuckles and brake callipers. The most significant application of the austempering process on ductile iron produces Austempered Ductile Iron (ADI) that has a strength-to-weight ratio that surpasses that of aluminium [114].

The chemical composition of the cast iron used in this study for laboratory experiments is 69.42 wt% Fe, 28.41 wt% C, 1.44 wt% Si and 0.73 wt% Cu and was obtained from Bay Zoltán Nonprofit Ltd. for Applied Research's Institute for Logistics and Production Systems-Miskolc.

3.1.2 Iron coated niobium carbide

Niobium, like titanium and vanadium, forms superhard MC carbides that remain relatively pure in special alloys on account of their low solubility in other metallic alloying elements. However, because they have a higher hardness than the precipitated chromium carbides commonly used for wear resistance, they are suitable as alternative hard phases. This work deals with new wear resistance steels and casting alloys containing niobium carbide. NbC has many physical and

chemical characteristics in common with TaC, such as a high melting point (3600 ˚C) and hardness (2800 HV) but the density of NbC (7.79 g/cm^3) is much lower than that of TaC (14.3 g/cm^3) [115], and the wettability with a binder of NbC is much better than TaC and TiC because of lower negative enthalpy [116]. Furthermore, compared with TaC, the reserves of NbC are very abundant, and its price is relatively low. These make NbC a promising alternative to TaC. In recent years, the researchers have been giving more attention to NbC for its attractive properties [117-120].

Although niobium carbide has been well known for decades, knowledge of its property profile remained limited. On the other hand, demand for niobium has increased significantly over the recent decades, mainly as a micro-alloying element in high strength and stainless steels. Within such alloys, niobium forms dispersed micro- or nano-sized niobium carbide particles, controlling the microstructure and thus improving mechanical properties [121, 122].

The mechanical and particularly tribological properties of NbC remain mostly unexplored. From a prior research, NbC is expected to be superior to WC in cutting tool applications, because NbC is nearly insoluble in Cr, Ni, Co or Fe at 1225 ˚C [123], whereas WC is fully soluble under the same conditions. The high solubility of WC in these metals is responsible for the chemical wear of WC. Nevertheless, NbC has occasionally been used as a secondary carbide phase in hard metals and cermets, castings and tool steels [110]. In these applications, it serves either as a grain refiner or as a hard phase helping to enhance wear resistance, limit grain growth and improve the hot hardness. It was recently shown that pure NbC, as well as metal, bonded NbC have a pronounced wear resistance under dry sliding conditions versus other monolithic ceramics and carbides, as well as increased tool life when compared to WC-Co [122, 124].

The niobium carbide material used in this study is iron coated niobium carbide (1-1.2 mm particles size), for laboratory experiments containing 53.04 wt% Nb, 25.73 wt% C, 19.74 wt% Fe and 1.5 wt% Al according to the scanning electron microscopy investigation as shown in Figure 1 and was obtained from Bay Zoltán

Nonprofit Ltd. for Applied Research's Industrial Laser Technology Laboratory - Budapest.

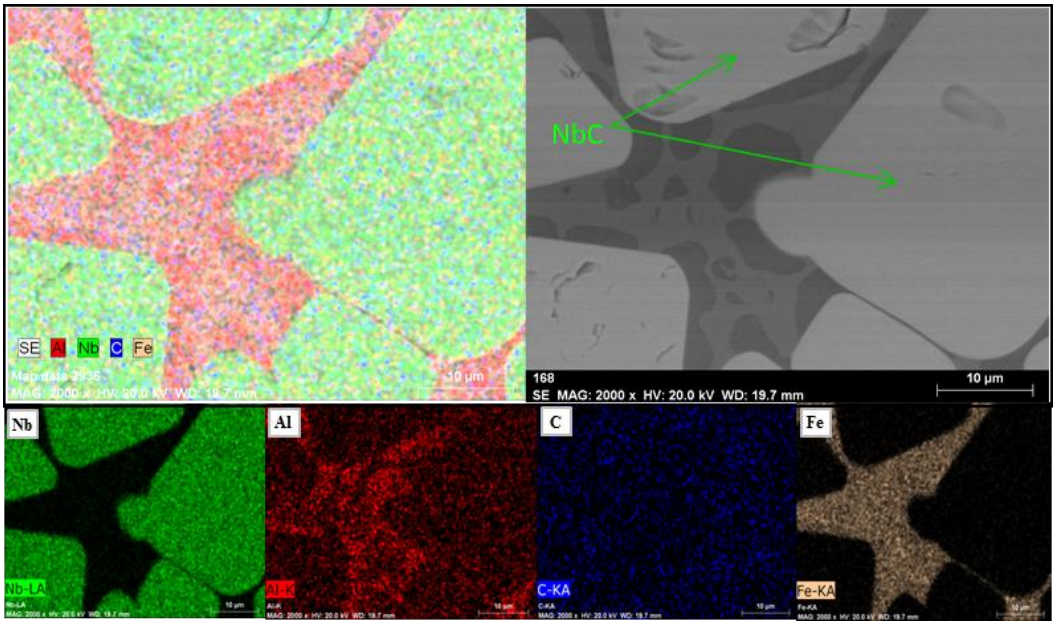

Figure 1. SEM and EDS images of initial iron coated NbC particles

From the SEM images in Fig. 1, and according to the energy dispersive X-Ray spectroscopy (EDS), it is possible to observe that the NbC particles are embedded in iron, which contains significant aluminium.

3.1.3 Silicon

Silicon is a solid material at room temperature with a melting point of 1.414 ˚C. Unlike most other substances but like water, it expands when it freezes and has a higher density in its liquid state than in its solid state [125].

Nb-based alloys with niobium silicides have been developed as the new class of heat-resistant structural materials because of their outstanding properties, i.e. low density (about 7 g/cm^3), high melting point (>1700 ˚C) and high strength at high temperatures [126]. Nevertheless, the intrinsic brittleness of silicides at room temperature hinders the practical applications of niobium silicide-based alloys. To overcome this drawback, many researchers took various measures including toughening and alloying. Silicon material (99.9 %, 2.5-5 mm particles size), was also obtained from Bay Zoltán Nonprofit Ltd. for Applied Research's Institute for Logistics and Production Systems-Miskolc

3.2 Methods

3.2.1 Planetary ball mill

One of the essential mills for conducting MA experiments is the planetary ball mill, which can mill a few hundred grams (up to 4×250 g) of the powder simultaneously [24]. The planetary ball mill got its name from the planet-like movement around their centres. These are arranged on a rotating disk and a particular drive mechanism causes them to rotate around their centres.

The centrifugal force generated by the pots rotating around their centres and that provided by the revolving support disk together act on the pot's contents, consisting of the material to be ground and the grinding balls. Since the pot and the supporting disk rotate in opposite directions, the centrifugal forces are alternately acting in different directions. These centrifugal forces cause the grinding balls to run down the inside wall of the pot-the friction effect-followed by the materials to be ground and the grinding balls lifting off and travelling through the internal chamber, colliding with the opposite wall of the pot (see Fig. 2).

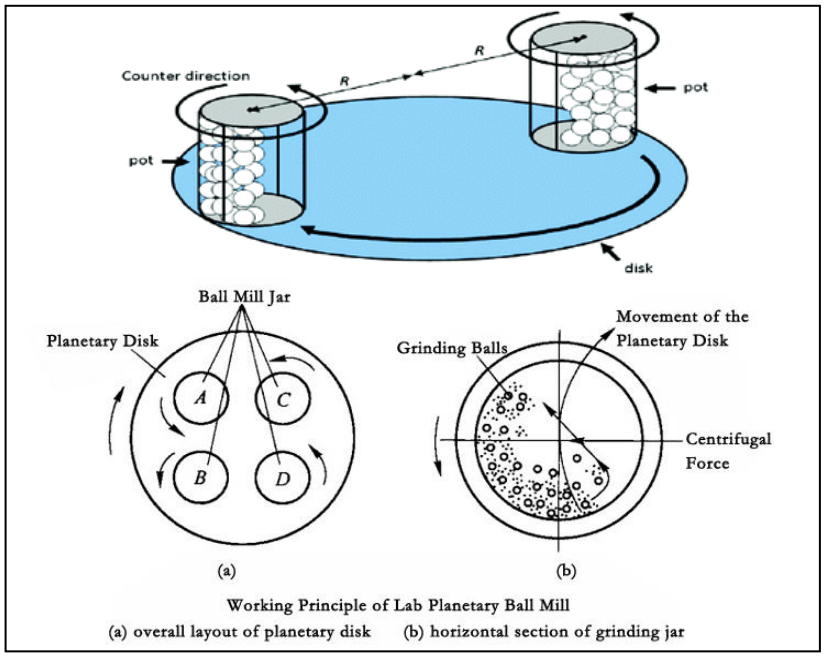

Figure 2. Schematic of the ball motion inside the planetary ball mill [151]

3.2.2 Stirred media mill

The stirred media mill is one of the most energy-efficient types of grinding equipment for wet ultrafine grinding, and it belongs to the group of mills with free-moving grinding media. The classical representative is the tumbling mill, consisting of a horizontally oriented rotating cylinder filled with up to 40% by volume with grinding media. Due to the rotation, the grinding media are lifted and get potential energy, which will convert into kinetic energy in a cascading manner. The feed material to be ground is dispersed within the grinding media and is stressed by pressure and friction between layers of media or by the impact of falling beads.

The wet grinding use of stirred media mills has many advantages [127]: reduced agglomeration tendency compared to dry grinding, no material loss avoided, no dust explosions or oxidations, easier handling of toxic materials, no need for air cleaning devices, improvement of heat transfer and others. Stirred media mills are used for dissipation and deagglomeration operations as well as for precise grinding of crystalline materials or the dissolution of micro-organisms. Stirred media mills are used for many applications in different industries and can be found especially where high product fineness is demanded [24] (see Figure 3).

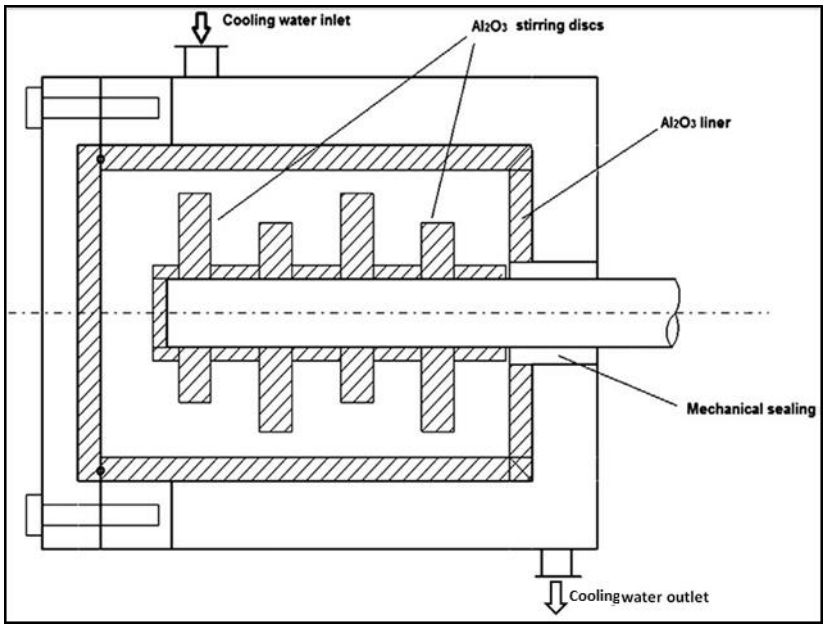

Figure 3. Laboratory scale stirred media mill [152]

3.2.4 Laser melt beam injection (LMI)

Laser melt beam injection is an interdisciplinary technology utilising laser technology, computer-aided design and manufacturing (CAD/CAM), robotics, sensors and control, and powder metallurgy. LMI employs a laser heat source to deposit a thin layer of the desired metal on a moving substrate (see Figure 4). With the powder injection method, the deposited material can be transmitted efficiently to the substrate. Among other methods, LMI by powder injection has been demonstrated to be the most effective method. During this process, the laser beam melts a segment of the powder particles and a thin layer of the moving substrate to deposit the powder particles on the substrate. Using LMI by powder injection, a wide variety of materials can be deposited on a substrate to form a layer with thicknesses ranging from 1-2 mm and widths as narrow as 3 mm. The type of laser used was solid-state Nd: YAG (Yttrium Aluminium Garnet) laser. The strongest output wavelength of neodymium-doped lasers is approximately 1064 nm with maximum power of 2700 W.

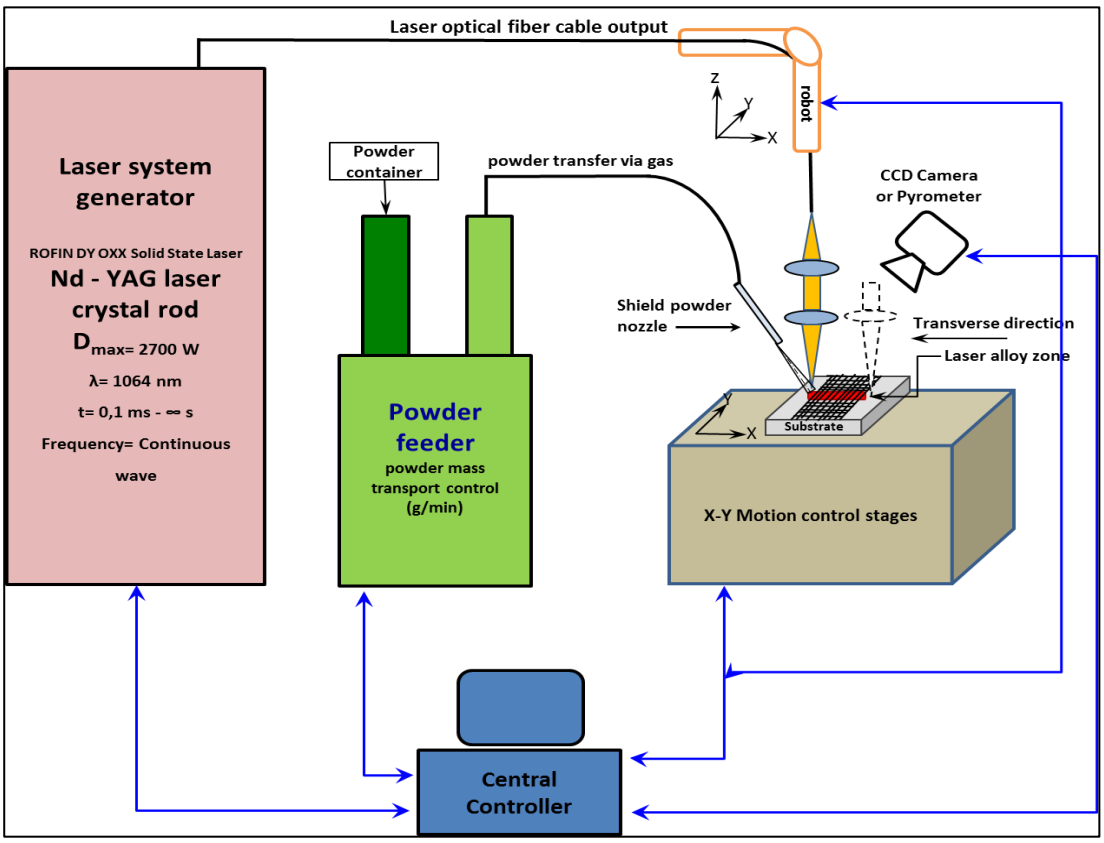

Figure 4. Closed-loop control of LMI device

3.2.5 Scanning electron microscopy (SEM) and energy dispersive X-ray spectroscopy (EDS)

Scanning electron microscopy is a powerful tool appropriate for investigating composite materials' surfaces/cross-sections. The application of a low-energy electron beam in the analysis of materials at the nanoscale is playing a significant role in many research areas. It employs decelerated primary electrons for better resolution and specificity of the resulting analysis [128]. The type of SEM and EDS used to investigate the samples was an S-4800 Hitachi with Bruker YAG energy dispersive detector. The primary beam energy was 20 kV, and Zeiss EVO M10 with thermal emission tungsten firing unit. The primary beam energy was 20 kV.

3.2.6 X-ray diffraction

The phase composition was determined by a Bruker D8 Advance XRD powder diffractometer (Cu-Kα radiation, 40 kV, 40 mA) in parallel beam geometry (Göbel-mirror). Patterns are recorded in 2-70° (2θ) range, with 0.007° (2θ) steps in 42 seconds, with a Vantec-1 position sensitive detector (1° window opening). Phase identification was made by Search/Match (multiple iterations) on ICDD PDF2-Release (2012). The specimen is rotated in sample plane during the measurement, to obtain data from the whole surface and to reduce in-plane preferred orientation effects. Crystallite size, strain and unit cell parameters were calculated by Rietveld refinement in TOPAS4, with empirical parametrization, instrumental parameters were defined on SRM 640a Si.

3.2.7 Vickers hardness test

The Vickers hardness test method is used to test the samples. The Vickers test is based on an optical measurement system. The microhardness test procedure assigns a domain of light loads using a diamond indenter to produce an indentation which is measured and converted into a hardness value. To enable measuring the size of the impression, the surface of the samples must be highly polished. Usually, on the Vickers scale, a diamond in the shaped of a square-based pyramid is used for testing on the Vickers scale. Microhardness measurements on

the cross sections of the samples were carried out using a Mitutoyo MVK H1 hardness tester, applying a load of 5-10 g with a holding time of 10 s.

3.2.8 Laser particle size analysis (LPSA)

Particle size distribution and geometrical specific surface area of the ground and mechanically alloyed material were measured and calculated by a Horiba LA-950V2 laser particle size analyser in an isopropanol medium. Calculation of particle size distribution from measured data was carried out using the Mie theory, taking into account the refraction index of the material.

Figure 5. Laser diffraction particle size analyser instrument

3.2.9 Dry sliding ball-on-disc wear resistance test

Dry sliding tests were carried out on specimens in the form of discs with a ball diameter of 4 mm using a ball-on-disc Tribometer T-01. Test parameters were selected considering recommendations of the ASTM G 99 standard. To simulate harsh service conditions, the higher load and smaller ball radius were chosen to increase the contact pressure. A single crystalline Al_2O_3 (99.99%) ball (5.69 mm diameter) was used as counter-body whose hardness is approximately 2000 HV. The Al_2O_3 ball rotates on the machined circular coating under a load of 5 N with a speed of 280.5 rpm (v = 0.06 cm/s), an air atmosphere and sample temperature of 28 ˚C. The total sliding distance L= 240 m (laps = 2000) was chosen. The wear experiments were carried out in the air at ambient temperature and completed after 65 min.

4 EXPERIMENTAL SECTIONS

4.1 Sample preparation

4.1.1 Grinding of iron coated NbC and Si powder by a planetary ball mill

The initial powder size of iron coated NbC (1-1.2 mm) was reduced by milling in a planetary ball mill for a few micrometres (≤ 63 μm). The aim was for the feed powder of the mechanical alloying process by a stirred media mill to be smaller than 63 μm. The container of the mill was made from iron and filled with steel balls. The grinding ball size was 40 mm, and three were in the grinding chamber. After the first grinding stage, the mill product was sieved at 63 μm, the fine size fraction was collected and the coarse fraction was fed into the mill again and ground until reaching a size finer than 63 μm (quantitatively ground). The scanning electron microscopy images of the iron coated NbC powder after the grinding process can be seen in Figure 7.

Figure 6. Milling equipment (planetary ball mill)

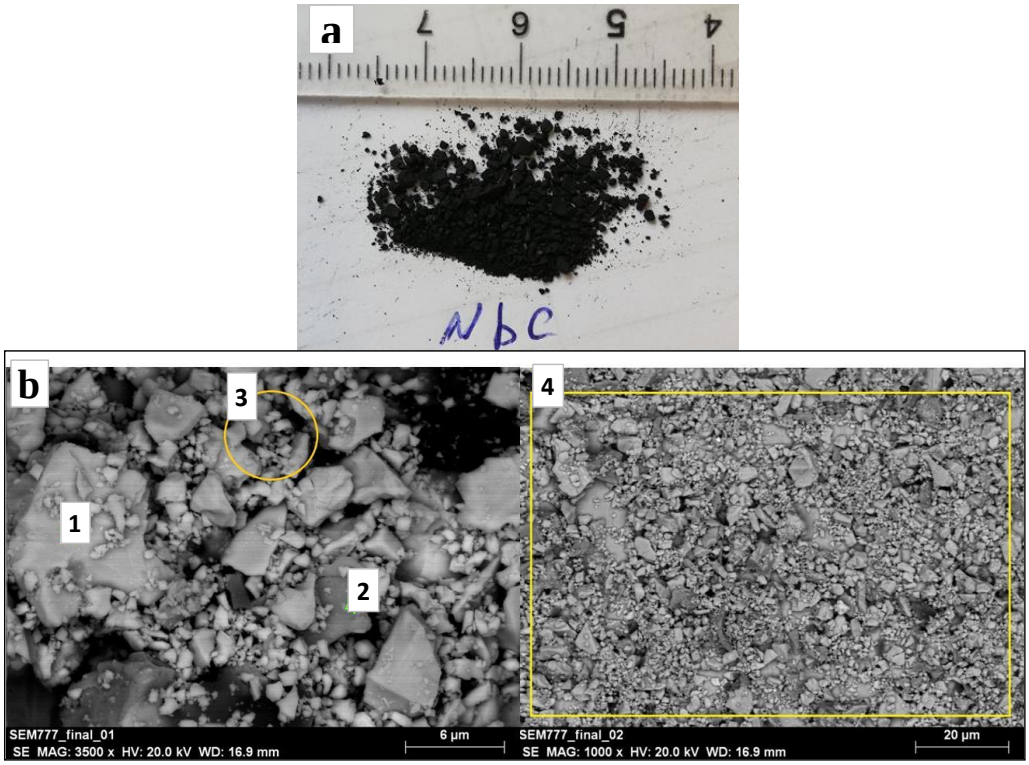

Figure 7. (a) Initial iron coated NbC powder (b) SEM images of the iron coated NbC powder after the grinding

In the EDS spectrum analysis of point 2 in Figure 8 of the SEM images in Fig. 7, Fe-Al-carbide particles are observed covering the NbC particles, which have been detached from between NbC particles during the milling process.

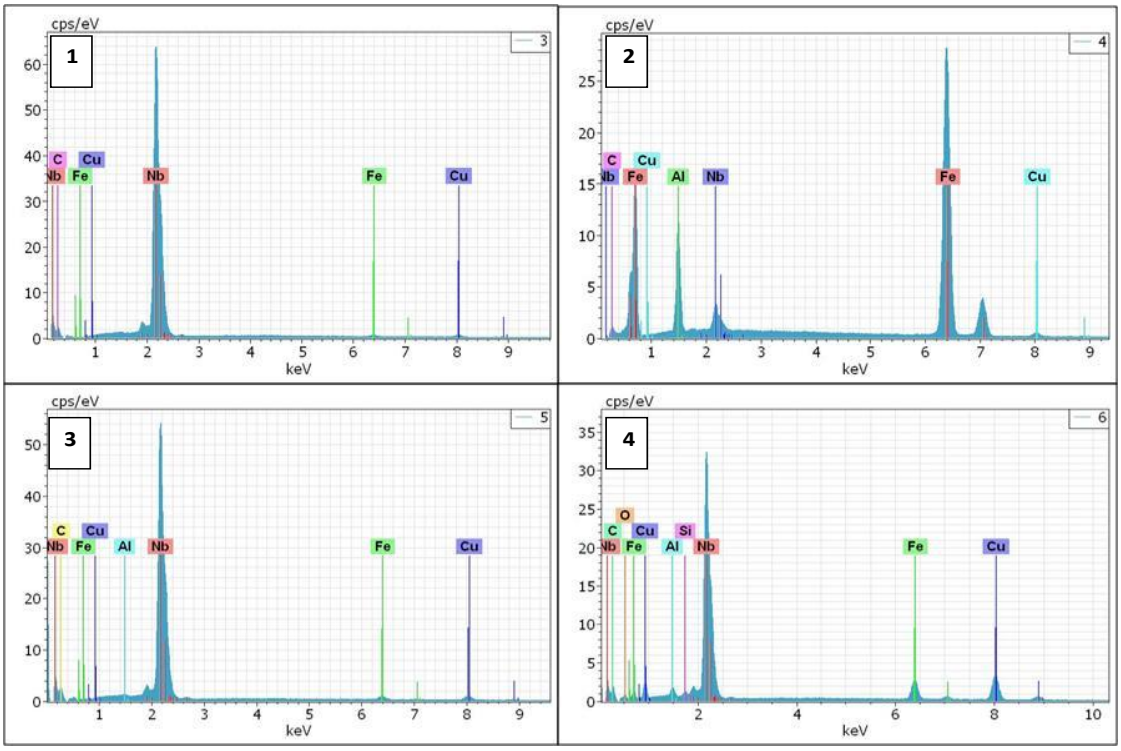

Figure 8. EDS spectra of SEM images in Fig. 7

Also, the initial powder size of Si (2.5-5 mm) was reduced by milling in a planetary ball mill to ≤ 63 µm. The container of the mill was made from iron and filled with steel balls. The grinding ball size was 40 mm, and three were the grinding chamber. After the first grinding stage, the mill product was sieved at 63 µm, the fine size fraction was collected and the coarse fraction was fed into the mill again and ground until reaching a size finer than 63 µm (quantitatively ground).

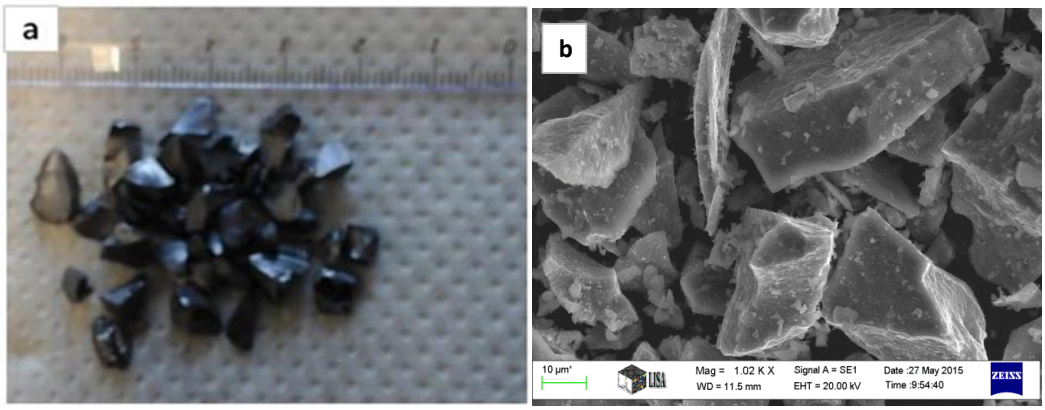

Figure 9. (a) Si before grinding (b) SEM image of Si powder after grinding

Scanning electron microscopy images of the silicon powder before and after grinding can be seen in Figure 9, where the effect of grinding on the particle size can be observed. The size was reduced from the initial 5 mm down to ≤ 63 µm. Furthermore, the shape of the particles became irregular with sharp edges compared to the original rounded particles. The characteristic particle sizes of silicon after preparation were as follows: median particle size d_{50} = 7.18 µm and 80% passing size d_{80} = 46.09 µm.

4.1.2 Preparation of cast iron samples

The samples of cast iron were prepared by cutting the rod of cast iron with cutting machine. The dimensions of the samples were 30×35×5 mm, as shown in Figure 10.

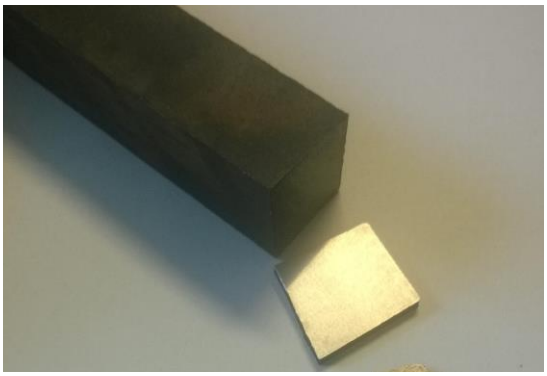

Figure 10. Cast iron sample

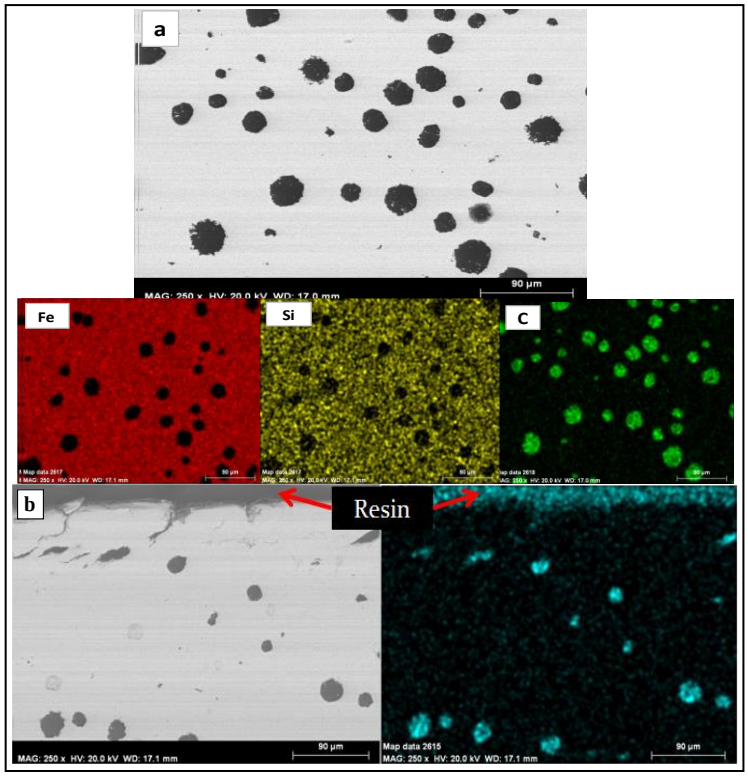

Figure 11. SEM images of the cross section of cast iron before the LMI process

In Figure 11 (b) of the cross-section of the cast iron sample, it can be observed that the surface is free from carbon particles for a few micrometres with many cracks. This causes poor surface hardness and lowers wear and abrasive resistance.

4.2 Mechanical alloying process (MA)

The previously prepared (grinded and sieved) iron coated NbC and silicon samples were mechanically alloyed in a batch stirred media mill with a grinding chamber volume of 530 cm^3. The milling chamber was equipped with a water jacket cooling system in order to control the temperature of the milling chamber. During the mechanical alloying experiments, the temperature of the milling chamber was a constant 30±2 ˚C. The stirrer consisted of perforated triangular disc rotors fixed on a drive shaft. The revolution number (circumferential speed of the rotor) can be adjusted by a frequency control unit. The electric power consumed during the experiments was measured by a microcomputer-controlled Carlo Gavazzi WM1-DIN digital energy meter for the characterisation of the specific grinding energy. The energy meter recorded the electric work in

cumulated form; in this way, the grinding work could be calculated as the difference between the initial and the final values. By measuring the no-load electric power consumption, the instantaneous power, and the mass of the product, the specific milling work can be determined as follows:

$$W_s = \frac{\int\big(P(t)\big)dt}{m_p} \tag{1}$$

where P(t) is the measured electric instantaneous power and m_p is the mass of the final product. The mechanical milling experiments were executed in a stirred media mill using different milling times: 5, 15, 30, 60, 120 and 240 minutes. The circumferential speed (tip speed) of the rotor in the stirred media mill was 10.56 ms^{-1}. The weight of the feed material is as follows: iron coated NbC 24.6 g and Si 4.35 g. Furthermore, to avoid several problems that arise in a dry mode milling, such as aggregation, agglomeration and sticking to the liners and the milling media, the isopropanol was added as a liquid medium (147.36 g for one batch). The media filling ratio was 70% during MA. The milling media were sintered zirconium silicate beads with a size range of 1.0-1.2 mm, its specific weight of 4.1 kgl^{-1}, and microhardness of 1000 HV. After the end of each work phase, all the operating data and details (grinding work, temperature and visual observation of the suspension) were noted as shown in Table 1.

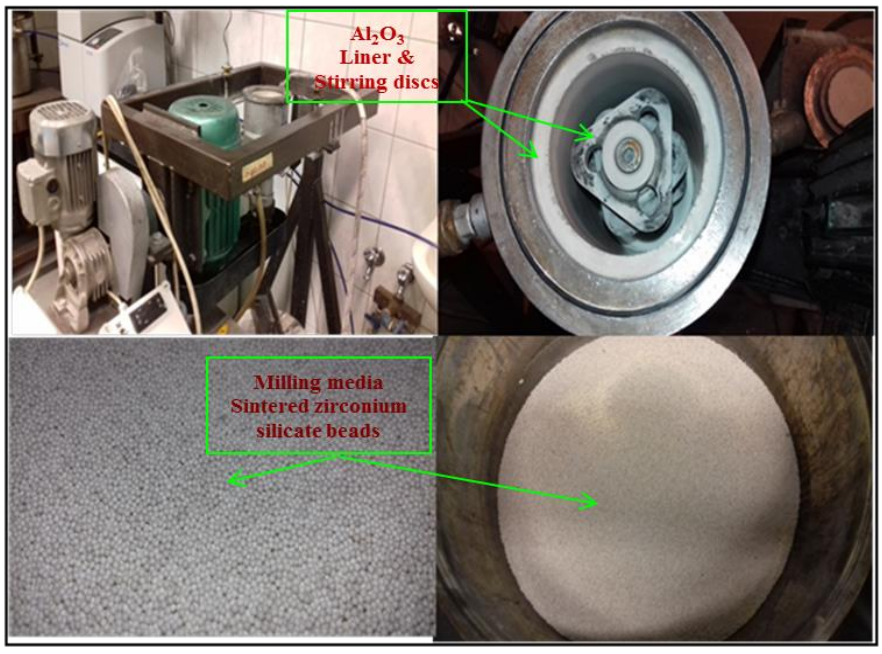

Figure 12. Stirred media mill and milling media

Table 1. Mechanical alloying conditions of iron coated NbC+Si powder

Milling time min	Grinding work Wh	Specific grinding energy kJ/kg	Temperature of the suspension ˚C
5	21	725	28.6
15	52	1796	31.1
30	94	3247	27.0
60	198	6839	32.6
120	406	14024	32.4
240	990	34197	31.8

4.3 Laser melt beam injection process

4.3.1 First part of the LMI experiment

The LMI experiments are performed in two parts. The first part involves selection the appropriate experimental conditions (laser energy, powder feed rate and laser spot width) that correspond to the powder type and sample type (cast iron). Different laser energies are applied ranging between 2000-2700 W, different powder feed rate 250-500 mm/min and different powder type: iron coated NbC, iron coated NbC+Si without MA and iron coated NbC+Si after MA, as shown in Table 2. Applying high laser power 2700 W leads to the melting and deformation of the surface of the sample, where the temperature is controlled by the energy of the laser (see Fig. 13), and resultant lower hardness values, therefore these values will not be taken into consideration. The final experimental conditions are selected depending on the experiment result that achieves the highest hardness value.

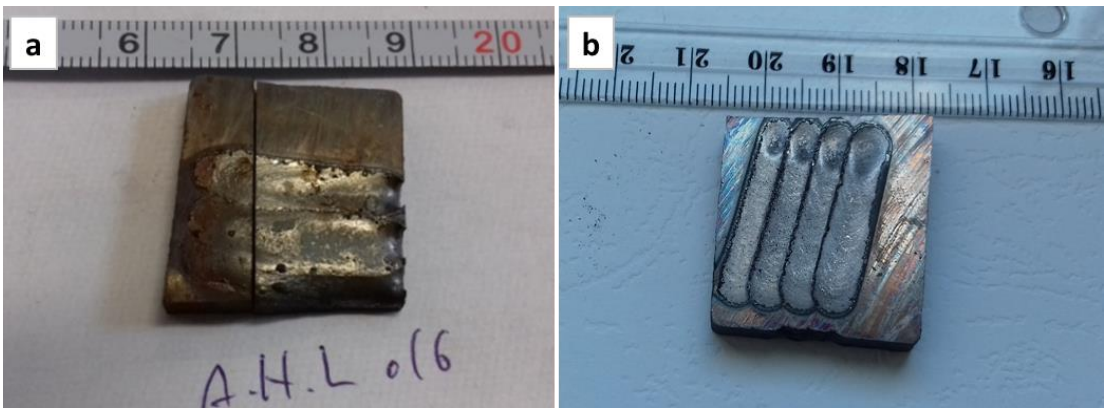

Figure 13. Cast iron samples after the LMI process (a) Laser energy 2700 W (b) Laser energy 2500 W

Table 2. Experimental conditions

Reinforcement powder	Laser energy W	Moving speed mm/min	Coating depth mm	Coating width mm
NbC	2500	500	1	3
NbC 85 wt% + Si 15 wt%	2500	500	1	3
NbC 85 wt% + Si 15 wt%	2250	250	1	3
NbC 85 wt% + Si 15 wt%	2000	250	1	3
NbC 85 wt% + Si 15 wt% After MA 240 min	2500	500	1	3
NbC 85 wt% + Si 15 wt% After MA 240 min	2500	250	1	3
NbC 85 wt% + Si 15 wt% After MA 240 min	2250	250	1	3
NbC 85 wt% + Si 15 wt% After MA 240 min	2000	250	1	3

4.3.2 Second part of the LMI experiment

In this part, the effect of powder type used in the LMI process on hardness and wear resistance values was studied, the cast iron sample 30×35×5 mm was used for reinforcing by iron coated niobium carbide-silicon powder, placed the powder in a container of the laser melt beam injection device. The distance between the sample and the nozzle must be 17 mm. The device is switched to start the process. The process was carried out with the argon gas to avoid oxidation of samples. According to the results of the LMI experiments in part one, the LMI conditions which will be applied in the second part of the experiments is 2500 W laser energy and 500 mm/min feed rate using iron coated niobium carbide-silicon powders without mechanical alloying and after the mechanical alloying process for different time periods (5, 15, 30, 60, 120 and 240 min). The details of each experiment are tabulated in Table 3.

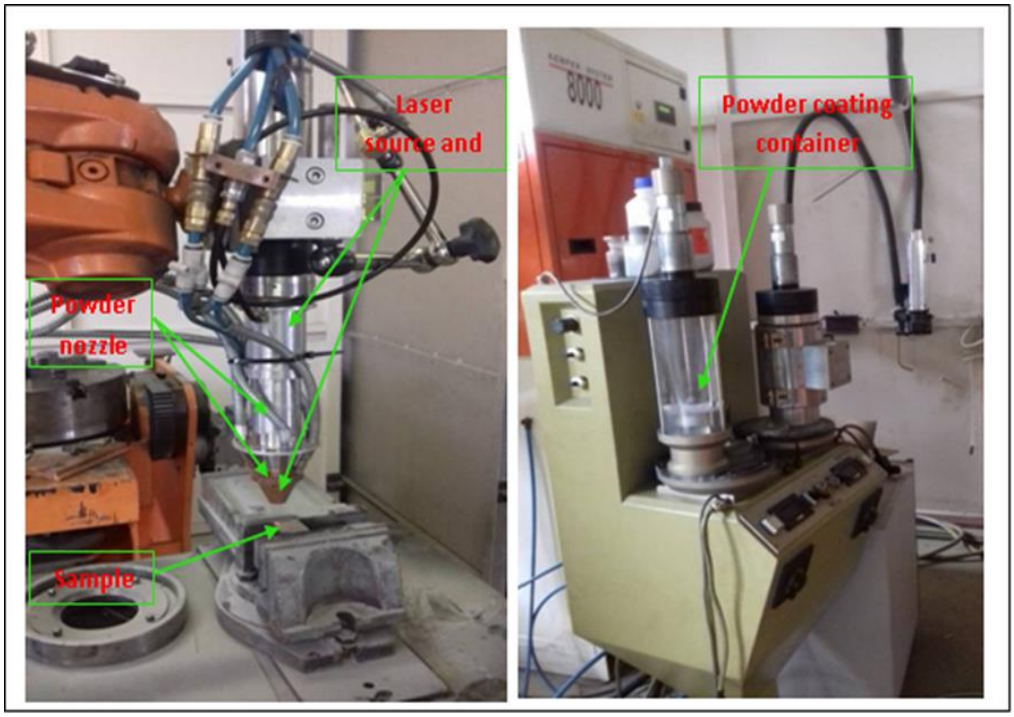

Figure 14. Laser melt beam injection instrument

Table 3. Experimental conditions

Coating powder	Power of laser W	Moving speed mm/min	Coating depth mm	Coating width mm
NbC 85 wt% + Si 15 wt%	2500	500	1	3
NbC 85 wt% + Si 15 wt% After MA 5 min	2500	500	1	3
NbC 85 wt% + Si 15 wt% After MA 15 min	2500	500	1	3
NbC 85 wt% + Si 15 wt% After MA 30 min	2500	500	1	3
NbC 85 wt% + Si 15 wt% After MA 60 min	2500	500	1	3
NbC 85 wt% + Si 15 wt% After MA 120 min	2500	500	1	3
NbC 85 wt% + Si 15 wt% After MA 240 min	2500	500	1	3

4.4 Brazing experiments

The spreading property of iron coated NbC+Si powder without or after mechanical alloying was examined by the sessile drop method for the nickel foil with the cast iron specimen. Where the surface of the cast iron substrate (10×15

mm) and the nickel foil (10×15 mm) was cleaned by sodium hydroxide (NaOH) solution then washed with distilled water and with alcohol (C_2H_5OH). The cast iron specimens covered by a layer of iron coated NbC+Si powder (without or after mechanical alloying for 240 min), then nickel alloy foil was placed on the top of the iron coated NbC+Si powder layer (see Fig. 15). After that, the specimens were placed in the vacuum furnace ($1 \cdot 10^{-4}$ mbar), then the furnace was heated up to 1100 ˚C, which is the molten temperature of nickel foil. The sample was kept at 1100 ˚C for 10 minutes. After 10 minutes, the furnace temperature was gradually reduced until the temperature inside the furnace reached 300 ˚C, at which point the furnace chamber was filled with nitrogen gas to avoid oxidation of the samples while continuing to reduce the furnace temperature till it reached room temperature (see Fig. 16).

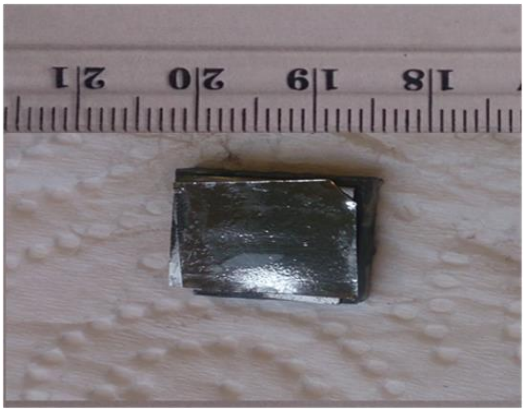

Figure 15. The cast iron sample covered with iron coated NbC+Si powder and Ni foil before being placed in the furnace

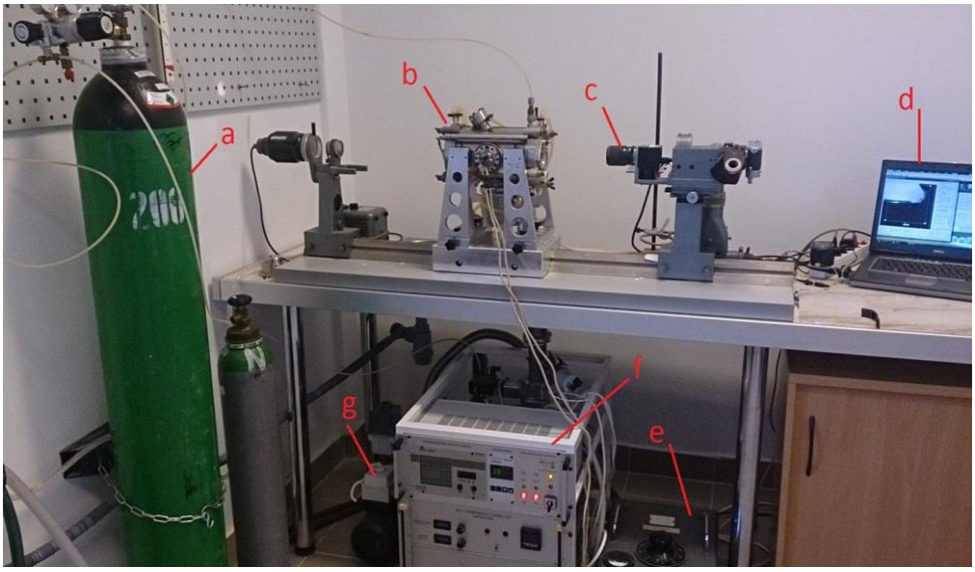

Figure 16. Brazing equipment (a: argon gas bottle, b: furnace, c-camera, d: laptop e: power supply, f: vacuum machine, g: assistant vacuum)

5 RESULTS AND DISCUSSION

5.1. Mechanical alloying process

5.1.1. Material fineness

A significant fluctuation can be observed in the particle size distribution of the iron coated NbC+Si powder after the mechanical alloying process.

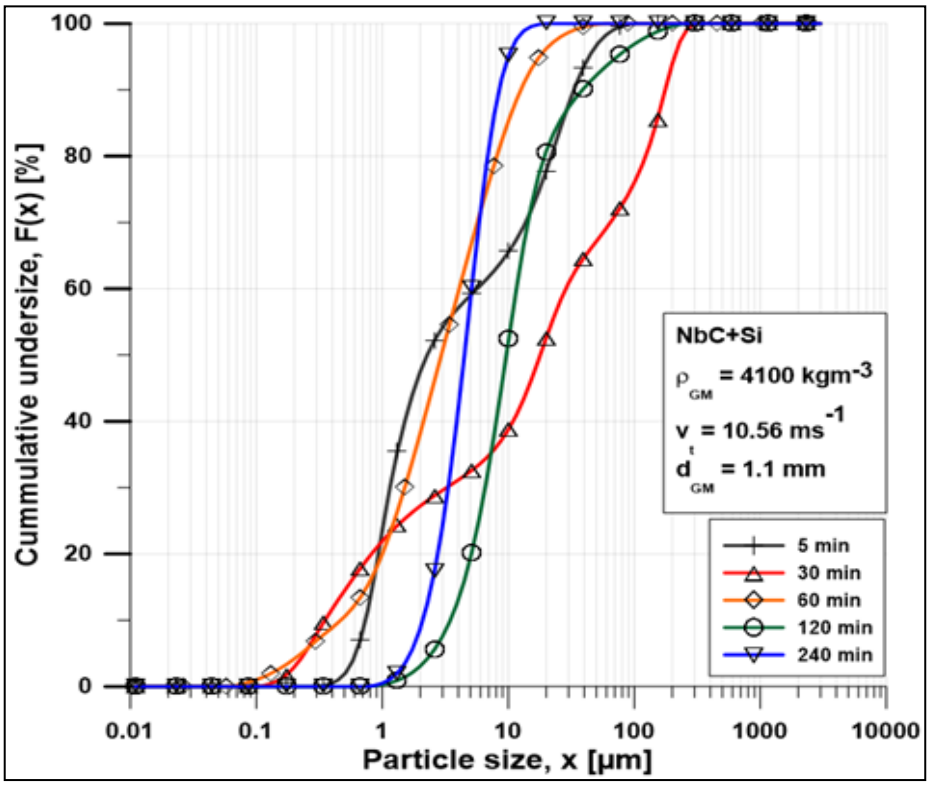

Figure 17. Cumulative particle size distribution curves of the MA (iron coated NbC+Si) powder

Figure 17 shows the cumulative particle size distribution curves of the mechanically alloyed iron coated NbC+Si particles. Remarkable coarsening of the particles appears at 30 min of residence time, probably due to the aggregation and/or agglomeration and/or mechanical alloying of the particles. After this, the iron coated NbC+Si ground material became finer, coarser, then finer again. No significant shift in particle size whether progressive or regressive was observed. However, this shift was to be expected as in the case of brittle materials in

general, but when the grinding kinetics was investigated, the non-brittle behaviour of the materials was found to be the cause behind this behaviour which results in more deformation and structural changing than particle size reduction.

Figure 18 shows the change of the particle size volume ratio of the mechanically alloyed iron coated NbC+Si particles.

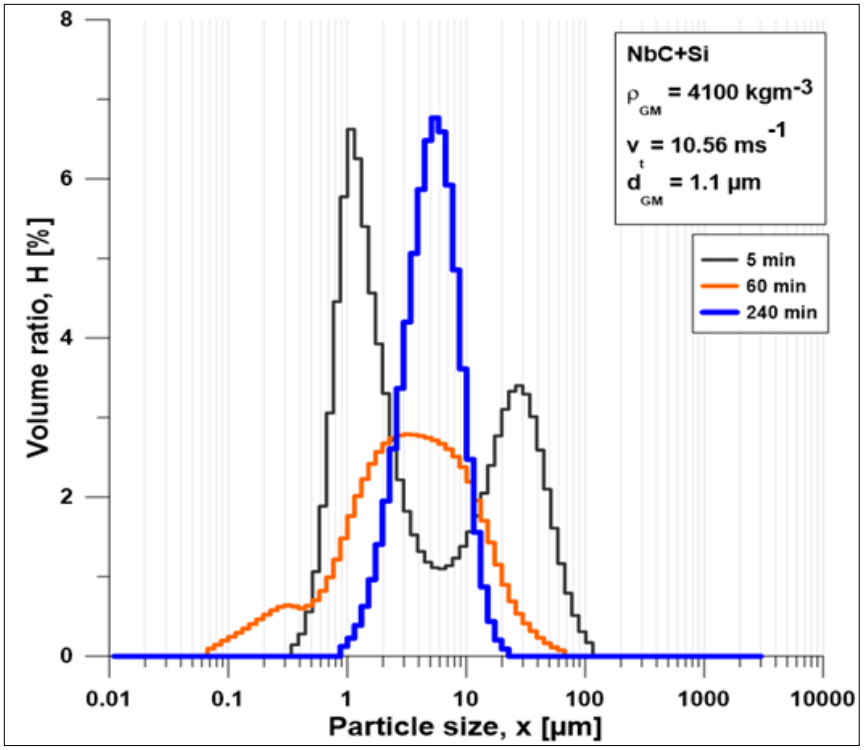

Figure 18. Frequency particle size distributions curves of the MA (iron coated NbC+Si) powder

Looking at Fig. 18, it can be stated that the shape of the curve is bimodal in the initial stages of the experiment and changes with residence time. After 60 min of residence time, the curve can be observed to shift from a bimodal to a unimodal shape, dominantly unimodal. The particle size range also changes as a function of time. The narrowest particle size range was produced after 240 min.

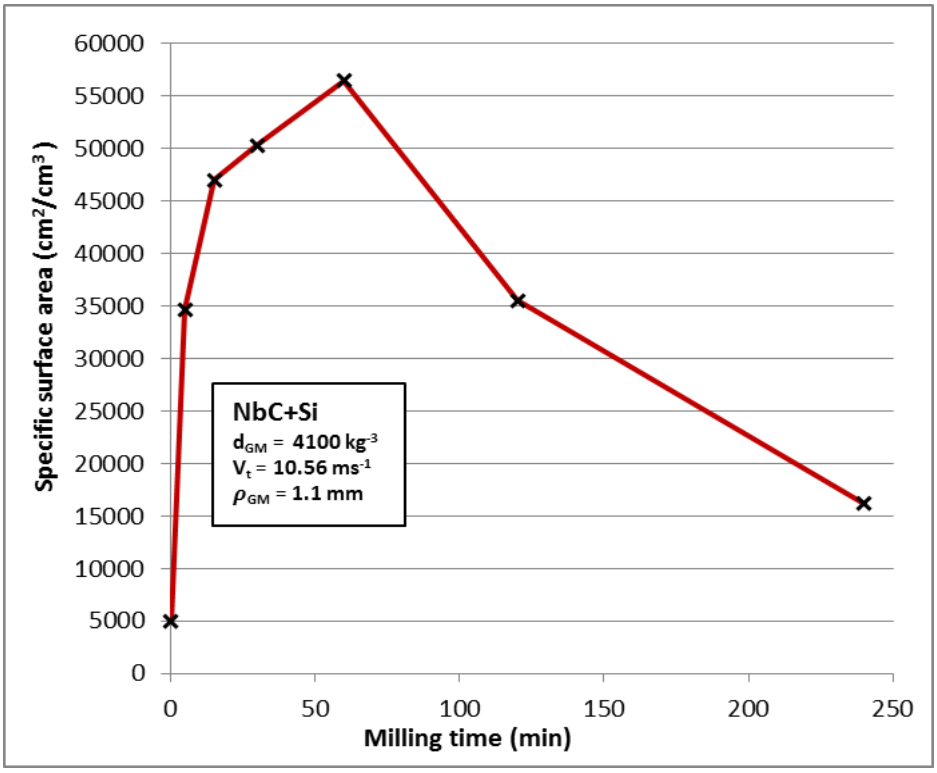

Figure 19. Diagram of a specific surface area as a function of milling time

In Figure 19, the geometric (outer) specific surface area is plotted as a function of milling time. A sudden decrease in specific surface area was noticed after 60 min of milling time in the stirred media mill. According to the kinetic considerations of the milling procedure, it can be divided into three main stages. In the first stage, the specific surface area rises linearly with the milling time (the so-called Rittinger section) with the maximum specific surface area 56500 cm^2cm^{-3} reached at 60 min of milling time. In the second stage, the slope of the specific surface area decreases (the section of aggregation), while in the third stage the specific surface area decreases drastically with the milling time (which can be explained by the phenomenon of agglomeration, where the bonding force between the particles becomes stronger than in the agglomeration phenomenon) down to 16000 cm^2cm^{-3}. However, from the cumulative undersize curves, no tendency can be observed; the specific surface areas calculated from it show the general trend [129] that was expected with brittle materials.

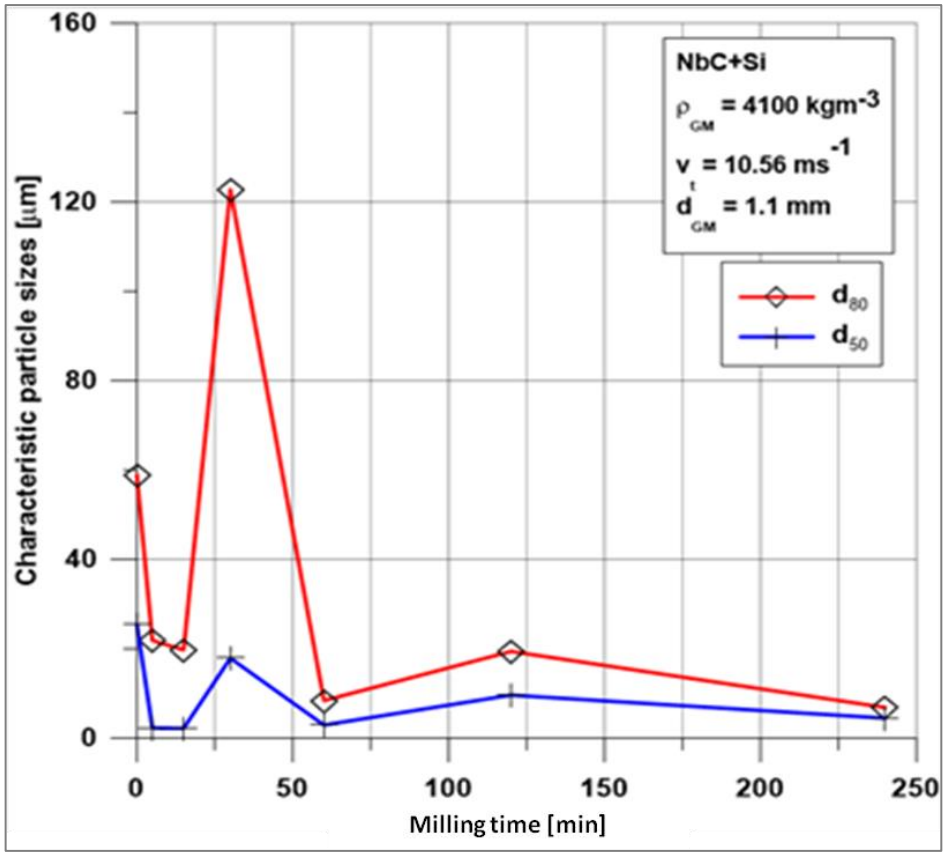

Figure 20. Diagram of diameter on cumulative% (x_{50} - x_{80}) as a function of milling time

Figure 20 shows the variation of the characteristic particle size values as a function of milling time for iron coated NbC+Si powder mixture, specifically with the median and 80% passing size plots. It is evident that the maximum particle size of the starting powder mixture was about 63 μm. Comparing with the growing trend depicted by diameter on cumulative d_{50}, the median particle size of iron coated NbC+Si powder mixture in diameter and d_{80} reaches a maximum at 30 min milling time and then stabilizes between 60 and 240 min. However, during this process, the primary niobium carbide and silicon particles suffer from the phenomenon of cold welding following the work hardening, resulting in the activation of the fracture mechanism, which is when the rate of cold welding and fracturing processes reach equilibrium and the steady state is achieved [130].

5.1.2. Microstructure

The samples for SEM analysis are prepared by taking a small amount of iron coated NbC+Si powder after each milling process at 5, 15, 30, 60, 120 and 240 min. Then the powder is placed in the resin mould. After the resin dried, the particles of powder were on the upper surface of the sample and ready for SEM investigation.

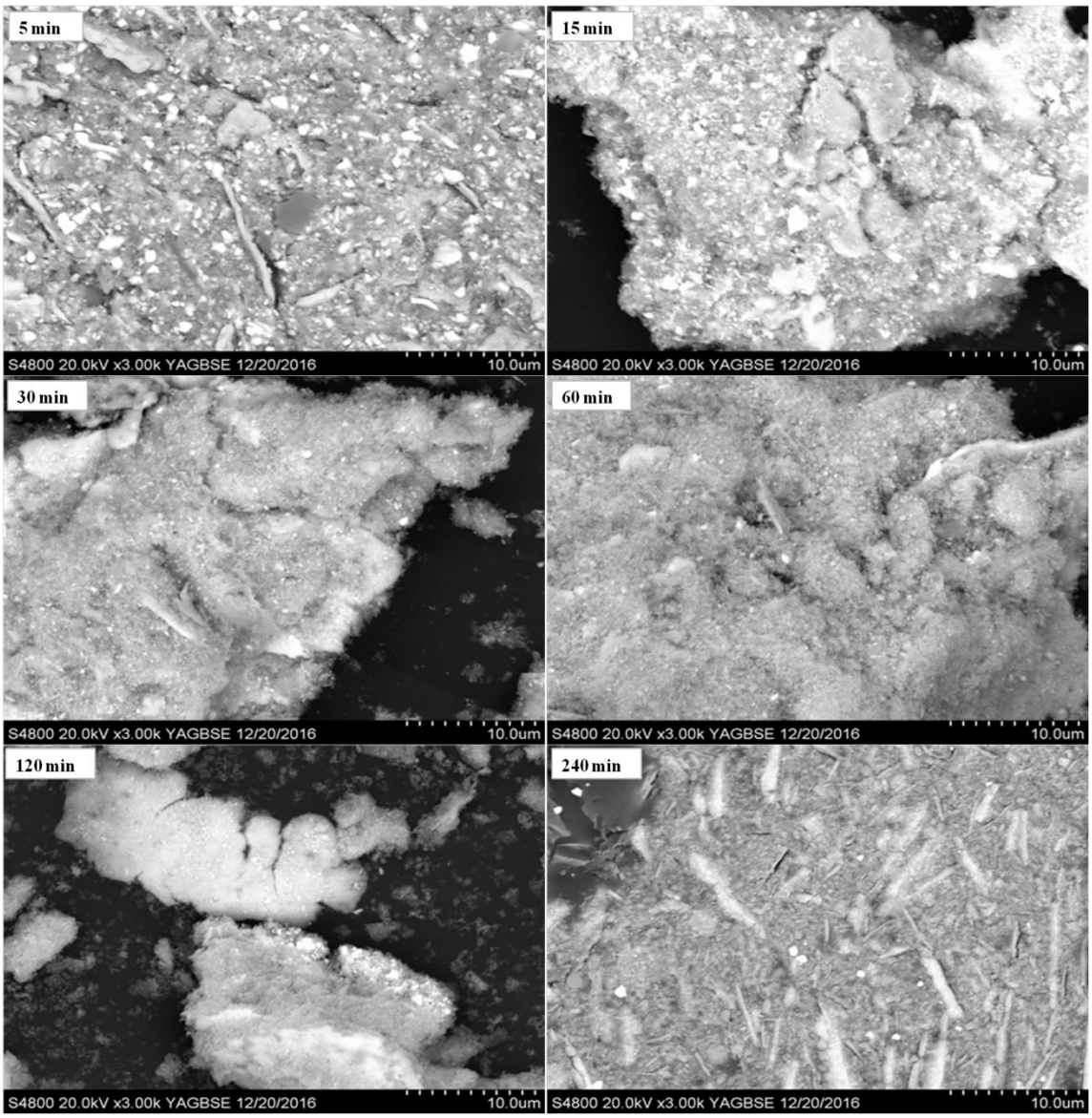

Figure 21. SEM images of the iron coated NbC+Si powder after MA for 5 - 240 min milling time

From the SEM images in Figure 21, the effect of milling for different periods of time (5-240 min) on the variation of the particle size of the iron coated NbC+Si powder can be seen. At the beginning of milling time (5 min), the particle size

starts to decrease, then the agglomeration stage can be noticed at the more extended milling time (240 min). It is not possible to distinguish particles of NbC from Si, due to the new homogeneous microstructure that formed with micrometer particles size.

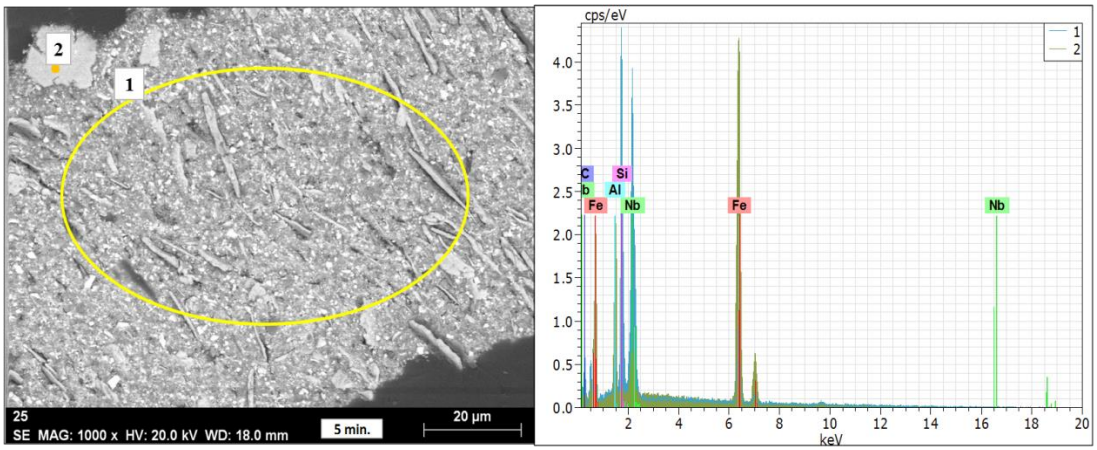

Figure 22. SEM and EDS images of the iron coated NbC+Si powder after MA for 5 min milling time

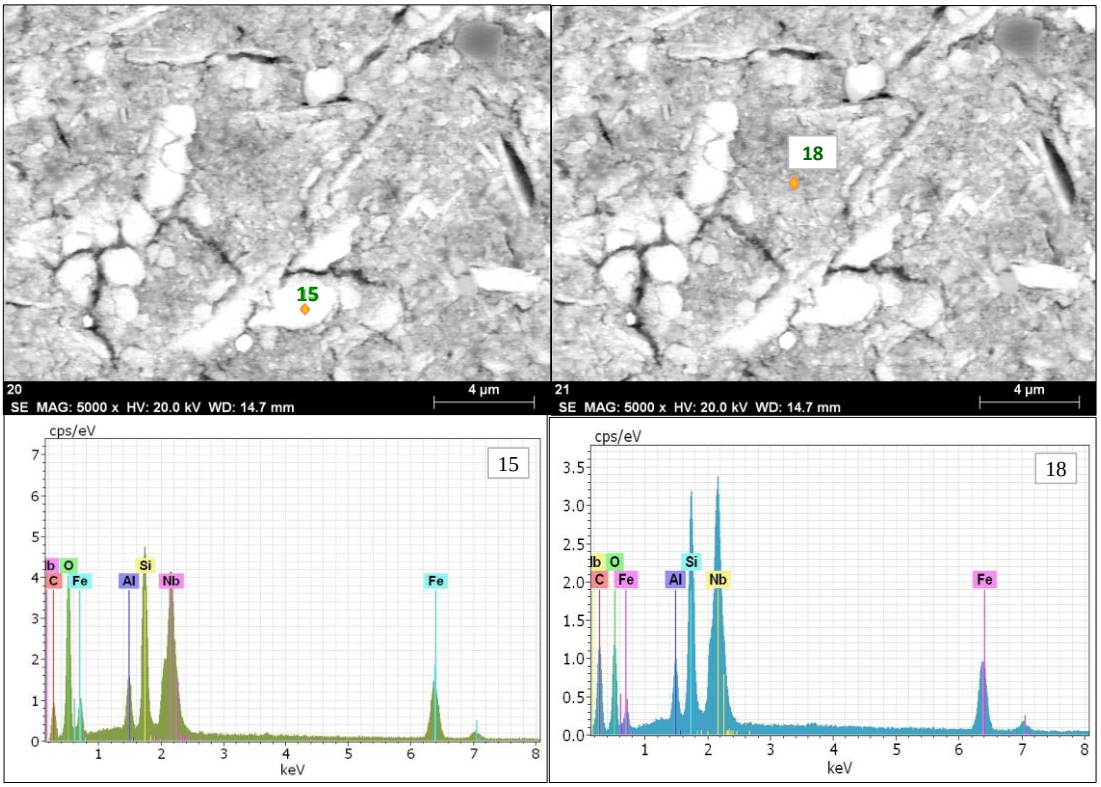

Figure 23. SEM and EDS images of the iron coated NbC+Si powder after MA for 240 min milling time

Figures 22 and 23 shows the SEM images and EDS spectra of the iron coated NbC+Si powder after 5 and 240 min of the MA process, where the effect of

milling can be seen for different times, namely the microstructure of the iron coated NbC+Si powder and the particle size. It is known that the MA process consists of three main stages: cold welding, fracturing and the steady-state condition [131]. Due to the extremely high surface energy of the fine particles and consequently the domination of cold welding and agglomeration over fracturing mechanisms, irregular-shaped powders with a wide particle size distribution are developed at the early stages of milling (e.g. 5 min).

By increasing the milling time, the powder particles are hardened, and due to the accumulation of strain energy [132], the particle hardness increases; therefore, the tendency of cold-welded powders for fracturing increases and the particle size is significantly reduced. Afterwards, a balance between the cold welding and fracturing rates is achieved, and the particle size reaches its steady-state condition [132, 133], which is associated with the narrow particle size is increasing as it is shown in Fig. 20.

The SEM image and the EDS images in Figs. 22, 23, clearly present that a short milling time (e.g. 5 min) there is a homogeneous element distribution. At sufficiently long milling time (e.g. 240 min), the elements distribution is homogeneous, and the difference between dark and light areas is the result of little difference in the intensity of the carbon element as shown in Fig. 23, thereby indicating a sufficient milling time for alloying.

5.1.3 Phase composition-Structural evolutions

Figure 24 shows the XRD spectra of the iron coated NbC+Si milled powder as a function of milling time. As seen from the patterns, in the initial powders mixtures, sharp diffraction peaks related to NbC, Si and Fe are evident. Also, minor phases such as Al-Fe-carbide and Fe-carbides are observed. By initiating milling, the development of nano-sized structure and the introduction of a high level of microstrain cause the sharp peaks to be considerably broadened. By further milling, the peaks of the initial materials gradually vanish.

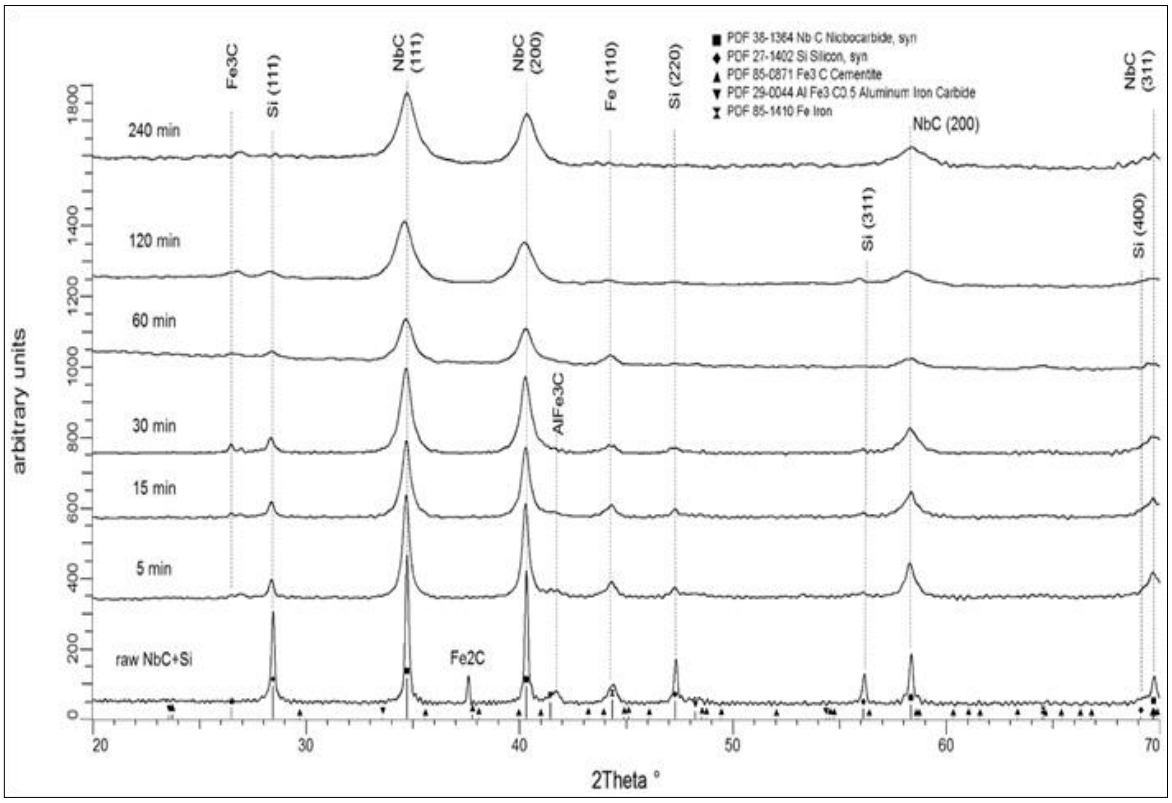

Figure 24. XRD patterns of iron coated NbC+Si powder after MA for different milling times

Further analysis of the XRD patterns indicates that increasing the milling time has a significant effect on the transformation of different phases in the powders. The peak broadening caused by crystallite size reduction is observed for each phase). Therefore, Rietveld refinement was used to calculated crystallite size and unit cell data is shown in Table 4. When examining the crystallite size, the significant fluctuation was observed, where the NbC crystallite size reduces 87.1

% after 240 min of milling, Si 93.8 %, Fe 52 %, and $AlFe_3C_{0.5}$ 54.5 %, but no crystalline Si-carbide is formed, while Nb_6C_5 is developed due to Si incorporation into with long milling time. With an increase in the milling operation, the polymorphic transformation can take place with mechanical alloying. The transformation is accompanied by a change in crystallite size and lattice distortion, and the crystallite size decreases and lattice distortion increases with an increase in grinding time. In general, the transformation shifts from unstable to stable forms [127].

Table 4. Crystallite size of iron coated NbC+Si powder after MA for different milling times

	Crystallite size (nm)						
MA time / Elements	**0 min**	**5 min**	**15 min**	**30 min**	**60 min**	**120 min**	**240 min**
Si	**65 ±15**	**40 ±10**	**26 ±6**	**19 ±5**	**13 ±3**	**4 ±1**	
NbC	**70 ±20**	**26 ±5**	**18 ±4**	**15 ±3**	**13 ±3**	**9 ±2**	**9 ±2**
Fe	**25 ±5**	**18 ±4**	**15 ±4**	**15 ±3**	**14 ±3**	**12 ±2**	
$AlFe_3C_{0.5}$	**22 ±2**	**9 ±2**	**9 ±2**	**10 ±2**	**16 ±3**	**10 ±2**	
Fe_3C cementite		**13 ±2**	**16 ±4**	**14 ±3**	**12 ±2**		
Nb_4C_3		**16 ±4**	**14 ±4**	**13 ±3**	**14 ±3**	**8 ±2**	**10 ±2**

With the silicon being significantly reduced already at the 5 min stage. After 240 min of milling, it was seen that the diffraction peak of Si has disappeared, and this is led to the Si changing into an amorphous phase. Since the formation of the amorphous phase during MA depends on several factors such as the milling conditions and the alloying system, different amorphisation reactions have been proposed [134]. One consists of a shift in the peak position and a continuous broadening of the XRD peaks due to a continuous reduction of the effective crystallite size being responsible for amorphisation of the present alloying system during MA. While the XRD peaks have revealed that the NbC(111) and NbC(200) phase powder mixtures exhibit a series of changes during milling

compared to the starting material, NbC phase demonstrates a lower and broader diffraction peaks, where the net height and net area increasing with the milling time until reaching the maximum value at 30 min of milling time can be observed, after which it tends to the drop until reaching the minimum value at 60 min and then going on to increase after 120 min of milling time.

This phenomenon demonstrates that the powder mixture only undergoes sub-microstructural changes of NbC phase owing to the severe plastic deformation of the NbC particles [135, 136]. The more extended milling time of 240 min leads to a remarkable broadening of NbC diffraction peaks and a decrease in the intensity of Si and Fe diffraction peaks. The peaks of Si and Fe disappear after 120 min of milling, indicating the formation of a solid solution (or secondary solid solution) of Si, C and Fe phases in NbC phase. It is well known that high velocity stirred media milling supplies an input of high energy to the powder system. During this process, a large number of flaws, including dislocations and new grain boundaries, are generated, rendering the diffusion between different components easy and in the occurrence of a solid solution of Si and Fe phase in NbC phase.

Milling in a stirred media mill provides the particles with an intense plastic deformation at an extremely high strain rate, resulting in the creation of high-density lattice defects and dislocations, as well as recovery phenomena [137, 138]. When the rate of the former is higher, the dislocations increase, resulting in a dislocated cell structure that ultimately creates low-angle grain boundaries. As the milling continues, low-angle grain boundaries transform into a whole nanocrystalline structure. In this stage, the crystallite size decreases and the lattice strain increases dramatically. The constant values of crystallite size and lattice strain reveal the balance of the appearance and disappearance of dislocations.

5.2 Laser melt beam injection process analysis

5.2.1 LMI experiments part 1

The original cast iron (ADI) substrate used in the experiments of the laser melt beam injection process has a surface hardness of 300 - 450 $HV_{0.05}$. After the LMI process, the samples were cut into halves and prepared for hardness test as shown in Figure 25.

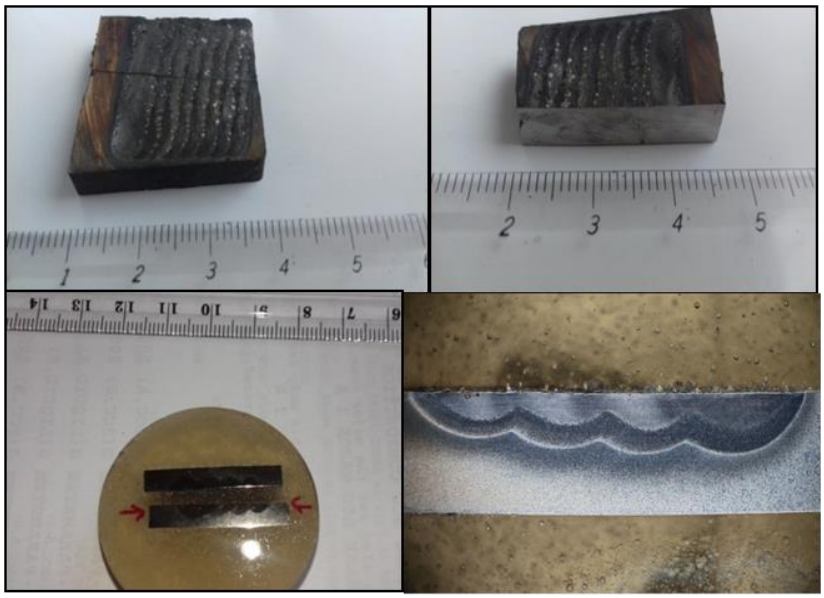

Figure 25. Cast iron samples after the laser melt beam injection process

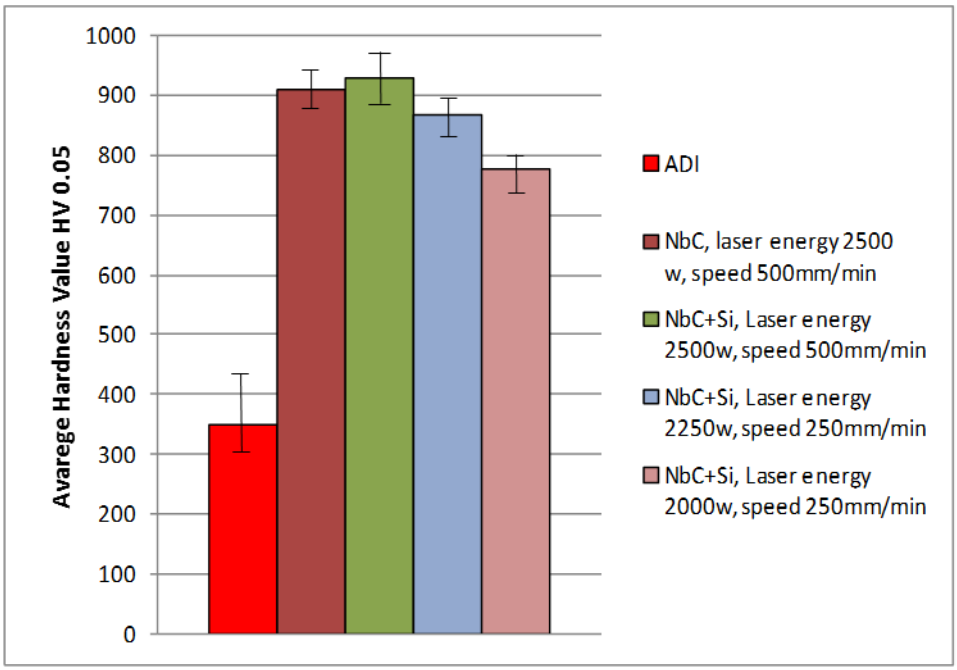

Figure 26. Average hardness value diagram of the LMI experiments, part 1

The graph of the average hardness value in Figure 26 shows the difference between the average hardness values of experiments, from maximum a value of 928 $HV_{0.05}$ to a minimum value a 780 $HV_{0.05}$. Depending on the conditions of the experiment and type of the reinforcing powder, the effect of the MA process for iron coated NbC+Si reinforcing powder is reducing the microhardness. A large increase in the microhardness value when using iron coated NbC as the reinforcement powder, was observed. The probable reason could be because the solubility of NbC is extremely low in Fe [139]. This means that micrometre-sized precipitates of NbC are virtually insoluble in iron and help prevent excessive grain growth in these steels. These act as a grain refinement process, ensuring both toughness and strength, besides inhibiting the heterogeneous grain growth causing hardness to increase [42].

Also, with the addition of Si to the iron coated NbC reinforcement powder, there was an observed increase in microhardness. The probable reason is the Si solid solution strengthens on NbC resulting from an increase in the concentration of Si in NbC solid solution, when it impedes dislocation mobility and increases the deformation resistance of the matrix [140], therefore improving the microhardness of NbC. Also, the Si increases the diffusivity of NbC in Fe at high temperatures over 948 ˚C [110], thus improving the microhardness of the iron matrix. Another probable reason for increasing microhardness with the addition of Si to the iron coated NbC powder is a precipitation hardening mechanism. Hard and brittle Fe_3C, Nb_4C_3 precipitates disperse in the NbC matrix, which would contribute to improving the microhardness of NbC solid solution [109].

Also the parameter of LMI process; laser energy from 2000-2700 W and the feed rate from 250-500 mm/min, where the decrease in the laser energy led to lower hardness values as well as when the feed rate speed was decreased.

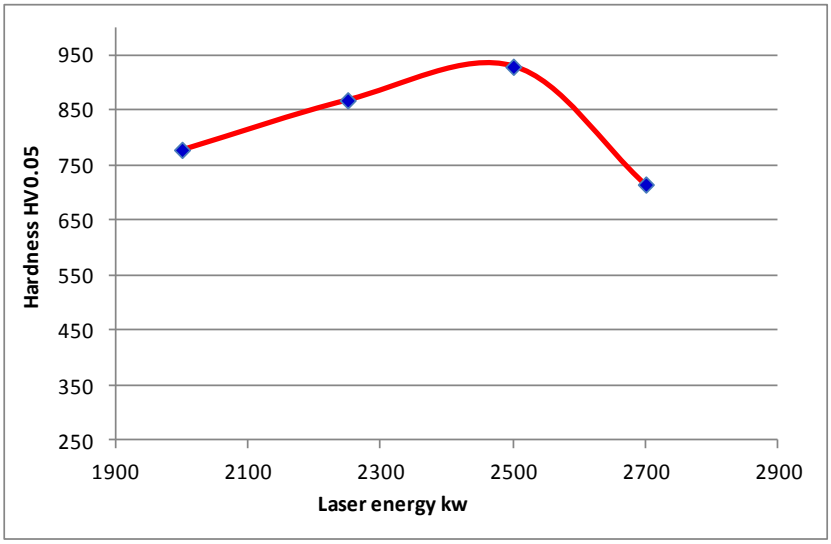

Figure 27. Effect of laser energy on the microhardness of cast iron after the LMI process

From Figure 27 it can be seen that the average hardness value of cast iron after the LMI process decreases with decreases in laser energy. The probable reason is that the lower energy of laser which means lower temperature and lower cooling rate in comparison with the previous experiments that used high laser energy the conditions that assess the niobium carbide particles to spreading better in the iron matrix. As previously mentioned, applying laser power above 2700 W leads to the melting of the surface of a sample, thus deforming it, which results in lower hardness values, therefore the LMI conditions which have been applied in the next LMI experiments are 2500 W laser energy and 500 mm/min feed rate.

5.2.2 SEM analysis of the LMI experiments part 2

In this part of the LMI experiment, the effect of powder type on the microstructure and hardness values was studied. In the SEM and EDS images in Figures 28 and 29 for the LMI experiment which used iron coated NbC powder only without Si, uniform spreading in the molten iron matrix of niobium particles < 10 µm was observed. Also, carbon particles aggregating on the border of the heat-affected zone of the laser in the form of arcs were found.

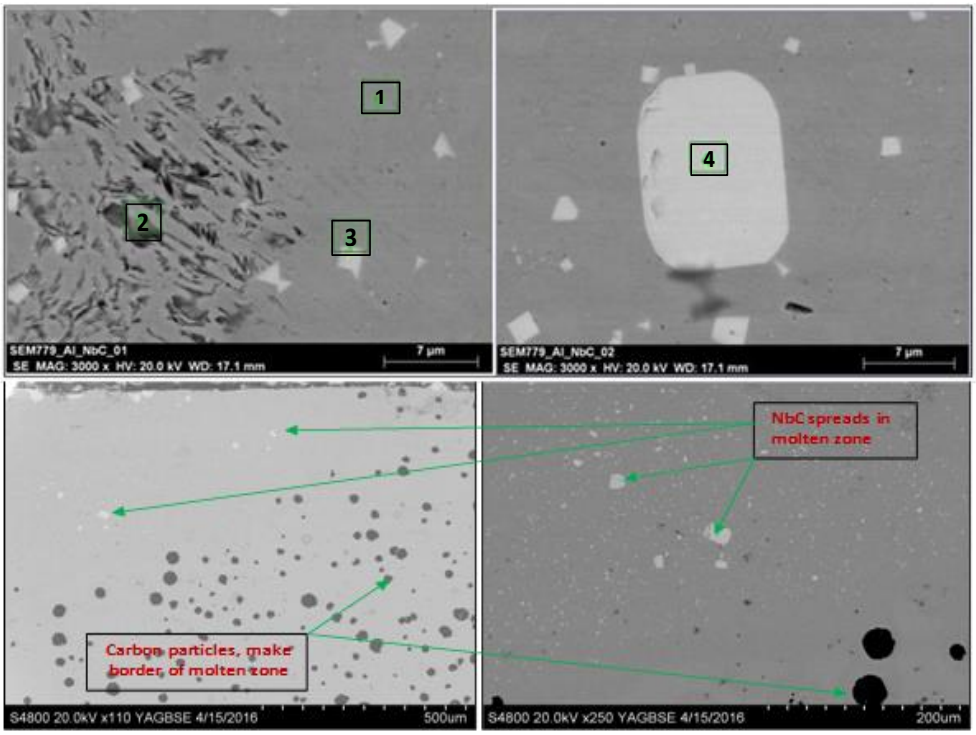

Figure 28. SEM images of the cross section of exp. No. 1 iron coated NbC powder only without Si

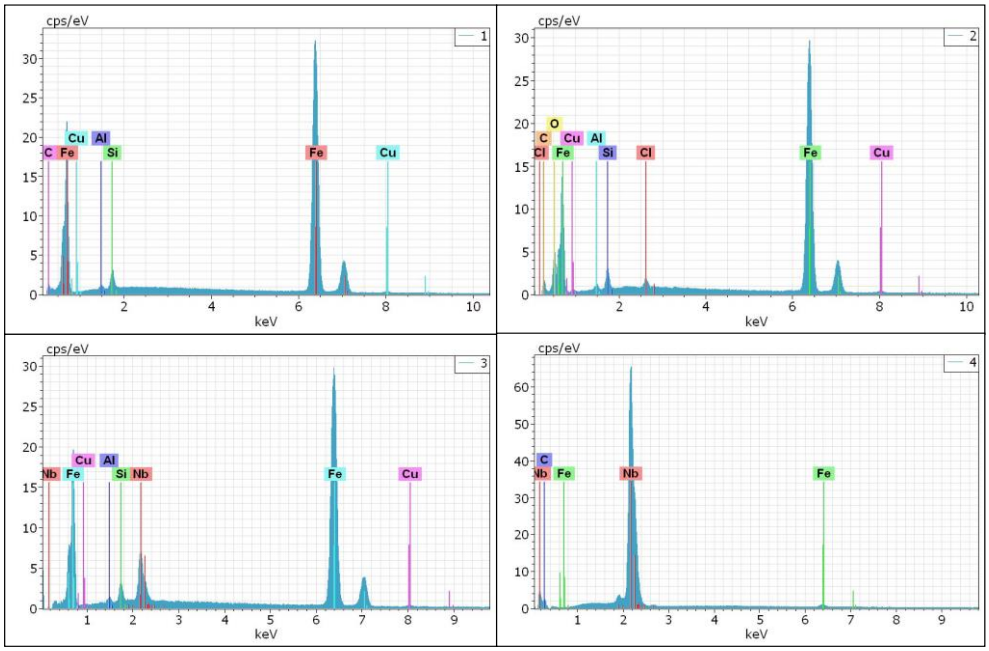

Figure 29. EDS spectrum of Points 1, 2, 3 and 4 in Fig. 28.

It should be noted that previous studies show that homogeneous nucleation of NbC can be as Nb and C atoms in the molten pool meeting [89]. During the LMI process and because of the high-temperature gradient and rapid cooling [141, 142], a certain amount of Nb particles remain unmelted and act as the substrate of NbC nucleation. The in-situ NbC particles, owing to its high melting point, it

precipitated out from the molten pool first, and the atoms of Al, Fe and Si were then squeezed into the interface between the NbC particles and the liquid phase.

5.2.2.1 LMI experiment using NbC+Si powder without the MA process

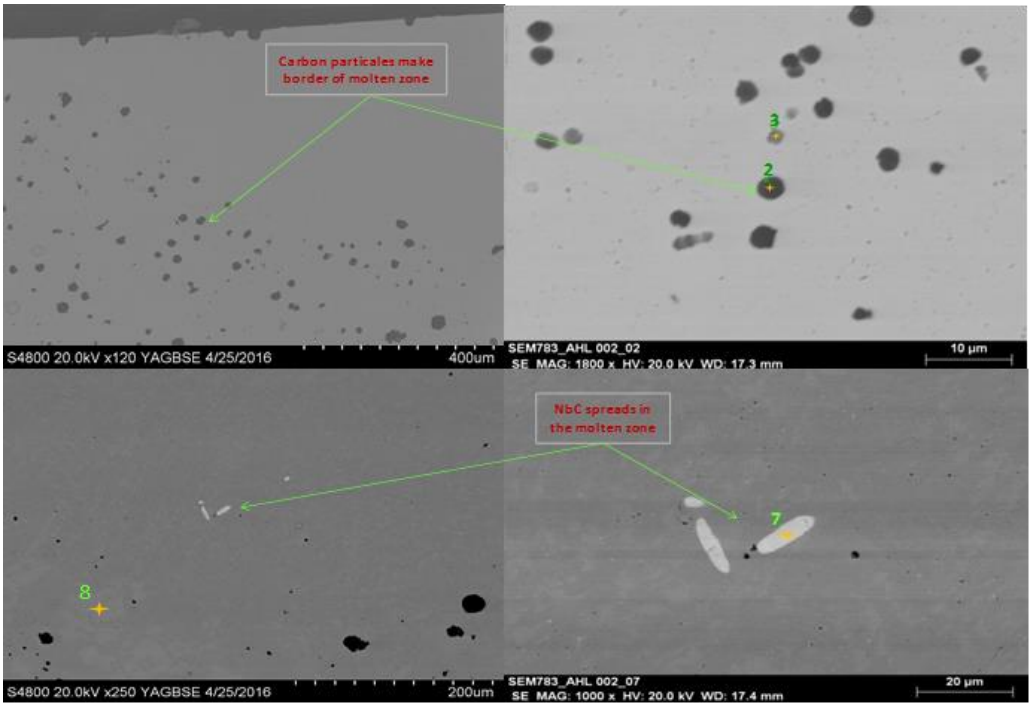

Figure 30. SEM images of the cross section of the cast iron sample of exp. (iron coated NbC 85 wt% with Si 15 wt%, without MA, laser energy 2500 W, moving speed 500 mm/min)

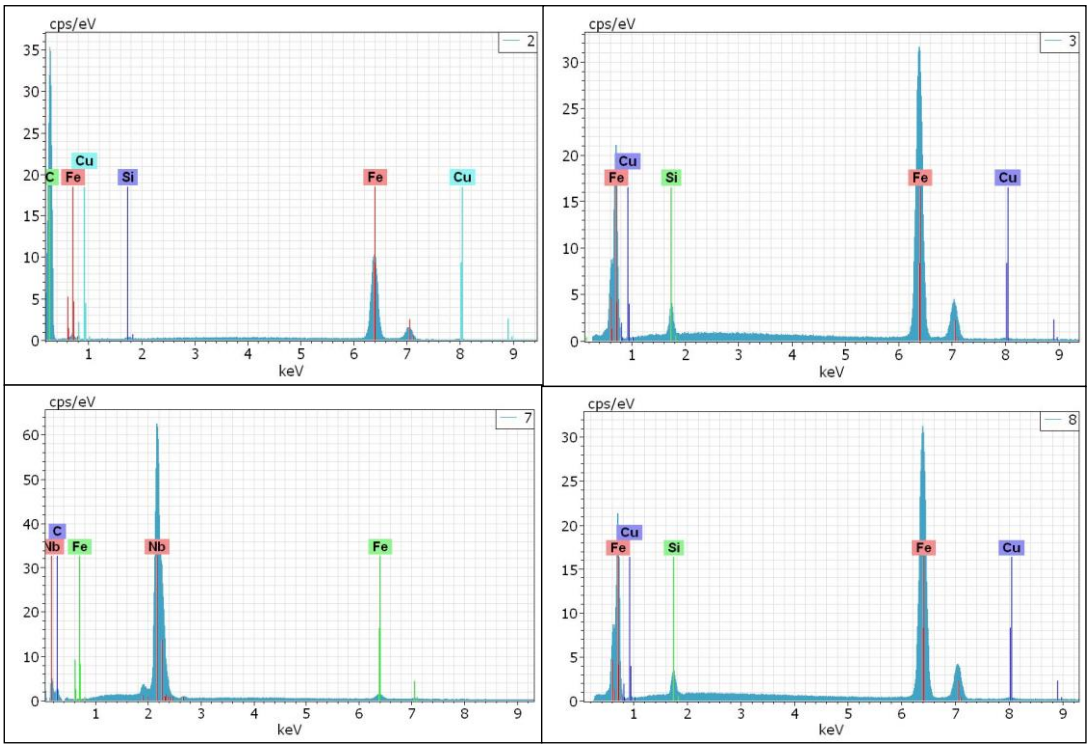

Figure 31. EDS spectrum of points 2, 3, 7 and 8 from Figure 30

From the SEM and EDS images in the Figures 30 and 31 of the experiment which used 85 wt% iron coated niobium carbide with 15 wt% silicon powder without MA. The effect of additional silicon on the microstructure of the cross section of cast iron samples after the LMI process can be observed the addition of silicon improved the diffusivity of niobium particles [110] in the melt iron matrix and promoted particle refinement [109], allowing it to form a homogeneous and fine microstructure with very few remaining niobium particles with size ≤ 20 µm, as shown in the Fig. 30.

5.2.2.2 LMI experiment using powder after 5 min MA

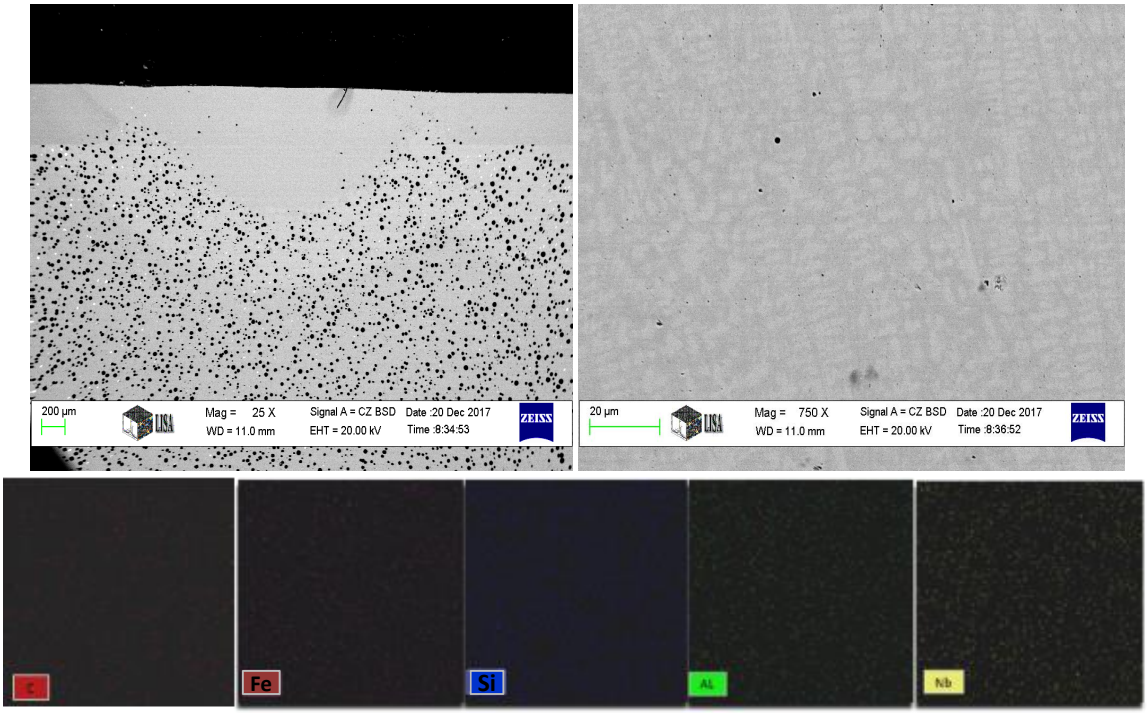

Figure 32. SEM and EDS images of the cross section of the cast iron coating sample of exp. (iron coated NbC 85 wt% + Si 15 wt%, after 5 min MA, 2500 W laser energy, moving speed 500 mm/min)

Table 5. The weight percentage of components in the melt pool zone in Figure 32

Elements	C	Si	Nb	Mn	Fe
wt %	2.37	2.67	4.9	0.47	89.57

In the EMS and EDS scan images of Figure 32 of the experiment which used iron coated niobium carbide 85 wt% with silicon 15 wt% powder after MA for 5 min, the effect of mechanical alloying on the components of the reinforcing powder

can be observed. It dissolved homogeneously in the iron matrix, and a eutectic microstructure (similar to ledeburite's microstructure) was formed during the terminal stages of solidification [86] due to the high temperature (2173-2375 K) generated during the LMI process and the following rapid cooling rate [143, 144].

5.2.2.3 LMI experiment using powder after 15 min MA

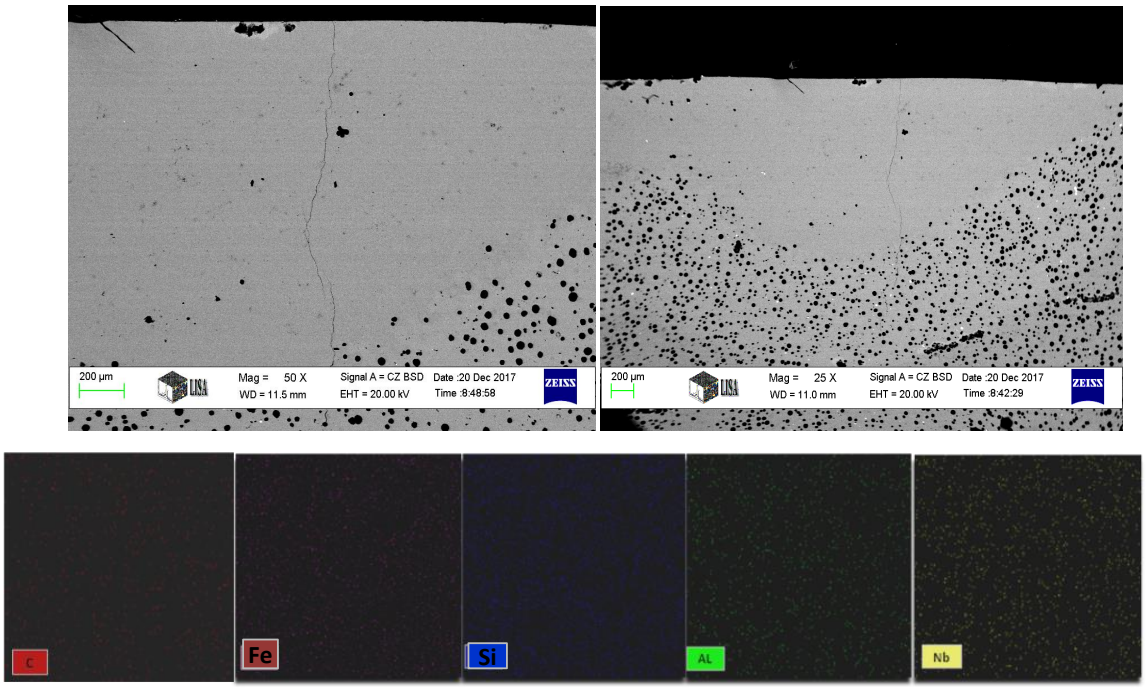

Figure 33. SEM and EDS images of the cross section of cast iron coating of exp. (iron coated NbC 85 wt% + Si 15 wt%, after 15 min MA, 2500 W laser energy, moving speed 500 mm/min)

Table 6. The weight percentage of components in the coated area in Figure 33

Element	C	Si	Nb	Mn	Fe
wt %	2.99	3.19	5.63	0.36	87.84

In the SEM and EDS images in Figure 33 of the experiment which used iron coated niobium carbide 85 wt% with silicon 15 wt% powder after MA for 15 min, it can be observed that the components of the powder have also dissolved homogeneously in the iron matrix.

5.2.2.4 LMI experiment using powder after 30 min MA

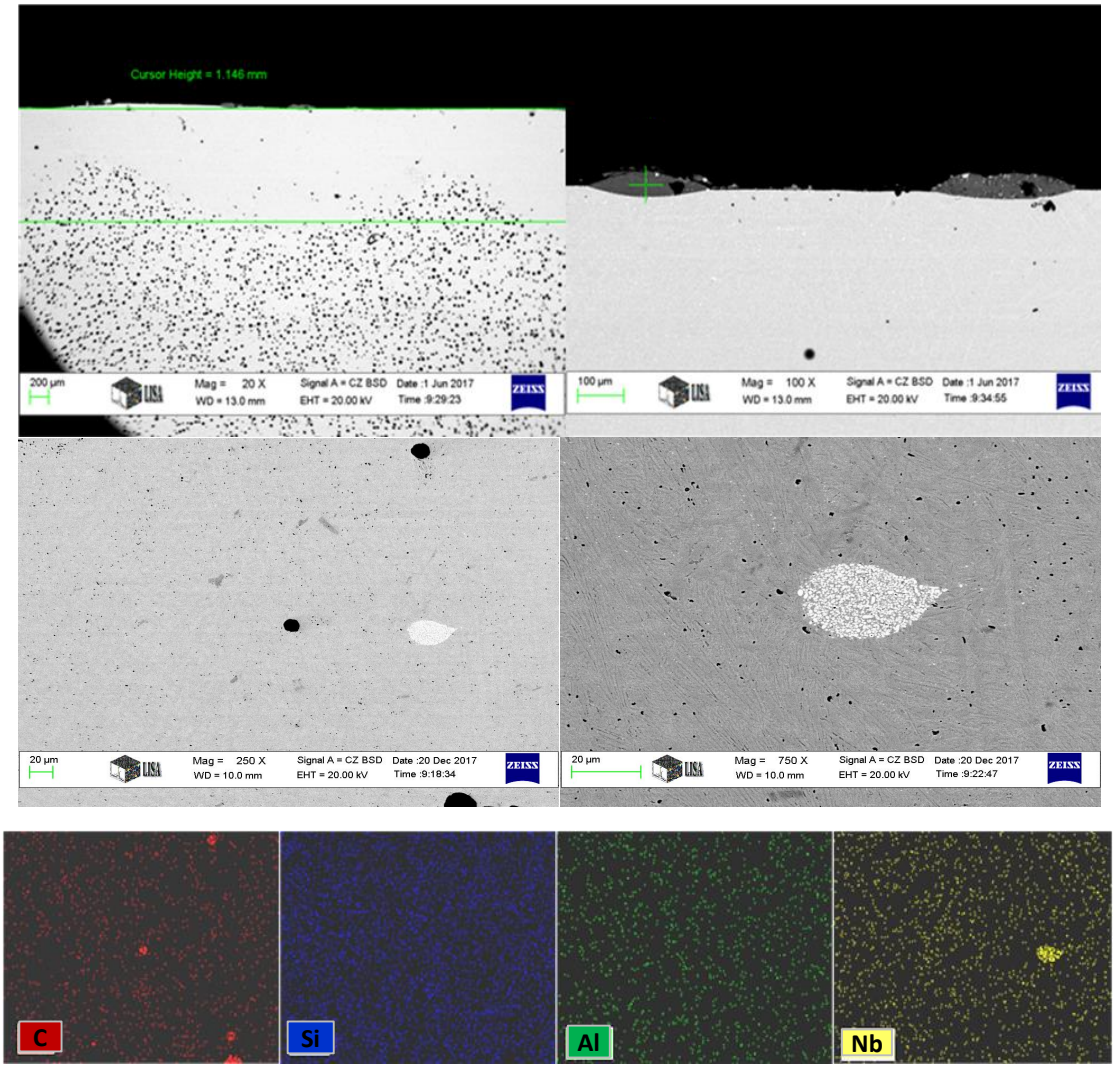

Figure 34. SEM and EDS images of the cross section of cast iron coating of exp. (iron coated NbC 85 wt% + Si 15 wt%, after 30 min MA, 2500 W laser energy, moving speed 500 mm/min)

From the SEM and EDS images in Figure 34, it can be observed that the melted aluminium formed a layer of slag on the coated surface and did not dissolve in the iron matrix because the wettability of aluminium with the iron is very low [145]. It can also be observed that the eutectic microstructure was created (similar to ledeburite's microstructure). The effect of MA on the specific surface area of particles (see the diagram of the specific surface area as a function of milling time in Fig. 19) can also been seen. Some particles of niobium agglomerates formed in small gatherings due to the effect of mechanical alloying time, which increased

the specific surface area and surface energy of niobium particles and reduced the wettability in the melted iron matrix.

5.2.2.5 LMI experiment using powder after 60 min MA

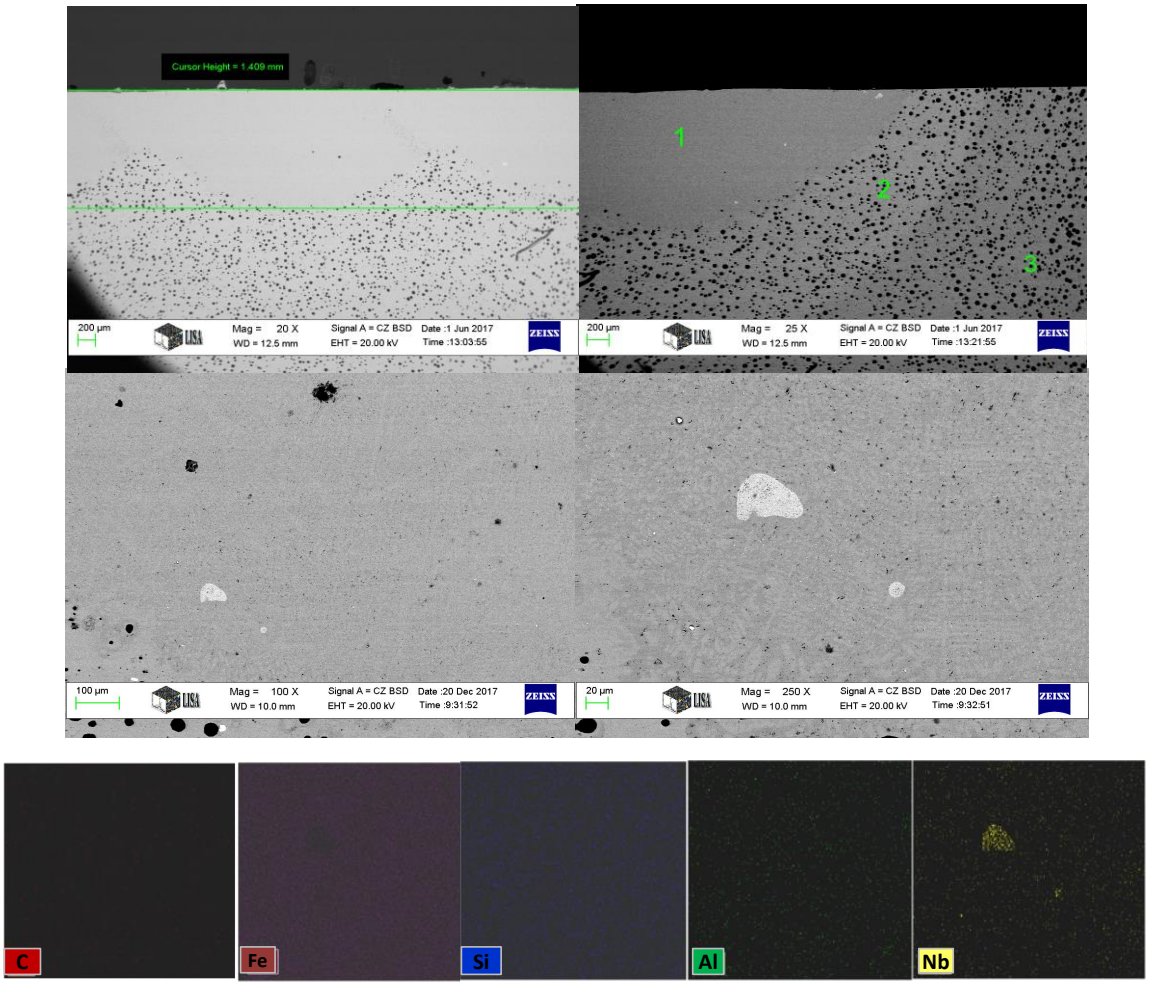

Figure 35. SEM and EDS images of the cross section of exp. (iron coated NbC 85 wt% + Si 15 wt%, after 60 min MA, 2500 W laser energy, moving speed 500 mm/min)

In Figure 35 the continuous effect of mechanical alloying time on the agglomerates of the niobium particles in small gatherings and increases in the area of the agglomerate with increasing MA time can be observed.

5.2.2.6 LMI experiment using powder after 120 min MA

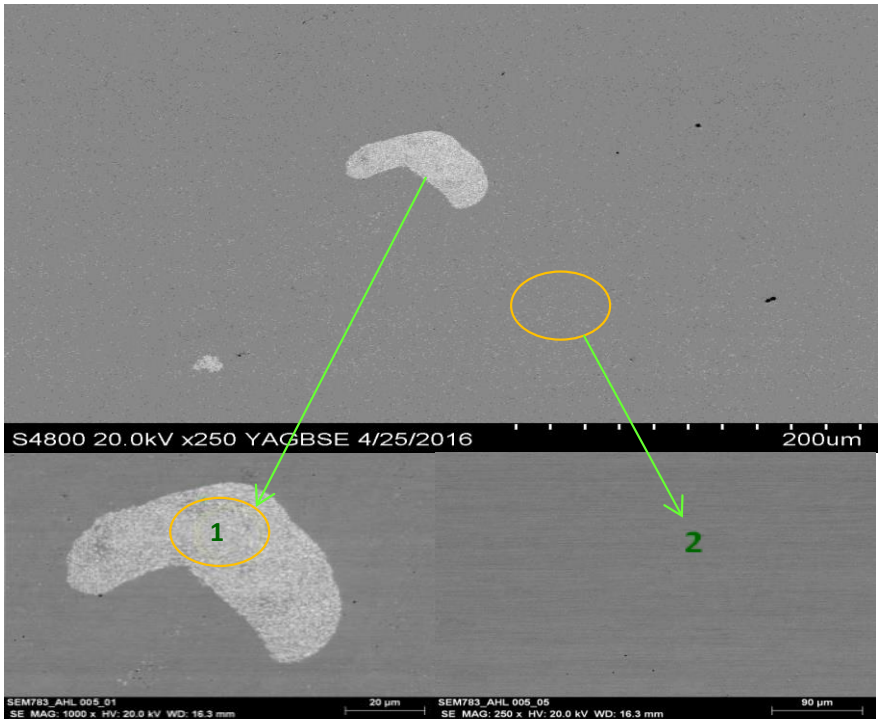

Figure 36. SEM images of the cross section of cast iron coating (iron coated NbC 85 wt% + Si 15 wt%, after 120 min MA, 2500 W laser energy, moving speed 500 mm/min)

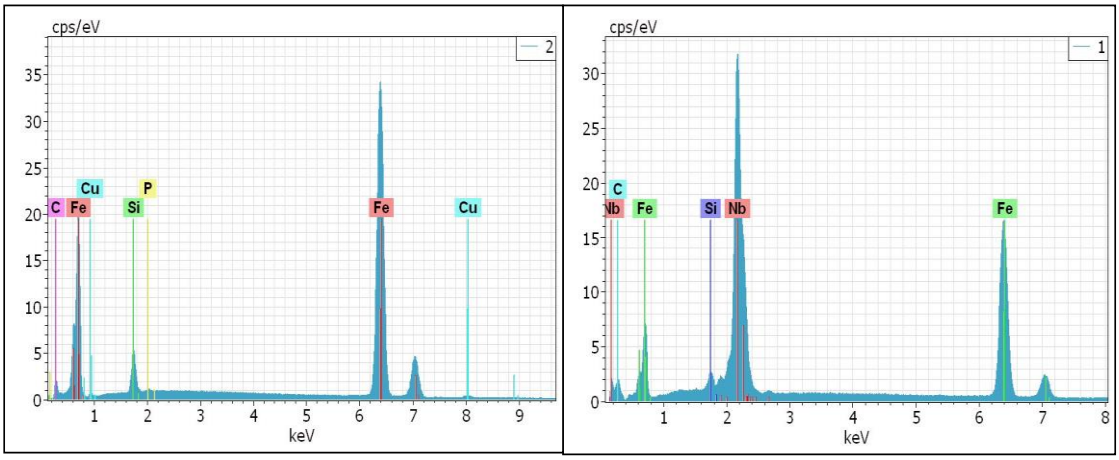

Figure 37. EDS spectrum of the points (1) and (2) in Figure 36

In Figure 36 it possible to observe the continuous effect of mechanical alloying time on the agglomerates of the niobium particles in the small gatherings: The area of agglomerate increased with increasing MA time when compared to the agglomerate area (according to the scale of SEM image) in the Figs. 34 and 35. Mechanical alloying increased the specific surface area and surface energy of niobium carbide particles and reduced the wettability in the iron matrix.

5.2.2.7 LMI experiment using powder after 240 min MA

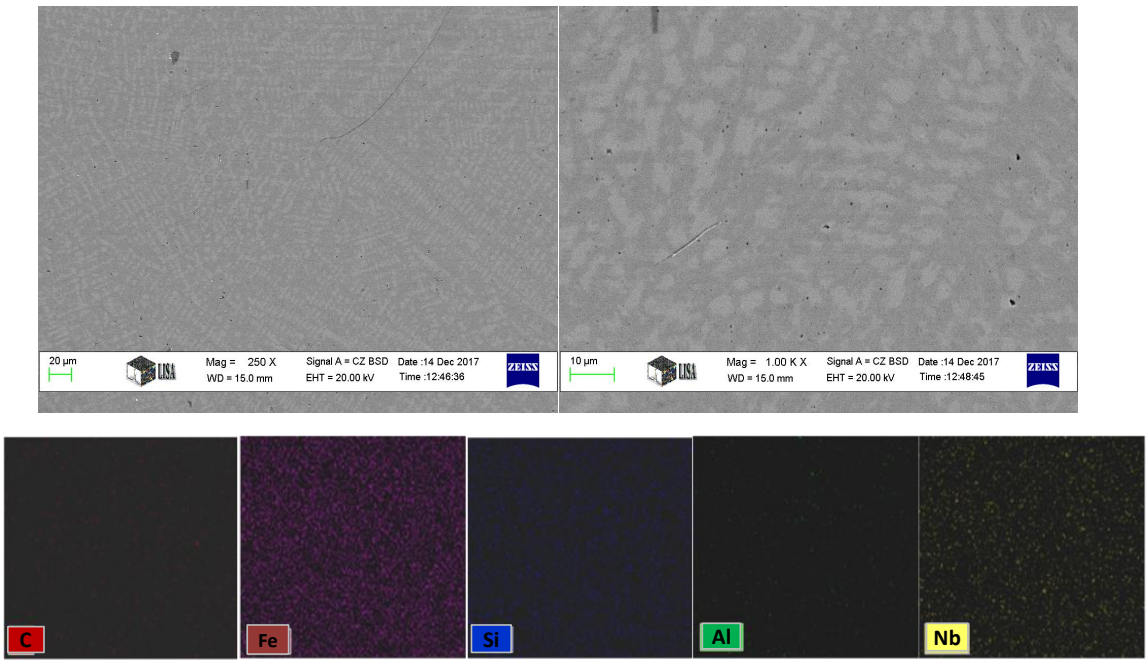

Figure 38. SEM and EDS images of the cast iron coating (iron coated NbC 85 wt% + Si 15 wt%, after 240 min MA, 2500 W laser energy, moving speed 500 mm/min)

In the SEM and EDS images Fig. 36 for experiments which use iron coated NbC+Si powder that was mechanically alloyed for 240 min, a significant difference in the microstructure of the cross section of the cast iron after the LMI process can be observed. This is due to the action of mechanical alloying on the components of the reinforcing powder for a longer time, where it dissolved homogeneously in the iron matrix without agglomeration areas of the niobium particles because of the new phases that were generated, as shown in Fig. 24 in XRD image of iron coated NbC+Si powder after MA for 240 min. The creation of a eutectic microstructure (similar to ledeburite microstructure) was also observed.

Figs. 30-38 show the effect of MA on the microstructure of the cross section of the cast iron samples after the LMI process in comparison with the diagram of the specific surface area as a function of MA time in Fig. 19, where some particles of niobium agglomerates in small gatherings were observed due to the effect of mechanical alloying time, which increased the specific surface area and surface energy of the niobium particles and reduced the wettability in the iron matrix. This effect increases with increasing MA time. The area of agglomerates of the

niobium particles in the small gatherings increase as of MA time increases for 30 min and 120 min if compared to the agglomerates areas in Figs. 34-36.

5.3 Brazing results

From the brazed cast iron samples, it can be observed that there are poor spreading results between cast iron substrates and nickel foil when using iron coated NbC+Si powder after the mechanical alloying for 240 min, as shown in Figures 39 and 40.

Figure 39. Cast iron sample after the brazing process (Ni alloy foil + iron coated NbC+Si powder without MA)

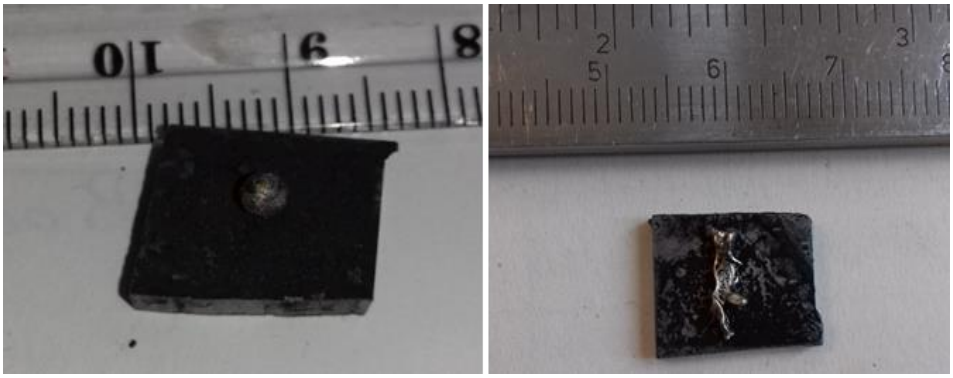

Figure 40. Cast iron samples after the brazing process (Ni alloy foil + iron coated NbC+Si) powder after MA 240 min

The probable reason is that the mechanical alloying process for iron coated NbC+Si powder causes a reduction in the spreading property of the melted metal due its increasing the specific surface area and surface energy of the powder particles and reducing the wettability.

5.4 Hardness investigation

5.4.1. Hardness investigation of the NbC powder

Hardness investigation was done on iron coated NbC powder before and after milling process to verify whether if there is an effect of milling (reduce the particles size) on hardness values.

Figure 41. Iron coated NbC powder in resin samples

Table 7. Hardness values of iron coated NbC powder

Powder	**Hardness $HV_{0.01}$**							**Average $HV_{0.01}$**
Raw NbC 1-1.2 mm	522	569	462	444	491	462	774	**579.6**
NbC ≤ 63µm (after milling in ball mill)	910	444	1208	490	496			**709.6**

From the hardness results in Table 7 the effect of milling on the hardness value of NbC particles can observed, although there was no possibility of measuring the hardness of powder after MA because the particles are too small to measure under 1µm. However, it is highly probable that the hardness will increase after the milling process (reducing the size particles) because during the milling process, the powder particles are work hardened and accumulate strain energy [146], therefore the particle hardness increases.

5.4.2 Vickers hardness investigation after the LMI process

Vickers hardness investigation was done on samples after the LMI process at horizontal and vertical direction using a raster pattern as shown in Figure 42.

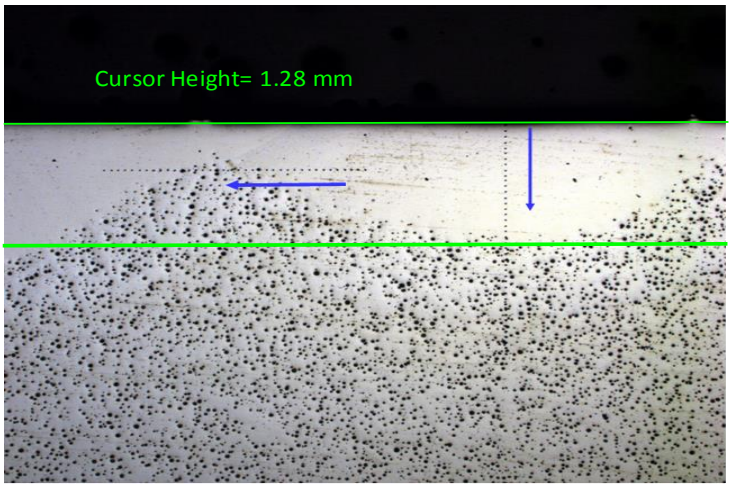

Figure 42. Hardness test after the LMI process in horizontal and vertical direction

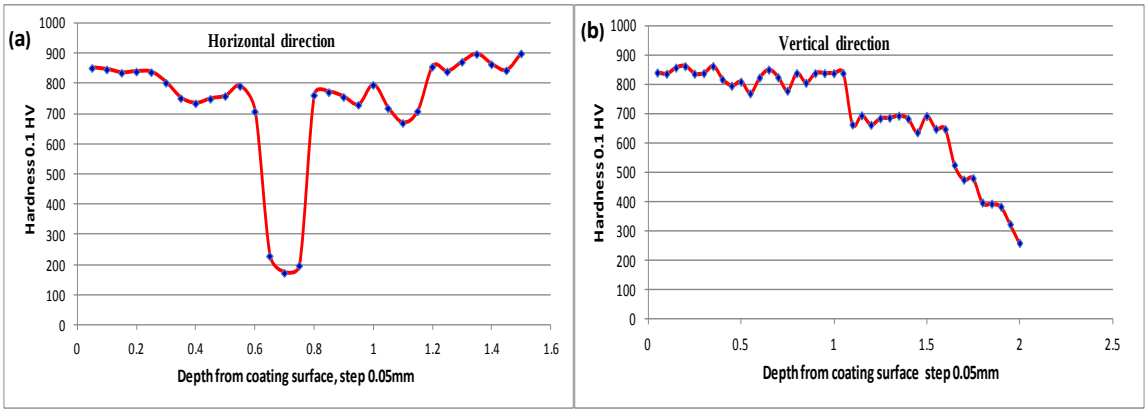

Figure 43. Hardness diagram in the (a) horizontal direction (b) vertical direction

Figure 43 (a) shows that the hardness values are relatively constant, but there is also a significant drop in the hardness value in the overlapping zone of the laser melting zone due to the aggregation of carbon particles in this area, which have low hardness. In Fig. 43 (b), it can be observed that the microhardness decreased whenever the depth from the surface of the substrate increased because the concentration of iron coated NbC+Si reinforcement powder decreased whenever the depth from the surface of the substrate increased, resulting in reduced microhardness.

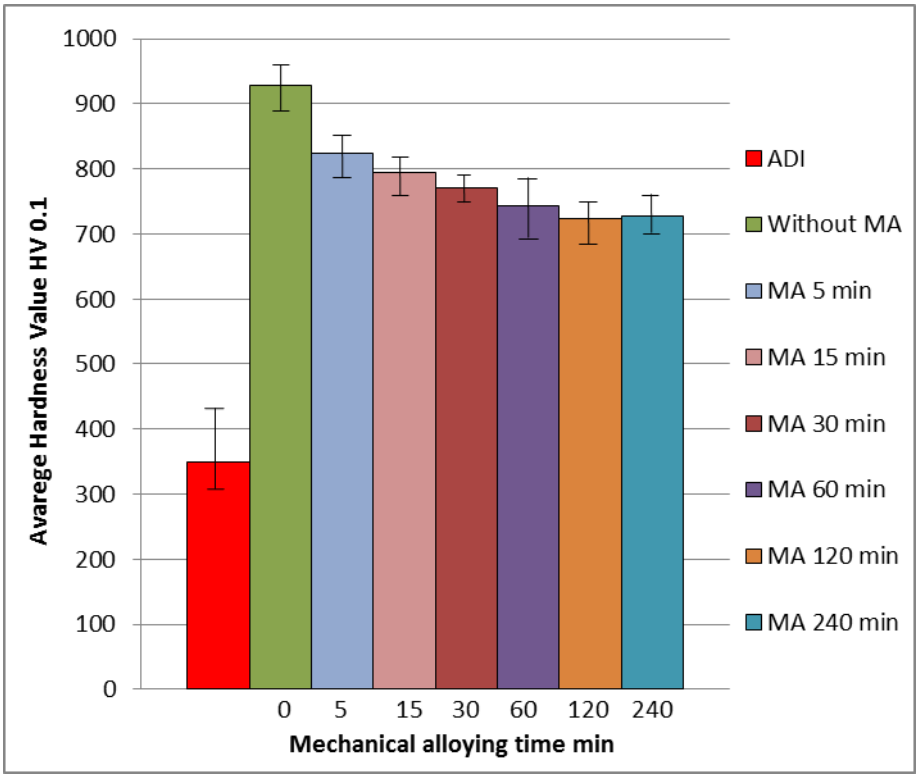

Figure 44. Diagram of the average hardness value of experiments (iron coated NbC 85 wt% + Si 15 wt%, laser energy 2500 W, moving speed 500 mm/min)

The average hardness value diagram in Figure 44 shows the difference between the average of hardness values of experiments, from a maximum value of 928 $HV_{0.1}$ to a minimum value of 777 $HV_{0.1}$, depending on the type of powder used in the laser coating and the laser properties (amount of laser energy and moving speed). The different reinforcing powder compositions have resulted in different microhardness values since the hardness of iron coated NbC+Si without MA is higher than the hardness of iron coated NbC+Si after MA. The probable reason is that the change in the observed microstructure of the iron coated NbC+Si powder after mechanical alloying affected the characteristic of diffusivity [110] and solubility [147] of powder components. SEM and EDS images show that niobium carbide tends to agglomerate in small areas and not regularly in the matrix of iron. Here it was noted that the mechanical alloying causes agglomeration of niobium carbide particles and prevents their spread regularly relatively within the melt iron matrix, which creates regions free from niobium carbide, causing low hardness in these regions.

Due to mechanical alloying, the crystalline size of the NbC particles decreases to 9±2 nm, which helps increase the solubility of the NbC precipitates in the melted iron matrix [147], therefore limiting their ability to prevent grain growth. As noted previously, it acts as an inhibitor for grain growth when it was in the micrometre size [42]. One more reason for decreases in the microhardness, as reported earlier, is that during the high-energy milling, the powders experience large mechanical deformation, so the products of MA can be compounds, composites, amorphous phases, nanocrystalline materials and metastable and/or supersaturated solid solutions. The same was observed from XRD patterns of iron coated NbC+Si powder, where the Si, Fe and Fe_2C peaks disappeared after 240 min of MA process, which has an effect on the diffusivity of Nb in the Fe and precipitation hardening. Hard and brittle Fe_3C and Nb_4C_3 precipitates disperse in the Nb matrix have a significant impact on the microhardness.

5.5 Wear resistance investigation

To select a proper method of wear resistance testing, it is necessary to accept the criteria considering service conditions and contact conditions, since the new coatings can be particularly effective.

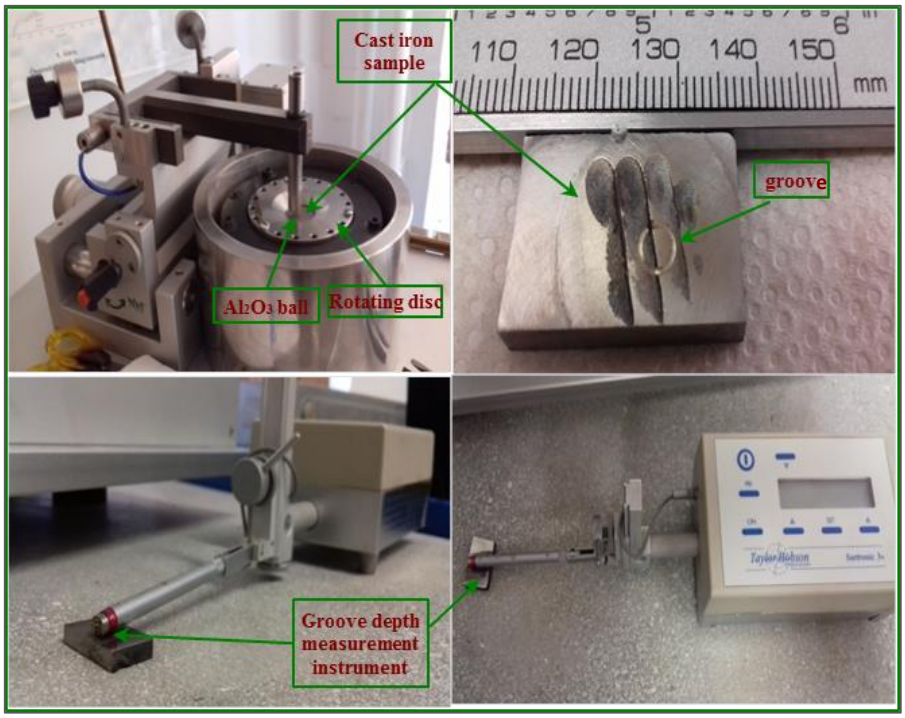

Figure 45. Wear-resistance tester instruments

It is assumed in this work that the layers alloyed with niobium carbide will show effective wear resistance in harsh conditions thanks to their high susceptibility to strain hardening, low coefficient of friction and resistance to surface degradation, thus the, wear resistance test was performed by dry sliding friction “ball on disc” as shown in Figure 45, to allow the evaluation of niobium as a modifier of the wear resistance of the cast iron covered and its influence on various mechanisms of wear.

Wear resistance properties are characterized using the mass loss of the specimen and by observing the wear scars and debris. This approximation was valid, in which the groove area generated by dry sliding an Al_2O_3 ball on the surface of the sample is calculated with the depth of the groove. Depending on these two parameters it is possible to measure the wear resistance value, where the lower value of depth and groove area means high wear resistance. The mass variation of the Al_2O_3 ball was not measured.

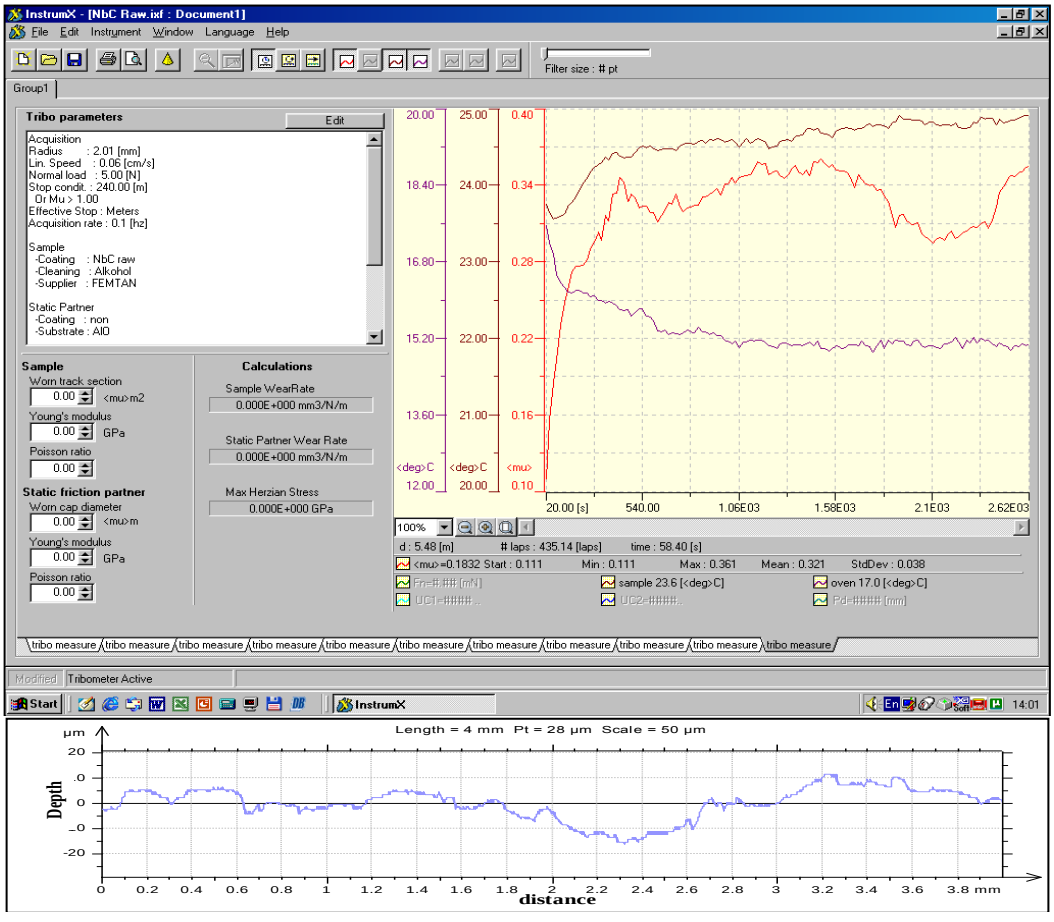

Figure 46. Friction coefficient as a function of wear test time for raw cast iron samples

Figure 46 presents the variations of the friction coefficient with the time of dry sliding wear examination for the cast iron samples before and after the LMI process with iron coated NbC+Si powder that was mechanically alloyed for different periods time (see Figs. 56-60). With specimens which used iron coated NbC+Si powder after MA for 240 min, the friction coefficient of the clad coating oscillates around 0.14, which is obviously smaller than that of the 0.30 % raw cast iron specimen, which oscillates around 0.40. With the niobium addition, the friction coefficient of the clad coating oscillates around 0.35. It can be concluded that the samples containing a clad layer produced by LMI with iron coated NbC+Si powder mechanically alloyed for different periods of time have excellent tribological performance and wear resistance under dry sliding friction against an Al_2O_3 ball wear test.

Table 8. Groove area values after wear resistance tests

LMI experiment conditions Coating powder	Groove area μm^2
Raw cast iron	9.458
NbC 85 wt% + Si 15 wt% *After MA 5 min.*	6.087
NbC 85 wt% + Si 15 wt% *After MA 15 min.*	2.046
NbC 85 wt% + Si 15 wt% *After MA 30 min.*	2.046
NbC 85 wt% + Si 15 wt% *After MA 60 min.*	2.034
NbC 85 wt% + Si 15 wt% *After MA 120 min.*	1.798
NbC 85 wt% + Si 15 wt% *After MA 240 min.*	1.289

Table 8 shows the results of the groove area values after dry sliding friction against an Al_2O_3 ball wear resistance test, where it can be observed the groove areas of the cast iron specimens decrease after the laser melt beam injection process, which means an increase in the wear resistance of samples.

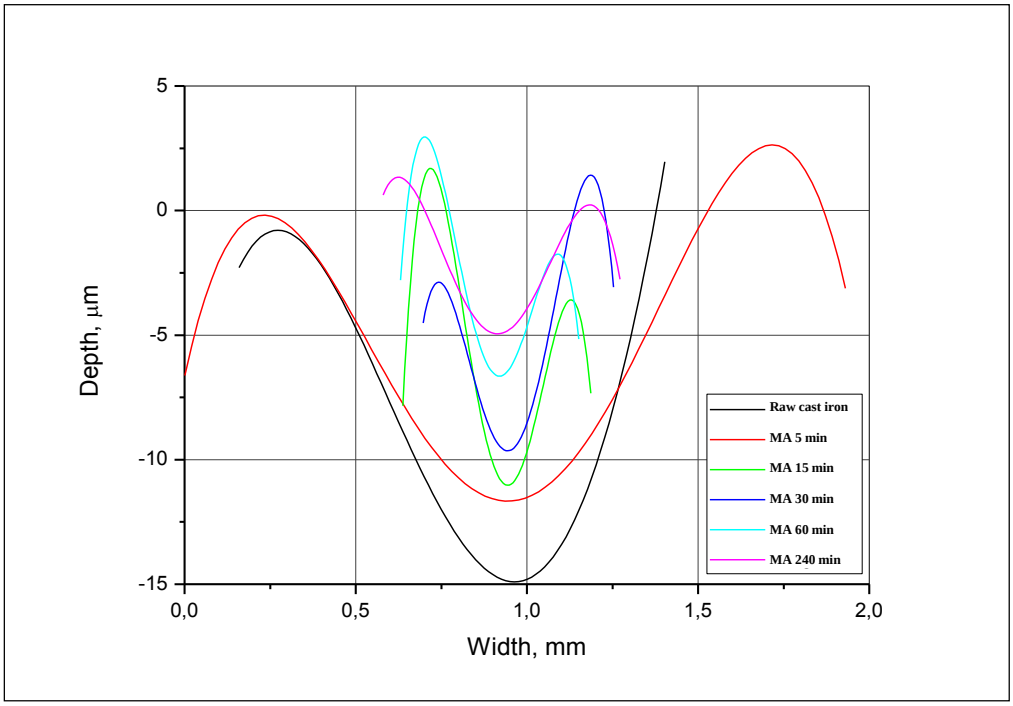

Figure 47. Average depth values of the dry sliding Al_2O_3 ball wear resistance test of castiron samples after the LMI process with iron coated NbC+Si powder

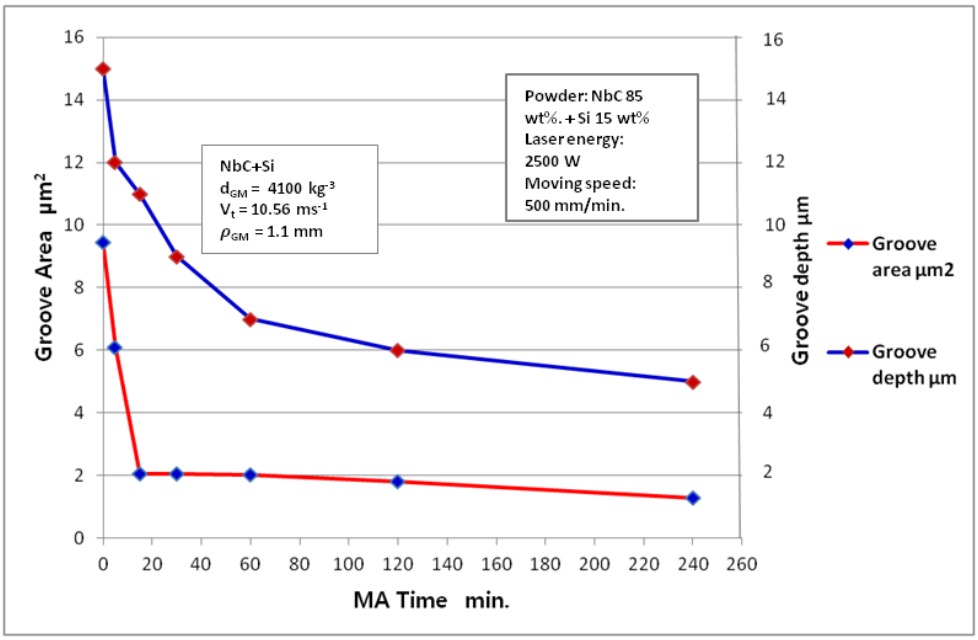

Figure 48. The groove area and depth values of the dry sliding Al_2O_3 ball on the cast iron substrate after the LMI process as a function of MA time

Figures 47 and 48 show the effect of MA time on the iron coated NbC+Si powder, which used as a reinforcing powder in the LMI process, on the groove depth values of the cast iron specimens after dry sliding friction against Al_2O_3 ball wear

resistance tests, where the depth value decreases with increasing MA time of the powder, indicating improvements in wear resistance values with the increasing mechanical alloying time of the iron coated NbC+Si powder. The dry sliding wear test results in Table 8 indicate that the wear resistance of the cast iron specimens processed by the laser melt beam injection process with iron coated NbC+Si powder is about 4.6-7.3 times higher than that of the raw cast iron specimen. Using iron coated NbC+Si powder after the MA process decreases the friction coefficient and increases the wear resistance of the cast iron that was processed by LMI. The new microstructure of the cast iron after the laser melt beam injection process becomes more uniform and finer when using iron coated NbC+Si powder after MA than used iron coated NbC+Si powder without MA as shown in Fig. 30. These novel microstructure characteristics ensure the LMI process provides an excellent wear resistance [148], especially the specimens which used iron coated NbC+Si powder after MA for 240 min, hence, the material removal rate is low as a consequence of adhesive deformation [149]. Some previous studies indicated that there was not always a positive correlation between the microhardness and wear resistance properties in all cases [60, 150] where the microstructure features can also determine the wear behaviours [148]. Accordingly, wear and friction were reduced because of grain refinement [150]. This explains the different behaviour of the microhardness with MA time of the reinforcement powder, therefore the effect of the microstructure features of powder on the LMI process is apparent, and the wear resistance has been improved under dry sliding friction against Al_2O_3 ball wear tests, So the wear resistance can be developed by changing the surface properties of solids by one or more types of surface engineering.

6 CONCLUSION

Based on all of the experimental results obtained in this work, the following conclusions could be drawn:

- The initial microhardness of iron coated NbC particles was 579.6 $HV_{0.1}$ and increased to 709.6 $HV_{0.1}$ after the milling process by planetary ball mill up to 63µm powder particle size.
- Mechanical alloying times in a stirred media mill have a significant effect on decreasing the particle size of iron coated niobium carbide and silicon at the beginning for 5 min with agglomeration at more extended milling periods of 240 min.
- An ultrafine nanocrystalline Nb-Si-Fe-C alloy with NbC powder is produced by green chemistry in stirred media milling at room temperature. During this process, the particles undergo cold welding, plastic deformation and work hardening and recovery stages. Milling time (stress number) is an influencing parameter in producing alloy powders. As the velocity reaches 1009 rpm, cold welding is the dominant mechanism during milling, and no solid solution has been observed even after milling for 240 min. The optimum milling conditions of 1009 rpm for 240 min lead to nanocrystalline Nb-Si-Fe and C alloy powder particles with a crystallite size under 9±2 nm.
- The surface hardness of cast iron increases after the laser melt beam injection process until reaching its maximum value (928-1001 $HV_{0.1}$).
- The surface hardness value depends on the type of powder used in the laser melting process and the laser parameters (amount of laser energy and laser moving speed), and the ideal conditions were found when using the iron coated NbC 85 wt% with Si 15 wt%, laser energy 2500 W and coating speed 500 mm/min. There is a regular gradient of hardness values from the surface to the bottom of the cast iron sample.

- Using mechanically alloyed iron coated NbC+Si powder results in lower hardness than non-alloyed powder for the cast iron samples processed by LMI.
- The wear resistance of cast iron surface increases during, the laser melt beam injection coating process until reach to the maximum value 7.3 times higher than the initial value.
- The wear resistance value depends on the type of powder used in the laser melting injection process, and the ideal result was found when using iron coated NbC 85 wt% with Si 15 wt%, after 240 min MA laser energy 2500 W and coating speed 500 mm/min.

7 Claims

1. Based on the scanning electron microscopy images, I established that the addition of 15 wt% of silicon powder to the 85 wt% iron coated niobium carbide powder, which was used as reinforcement powder in the laser melt beam injection process (LMI), improves the diffusivity of niobium carbide particles in the melted iron matrix and promotes particle refinement and form an fine microstructure, and changed the form of niobium particles from the polygon grains (Figure A/a) to longitudinal grains (Figure A/b), which would be under the size of 20 µm, if at all they remain dispersed in the iron matrix.

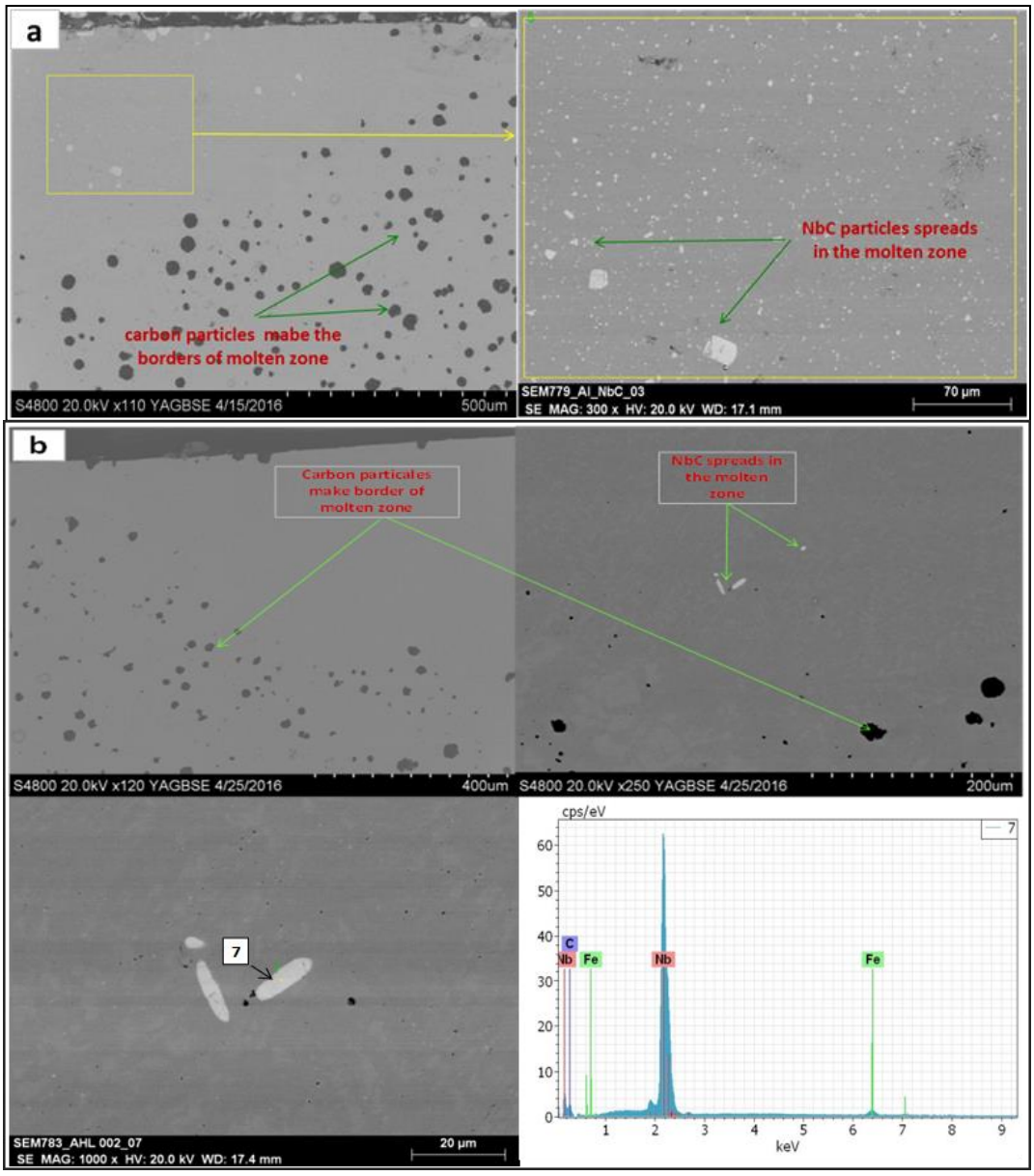

Figure A. SEM and EDS image of a cross section of cast iron samples after laser melt beam injection process (a) iron coated NbC powder (b) iron coated NbC+Si powder

2. I established that mechanical alloying (MA) of the iron coated NbC 85 wt% + Si 15 wt% powder from 5 min to 240 min improved the solubility of the powder components in the liquid iron matrix during the laser melt beam injection (LMI) process, as shown in Figure B.

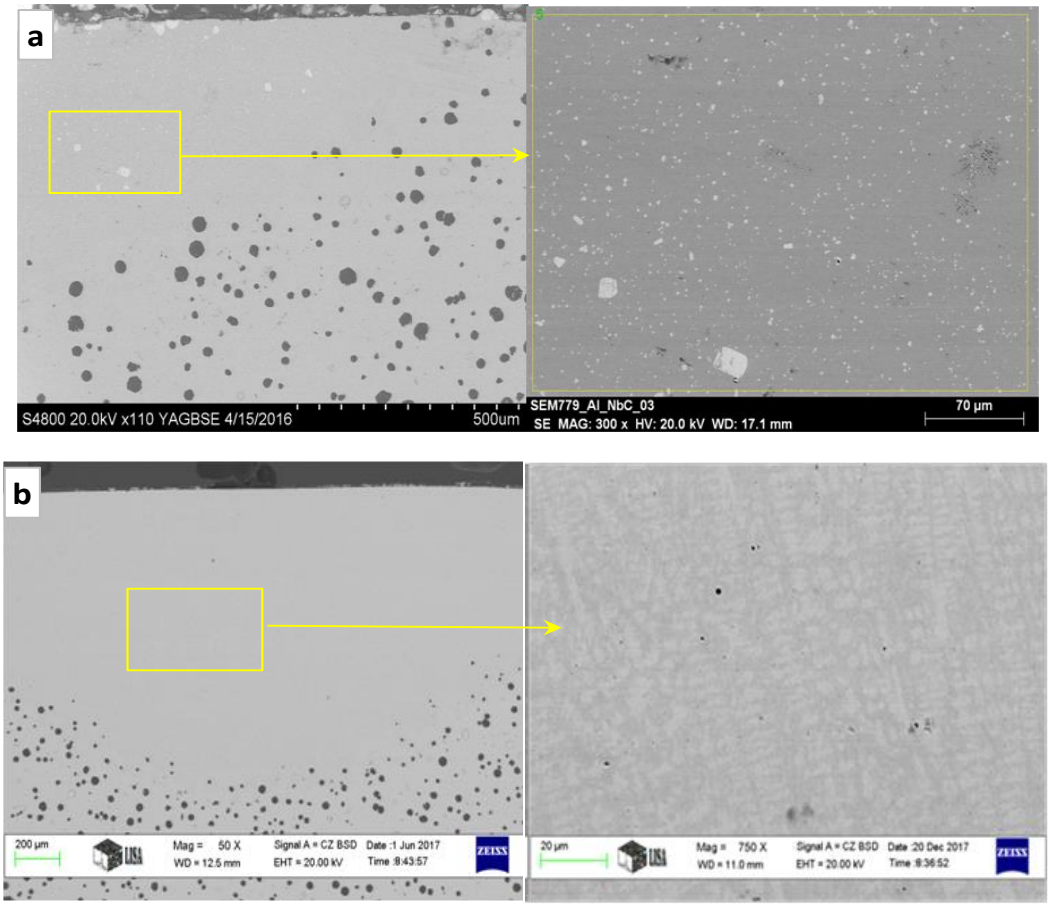

Figure B. SEM images for the cross section of cast iron samples after the LMI process (a) Iron coated NbC+Si powder without MA (b) Iron coated NbC+Si powder after MA for 240 min

3. I determined that the mechanical alloying process for iron coated NbC+Si powder causes reduce the spreading property of the melted metal due to mechanical alloying time and milling energy increasing the specific surface area and surface energy of powder particles and reducing the wettability, see Figures C and D.

Figure C. Cast iron sample after the brazing process (Ni alloy foil+ iron coated NbC+Si powder without MA)

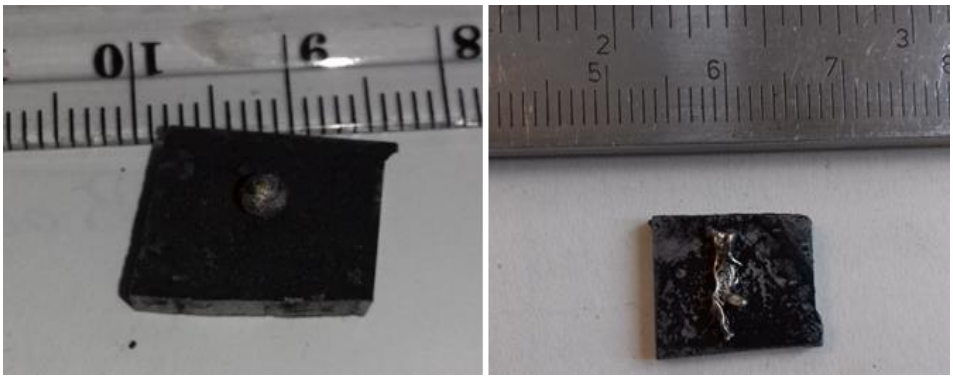

Figure D. Cast iron samples after the brazing process (Ni alloy foil + iron coated NbC+Si powder after MA)

4. I established that the increase in the mechanical alloying (MA) time and specific milling energy of iron coated NbC 85 wt% + Si 15 wt% powder, which used as reinforcing powder in the laser melt beam injection (LMI) process, caused the hardness values of the cross section of cast iron treated by LMI process to decrease, from a maximum 928 $HV_{0.1}$ to a minimum 777 $HV_{0.1}$, as shown in the Figure E. The probable reason is that due to mechanical alloying, the size of the NbC particles decreases to the nanocrystalline size, increasing the specific surface area, which helps increase the solubility of the NbC precipitates in the melted iron matrix, therefore limiting their ability to prevent grain growth. As noted previously, it acts as an inhibitor for grain growth when it was in the micrometre size. One more reason for decreases in the microhardness, as reported earlier, is that during high-energy milling (MA), the powders experience large mechanical deformation, therefore, the products of MA can be compounds, composites, amorphous phases, nanocrystalline materials and metastable and/or supersaturated

solid solutions. The same was observed from XRD patterns of iron coated NbC+Si powder, where the Si, Fe and Fe_2C peaks disappeared after 240 min of the MA process, which has an effect on the diffusivity of Nb in the Fe and precipitation hardening. Hard and brittle Fe_3C and Nb_4C_3 precipitates disperse in the NbC matrix and have a significant impact on the microhardness.

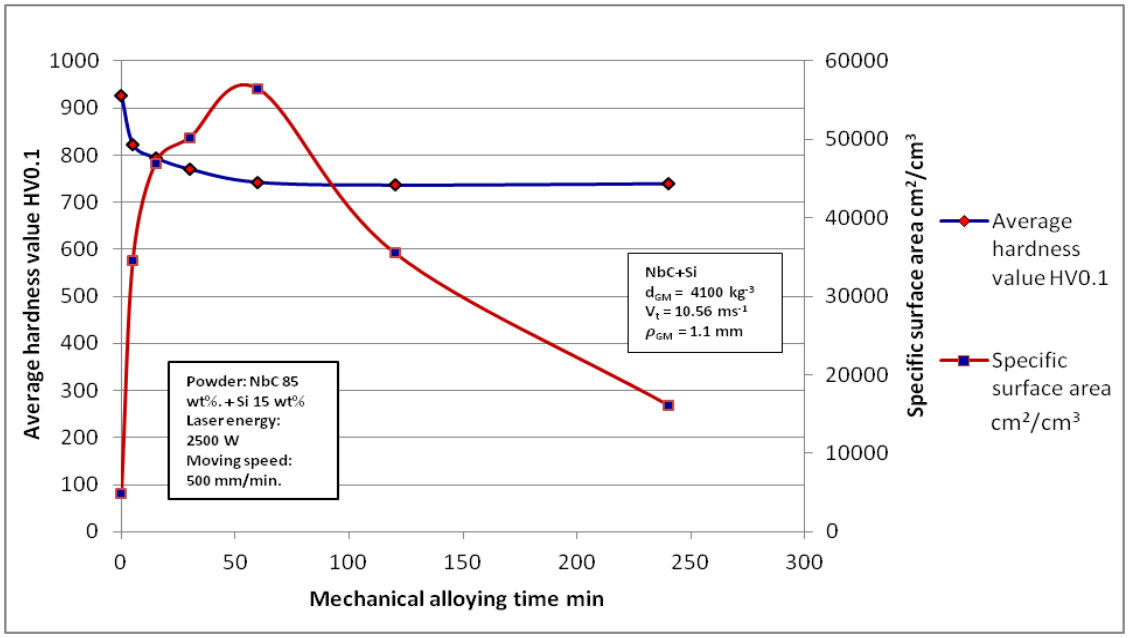

Figure E. Average hardness values of cast iron samples after the LMI process as a function of MA time and specific surface area of iron coated NbC+Si powder

5. I established that the wear resistance values of the cross section of the cast iron that was treated by the laser melt beam injection (LMI) process increases with increasing in mechanical alloying (MA) time of the iron coated NbC 85 wt%+ Si 15 wt% powder, as shown in Figure F, which shows the results of the groove area and/or groove depth values after dry sliding wear resistance tests, where the groove area decrease from 9.458 µm to 1.289 µm. The new microstructure of cast iron surface after the LMI process became more uniform and finer when using mechanically alloyed iron coated NbC+Si powder than when using iron coated NbC+Si powder without MA, especially the specimens which used iron coated NbC+Si powder after MA for 240 min as shown in Figure G. The novel microstructure characteristics ensure the laser melt beam injection process has excellent wear resistance. The microstructure features can also determine the wear

behaviours, and accordingly, wear and friction were reduced because of grain refinement. This explains the different behaviour of the microhardness with MA time of the reinforcement powder. Consequently the effect of microstructure features of iron coated NbC+Si powder on the LMI process is obvious, and the wear resistance has been improved and confirmed under dry the sliding wear test.

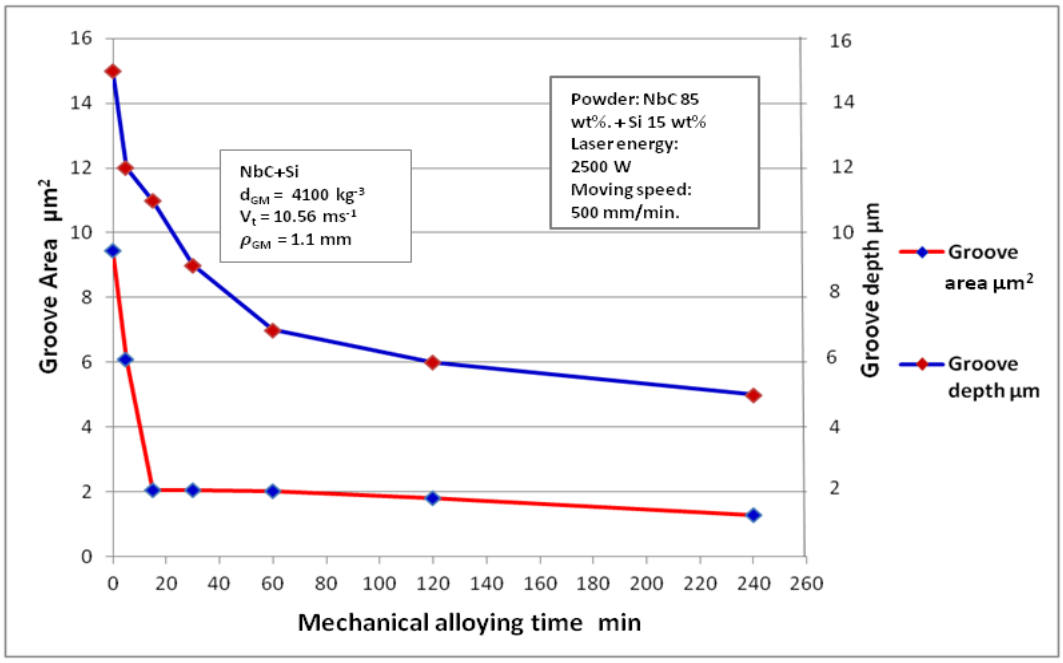

Figure F. The groove area &depth values of the dry sliding Al_2O_3 ball on the cast iron substrate after the LMI process as a function of MA time

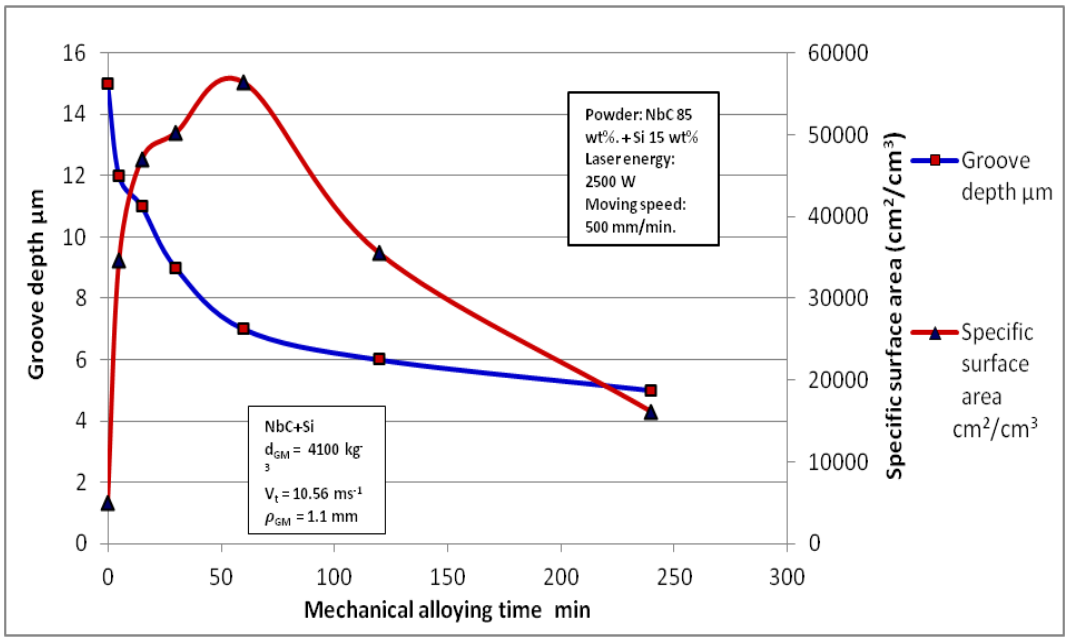

Figure G. The groove area &depth values of the dry sliding Al_2O_3 ball on the cast iron substrate after the LMI process as a function of MA time and specific surface area of iron coated NbC+Si powder

8 Publications related to this dissertation work

8.1 Scientific publication

1. Al-Azzawi Ali, Péter Baumli: Methods of composite coating: a review, Materials Science and Engineering, University of Miskolc HU ISSN 2063-6792, 40 (1) (2015) 26-32.
2. Al-Azzawi Ali, Péter Baumli, Gábor Mucsi: Mechanical Alloying and Milling. Conference paper: MultiScience-XXIX. microCAD International Multidisciplinary Scientific Conference. DOI: 10.26649/musci.2015.017.
3. H. Al-Azzawi, J. Sytchev, P. Baumli: Increasing the surface hardness of a Cast Iron Surface by Electrodeposition of Boron from Molten Salts, Arch. Metall. Mater. 62 (2017), 2B, 1015-1018
4. Al-Azzawi, Péter Baumli: Coating of 1.4404 stainless steel by a combination of brazing and nitriding. Journal of Metallurgical and Materials Engineering. 24(3) (2018) 209-218.
5. Ali Al-Azzawi, Ferenc Kristály, Ádám Rácz, Péter Baumli and Gábor Mucsi: Mechanical alloying of NbC and Si in a stirred media mill, (Accepted manuscript DOI: 10.2298/JMMB181124016A, Journal of Mining and Metallurgy Section B: Metallurgy).

8.2 Oral and Poster Presentations

1. Ali Al-Azzawi, George Kaptay, Gabor Mucsi: Preparation of nano- and microparticles with high mechanical properties, EUROMAT 2015, Warsaw, Poland, September 20-24, 2015, poster.
2. Ali Al-Azzawi, Jaroslav Sytchev, Péter Baumli: Surface Hardening of Steels, 14th International Symposium on Novel and Nano Materials (ISNNM-2016), 2016 Júl. 3-júl 8, poster.
3. Mechanical alloying of NbC and Si in a stirred media mill, A. Al-Azzawi, P. Baumli, F. Kristaly A. Racz, G. Mucsi. 9th International

Conference on Mechanochemistry and Mechanical Alloying (INCOME 2017), September 3-7, 2017, Kosice, Slovakia, poster.

4. Al-Azzawi Ali, Péter Baumli, Gábor Mucsi: Mechanical alloying and milling, MicroCAD Miskolc, 2015 április 9-10, Oral presentation, SESSIONS B: Applied materials.
5. Ali H. Hasan Al-Azzawi, Sytchev Jaroslav, Péter Baumli: Modification of a Cast Iron Surface by Electrodeposition of Boron from Molten Salts, MicroCAD 2016 április, conference, Miskolc.
6. Al-Azzawi Ali, Péter Baumli, Gábor Mucsi: Preliminary grinding experiments of Niobium carbide and silicon, MicroCAD Miskolc, 2017 April 20-21.
7. Al-Azzawi Ali, Péter Baumli: Coating of 1.4404 stainless steel by a combination of brazing and nitriding, (ISCAME 2018) October 11-12, Debrecen, poster.

9 REFERENCES

[1] Mostaed A, Mostaed E, Shokuhfar A, Saghafian H, Rezaie HR. The influence of milling time and impact force on the mutual diffusion of Al and Cu during synthesis of Al- 4.5 wt% Cu alloy via mechanical alloying. J. Defect Diffusion Forum. 283 (2009).Pp. 494-498.

[2] Hellstern E, Fecht HJ, Fu Z, Johnson WL. Structural and thermodynamic properties of heavily mechanically deformed Ru and AlRu. J. Appl. Phys, 65(1989).Pp. 305-310.

[3] Enayati MH, Aryanpour GR, Ebnonnasir A. Production of nanostructured WC-Co powder by ball milling. Int. J. Refract Metals Hard Mater, 27 (2009). Pp. 159-163.

[4] Panigrahi BB. Sintering and grain growth kinetics of ball milled nanocrystalline nickel powder. J. Mater Sci Eng A, (2007). Pp. 460-461:7-13.

[5] B.S. Murty, M. Mohan Rao, S. Ranganathan. Milling maps and amorphization during mechanical alloying. J. Acta Metallurgica et Materialia.43(1995).Pp. 2443-2450.

[6] M. Nazareth R.V. Perdigao, Jose A.R. Jordao, Claudio S. Kiminami, Walter J. Botta F. Phase transformation in Nb-16 at. %Si processed by high-energy ball milling. J. Non-Crystalline Solids. 219(1997). Pp. 170-175.

[7] K. Lu. Nanocrystalline metals crystallized from amorphous solids: nanocrystallization, structure, and properties. J. Materials Science and Engineering: R: Reports. 16(1996).Pp. 161-242

[8] Z. Peng, C. Suryanarayana, F.H. Froes. Synthesis of metastable phases in Al-Nb powders by mechanical alloying. J. Scripta Metall. Mater. 27 (1992). Pp. 475

[9] M.G Mendiratta, D.M Dimiduk. Phase relations and transformation kinetics in the high Nb region of the Nb-Si system. J. Scripta Metallurgica et Materialia.25 (1991). Pp. 237-242.

[10] M.T. Marques, V. Livramento, J.B. Correia, A. Almeida, R. Vilar. Production of copper-niobium carbide nanocomposite powders via mechanical alloying. J Materials Science and Engineering A. 399 (2005).Pp. 382-386

[11] R. Colaco, R. Vilar, Abrasive wear of metallic matrix reinforced materials. J. Wear, 255 (2003). Pp. 643-650.

[12] L. Bourithis, G.D. Papadimitriou, Synthesizing a class “M” high-speed steel on the surface of plain steel using the plasma transferred arc (PTA) alloying technique: microstructure and wear properties. J. Mater. Sci. Eng. A 361 (2003). Pp. 165-172.

[13] Q.Y. Hou, J.S. Gao, F. Zhou. Microstructure and wear characteristics of cobalt-based alloy deposited by plasma transferred arc weld surfacing. J. Surf. Coat. Technol. 194 (2005). Pp. 238-243.

[14] G. Abbas, U. Ghazanfar. Two-body abrasive wear studies of laser produced stainless steel and stainless steel + SiC composite clads. J. Wear. 258 (2005). Pp. 258-264.

[15] J. Mazumder, A. Schifferer, J. Choi. Direct materials deposition: designed mecro- and microstructure. J. Mater. Res. Innovations, 3 (1999).Pp. 118-131.

[16] R. Vilar: Laser Cladding. Journal of Laser Application.11 (1999).Pp. 64-79.

[17] R. Colac, R. Vilar. laser rapid-alloy prototyping for the development of wear-resistance Fe-Cr-C/NbC composite materials. Journal of Laser Application.15 (2003).Pp. 267-272.

[18] Hidenoriterasaki, S. Urakaw, David C. Rubie. Interfacial tension of Fe-Si liquid at high pressure, J. Physics of the Earth and Planetary Interiors. Vol. 202-203(2012).Pp. 1-6.

[19] C. Suryanarayana, E. Ivanov, V.V. Boldyrev: The science and technology of mechanical alloying. J. Materials Science and Eng., A 304-306 (2001). Pp. 151-153.

[20] P. Balaz, M. Achimovicová. Mechano-chemical leaching in hydrometallurgy of complex sulphides. J. Hydrometallurgy. 84 (2006).Pp. 60-68.

[21] HJ. Fecht, Yu. Ivanisenko: Nanostructured Materials and Composites Prepared by Solid State Processing. Book Nanostructured Materials. Processing, Properties, and Applications. 2nd (2007). Pp. 119-172

[22] P. Baláz. Extractive metallurgy of activated minerals. Elsevier, Amsterdam, 2000, Pp. 278.

[23] K. Tkácová. Mechanical activation of minerals, Elsevier, Amsterdam, (1989).Pp. 293.

[24] Suryanarayana C. mechanical alloying and milling. J. Intermetallics. 3 (1995).Pp. 153-160.

[25] A. Kwade, J. Schwedes. Wet comminution in stirred media mills. J. KONA Powder and Particle, 15 (1997). Pp. 91-101.

[26] S. Mende, F. Stenger. W. Peukert, J. Schwedes. Mechanical production and stabilization of submicron particles in stirred media mills. J. Powder Technology, 132 (2003). Pp. 64-73

[27] A. Kwade, J. Schwedes. Breaking characteristics of different materials and their effect on stress intensity and stress number in stirred media mills. J. Powder Technol. 122 (2002).Pp. 109-121.

[28] Aggarwal G, Park SJ, Smid I. Development of niobium powder injection molding. Part I: Feedstock and injection molding. Int. J. Refract Metals Hard Mater. 24(2006).Pp. 253-262.

[29] Aggarwal G, Smid I, Park SJ, German RM. Development of niobium powder injection molding. Part II: Debinding and sintering. Int. J. Refract Metals Hard Mater. 25 (2006).Pp. 226-236.

[30] Kim WY, Tanaka H, Kasama A, Hanada S. Effect of carbon on the tensile properties of Nb-Mo-W alloys at 1773 K. J. Alloys Compd. 333 (2002).Pp. 170-180.

[31] Ostermann F. Controlling carbide dispersions in niobium-base alloys. J. Less-Common Met. 25 (1971). Pp. 243-256.

[32] Zheng X, Chen SK, Li ZK, Zhang TJ, Fu J, Wang DH. Formation and evolution of secondary phases in a Nb-W-Mo-Zr-C Alloy. Chin. J. Rare Met. 35 (2009).Pp.1-5.

[33] Tan Y, Ma CL, Kasama A, Tanaka R, Yang JM. High temperature mechanical behavior of Nb-Mo-ZrC alloys. J. Mater Sci. Eng. A. 355 (2003).Pp. 260-266.

[34] Zheng X, Zhang TJ, Li ZK, Chen SK, Ding X, Yang XM, Fu J. Microstructure and properties of deposit strengthened Nb-W-Mo-Zr-C Alloy. J. Rare Metal Mater Eng. 36 (2007).Pp. 1886-1990.

[35] Bukhanovsky VV, Mamuzic I. The effect of temperature onmechanical characteristics of niobium alloys of the system Nb-W-Mo-Zr. J. Metalurgija. 42 (2003).Pp. 85-90.

[36] Bukhanovskii VV, Mamuzic I. Effect of high-temperature gas medium on the structure and mechanical characteristics of niobium alloy 10 VMTs. J. Met Sci Heat Treat. 55 (2008).Pp. 123-128.

[37] Kim WY, Tanaka H, Kim MS, Hanada S. High temperature strength and room temperature fracture toughness of Nb-Mo-Wrefractory alloys with and without carbide dispersoids. J. Mater Sci Eng A. 346 (2003) Pp. 65-74.

[38] Aggarwal G, Smid I, Park SJ, German RM. Development of niobium powder injection molding. Part II: Debinding and sintering. Int. J. Refract Metals Hard Mater. 25 (2006).Pp. 226-236.

[39] J. Mazumder, A. Schifferer: Direct materials deposition: designed macro and microstructure. J. Mater. Res. Innovations 3 (1999).Pp. 118-131.

[40] T. Takahashi, Y. Hashimoto. Preparation of dispersion-strengthened coppers with NbC and TaC by mechanical alloying. J. Mater. Trans. JIM 32 (1991).Pp. 389-397.

[41] B.R. Murphy, T.H. Courtney. Mechanochemically synthesized NbC cermets: Part I. Synthesis and structural development. J. Mater. Res. 14 (1999).Pp.4274-4284.

[42] A.G.P. Da Silva, C.P. De Souza, U.U. Gomes, F.F.P. Medeiros, C. Ciaravino, M. Roubin: A low temperature synthesized NbC as a grain growth inhibitor for WC-Co composites. J. Materials Science and Engineering A. 293 (2000). Pp. 242-246

[43] Marques, M. T., et al. XRD, XPS and SEM characterisation of Cu-NbC nanocomposite produced by mechanical alloying. J. Materials Chemistry and Physics 109.1 (2008)Pp.174-180.

[44] M.T. Marques, V. Livramento, J.B. Correia, A. Almeida, R. Vilar: Production of copper-niobium carbide nanocomposite powders via mechanical alloying. J. Materials Science and Engineering: A 399 (2005).Pp.382-386.

[45] Panigrahi BB. Sintering and grain growth kinetics of ball milled nanocrystalline nickel powder. J. Mater Sci. Eng. A 460 (2007).Pp.7-13.

[46] Groza JR, Dowding RJ: Nanoparticulate materials densification. J. Nanostruct Mater. 7(1996).Pp.749-768.

[47] Wang HT, Fang ZZ, Hwang KS, Zhang HB, Dave S. Sinter-ability of nanocrystalline tungsten powder. Int. J. Refract Metals Hard Mater. 28 (2010).Pp.312-316.

[48] Koch CC. The synthesis and structure of nanocrystalline materials produced by mechanical attrition: a review. J. Nanostructured Materials. 2 (1993) Pp.109-129.

[49] G. Cocco, G. Mulas, L. Schiffini: Mechanical Alloying Processes and Reactive Milling. J. Materials Transactions. 36 (2005) pp. 150-160

[50] A.P. Randlinski, A. Calka: The crystallization process of amorphous alloy powders prepared by ball milling. J. Mater. Sci. Eng. A134 (1991).Pp. l 376.

[51] K.S. Kumar, S.K. Mannan: High-Temperature Ordered Intermetallic Alloys, J. Mater. Res. Soc. Symp. Proc. 133 (1989).Pp. 415.

[52] A.R. Yavari and O. Drbohlav: Mechanisms of nanocrystallization of Fe- and Al-based amorphous precursors. J. Mater. Sci. Forum 225-227(1996).Pp. 305

[53] M.L. Trudeau, L. Dignard-Bailey, R. Schulz, D. Dusdault: Fabrication of nanocrystalline iron-based alloys by the mechanical crystallization of amorphous materials. J. Nanostructured Materials. 2 (1993). Pp. 361-368.

[54] A.Ye. Yermakov, Ye. Yurchikov, V.H. Barinov: Magnetic properties of amorphous powders of Y-Co alloys produced by grinding. J. Phys. Metals Metallogr. 52 (1981).Pp. 50-58.

[55] D.L. Zhang, T.B. Massalski, M.R. Paruchuri: Formation of metastable and equilibrium phase during mechanical alloying of Al and Mg powder. J. Metall. Mater. Trans. A 25 (1994). Pp. 73-79.

[56] M.N.R.V. Perdigao, J.A.R. Jordao, C.S. Kiminami, W.J. Botta: Processing Parameters On Self-Propagating High-Temperature Synthesis Of Al_2O_3-Zro_2-Nb Composites. J. Mater. Sci. 235-238 (1997).Pp. 151.

[57] Anderson M, Patwa P, Shin YC: Laser-assisted machining of Inconel 718 with an economic analysis. Int. J. Mach. Tools Manuf. 46 (2006) Pp. 1879-1891.

[58] Tavakoli S, Attia H, Vargas R, Thomson V: Laser-assisted finish turning of Inconel 718-process optimization. Proceedings of the ASME International manufacturing science and engineering conference 2009, MSEC2009. 1 (2009).Pp. 833-840.

[59] Chien W, Hou S. Investigating there cast layer formed during the laser trepan drilling of Inconel 718 using the Taguchi method. Int J. Adv. Manuf. Technol. 33(2007).Pp. 308-316.

[60] William M. Steen. Jyotirmoy Mazumder. Laser Material Processing. Book, Springer London Dordrecht Heidelberg New York, 4th (2010).Pp. 295-347.

[61] M. Alimardani, C.P.P aul, E. Toyserkani, A. Khajepour. 24 - Multiphysics modelling of laser solid freeform fabrication techniques. J. Advances in Laser Materials Processing. (2010). Pp. 765-791.

[62] E. C. Santos, M. Shiomi, K. Osakada, T. Laoui. Rapid manufacturing of metal components by laser forming. Int. J. Machine Tools and Manufacture. 46 (2006). Pp. 1459-1468.

[63] John C. Ion. Book Laser Processing of Engineering Materials Principles, Procedure and Industrial Application (2005). Pp. 296-326.

[64] Z. Dawei, T. Li, T.C. Lei. Laser cladding of Ni-Cr3C2/(Ni+Cr) composite coating. J. Surface and Coatings Technology 110 (1998).Pp. 81-85.

[65] Y.T. Pei, J.H. Ouyang, T.C. Lei, Y. Zhou. Microstructure of laser-clad SiC-(Ni alloy) composite coating. J. Materials Science and Engineering A194 (1995).Pp. 219-224.

[66] P. Di Pietro, Y.L. Yao. An investigation into characterizing and optimizing laser cutting quality - A review. Int. J. Machine Tools and Manufacture. 341(1994).Pp. 225-243.

[67] M. Zhong, W. Liu, Laser surface cladding. The state of the art and challenges. J. Mechanical Engineering Science C. 224 (2010).Pp. 1041-1060.

[68] H. Alemohammad, S. Esmaeili, E. Toyserkani. Deposition of Co-Ti alloy on mild steel substrate using laser cladding. J. Materials Science and Engineering A. 456 (2007). Pp. 156-161.

[69] R. Colaco, R. Vilar. Abrasive wear of metallic matrix reinforced materials. J Wear. 255 (2003).Pp. 643-650.

[70] Fei-Yi Hung, Zao-YouYan, Li-Hui Chen, Truan-Sheng Lui. Microstructural characteristics of PTA-overlayed NbC on pure Ti. J. Surface and Coatings Technology. 200 (2006).Pp. 6881-6887.

[71] K. Van Acker, D. Vanhoyweghen, R. Persoons, J. Vangrunderbeek. Influence of tungsten carbide particle size and distribution on the wear resistance of laser clad WC/Ni coatings. J. Wear, 258(2005).Pp. 194-202.

[72] S.W Huang, M. Samandi, M. Brandt: Abrasive wear performance and microstructure of laser clad WC/Ni layers Author links open overlay panel. J. Wear. 256 (2004).Pp. 1095-110.

[73] Q. Ming, L.C. Lim, Z.D. Chen. Laser cladding of nickel-based hardfacing alloys. J. Surface and Coatings Technology. 106 (1998). Pp. 174-182.

[74] Q. Li, T.C. Lei, W.Z. Chen: Microstructural characterization of WCp reinforced Ni-Cr-B-Si-C composite coatings. J. Surface and Coatings Technology.114 (1999) Pp. 285-291.

[75] Y.T Pei, T.C Zuo. Gradient microstructure in laser clad TiC-reinforced Ni-alloy composite coating. J. Materials Science and Engineering: A 241 (1-2) (1998).Pp. 259-263.

[76] Y.T. Pei, J.H. Ouyang, T.C. Lei, Y. Zhou: Microstructure of laser-clad SiC-(Ni alloy) composite coating. J. Materials Science and Engineering A.194 (1995). Pp. 219-224.

[77] Z. Dawei, T. Li, T.C. Lei. Laser cladding of Ni-Cr3C2/(Ni+Cr) composite coating. J. Surface and Coatings Technology 110 (1998). Pp. 81-85.

[78] D.-W. Zhang, T.C. Leib, F.-J. Lia. Laser cladding of stainless steel with Ni-Cr3C2 for improved wear performance. J. Wear.251 (2001). Pp. 1372-1376.

[79] D.-W. Zhang, T.C Lei: The microstructure and erosive-corrosive wear performance of laser-clad Ni-Cr3C2 composite coating. J. Wear.255 (2003).Pp. 129-133.

[80] Q. Li, T.C. Lei, W.Z. Chen. Microstructural characterization of laser-clad TiCp-reinforced Ni-Cr-B-Si-C composite coatings on steel. J. Surface and Coatings Technology 114 (1999). Pp. 278-284.

[81] J.H. Ouyang, Y.T. Pei, T.C. Lei, Y. Zhou. Tribological behaviour of laser-clad TiCp, composite coating. J. Wear, 185 (1995). Pp. 167-172.

[82] S. Suna, H. Fua, X. Pinga, Jian Lina, Y. Leia, W. Wub, J. Zhoub. Reinforcing behavior and microstructure evolution of NbC in laser cladded Ni45 coating. J. Applied Surface Science. 455 (2018).Pp. 160-170.

[83] Qingtang Li, Yongping Lei, Hanguang Fu. Growth Characteristics and Reinforcing Behavior of In-situ NbC_p in Laser Cladded Fe-based Composite Coating. J. Materials Science & Technology.31 (2015). Pp. 766-772.

[84] Sen Yanga, Wenjin Liua, Minlin Zhonga, Zhanjie Wangb. TiC reinforced composite coating produced by powder feeding laser cladding. J. Materials Letters. 58 (2004).Pp. 2958-2962.

[85] Ya-bin Cao, Hong-ting Ren, Chao-shuai Hu, Qing-xin Meng, Qing Liu. In-situ formation behavior of NbC-reinforced Fe based laser cladding coatings. J. Materials Letters. 147(2015).Pp. 61-63.

[86] Ya-bin Cao, Shi-xin Zhi, Qi Gao, Xin-tao Tian, Tao Geng, Xin Guan, Cha Qin. Formation behavior of in-situ NbC in Fe-based laser cladding coatings. J. Materials Characterization.119 (2016).Pp. 159-165.

[87] Kaptay Gy. Interfacial Phenomena during Melt Processing of Ceramic Particle-Reinforced Metal Matrix Composites. Part I. Introduction (incorporation) of solid particles into melts. J. Materials Science Forum.215-216, (1996). Pp. 459-466.

[88] Kaptay Gy. Kerámiával erősített fémmátrixú kompozitok gyártásának határfelületi vonatkozásai I.A határfelületi kritériumok levezetése (Interfacial aspects of producing MMCs. Part I/1. Derivation of interfacial criteria) (in Hungarian). BKL. Kohászat. 130 (5-6), (1997). Pp. 201-208.

[89] Jano V. Buza G. Kalazi Z. Diszperz eloszlású.fémmatrixú kerámia kompozitréteg létrehozása lézersugaras felületkezeléssel (Formation of a dispersedly distributed metal matrix ceramic composite coating by laser surface treatment). Bányászati és KohászatiLapok. 138 (3), (2005). Pp. 39-44.

[90] O. Verezub, Z. Kálazi, G. Buza, N. V. Verezub, G. Kaptay. In-situ synthesis of a carbide reinforced steel matrix surface nanocomposite by laser melt injection technology and subsequent heat treatment. J. Surface & Coatings Technology. 203 (2009). Pp. 3049-3057.

[91] Pe, Y. T. Ocelik, V. De Hosson, J. T. M.: $SiCp/Ti_6A_{l4}V$ functionally graded materials produced by laser melt injection. J. Acta Materialia.50, (2002).Pp. 2035-2051.

[92] Mridha, S. Baker, T. N. Incorporation of 3μm SiCp into Titanium surfaces using a 2.8kW laser beam of 186 and 373 MJm−2 energy densities in a nitrogen environment. J. Materials Processing Technology.185 (2007).Pp. 38-45.

[93] Vreeling, J. A. Ocelik, V. Hosson, J. T. M. De. Ti-6Al-4V strengthened by laser melt injection of WCp particles. J. Acta Materialia. 50(2002). Pp. 4913-4924

[94] F. Chen, Y. Liu, D. Li, F. L. WCp/Ti-6Al-4V graded metal matrix composites layer produced by laser melt injection. J. Surface & Coatings Technology. 202 (2008).Pp. 4780-4787.

[95] Agarwal, A. Dahotre, N. B. Laser surface engineering of steel for hard refractory ceramic composite coating. Int. J. Refractory Metals & Hard Materials. 17 (1999).Pp. 283-293.

[96] Liu D, Li L, Li F, Chen Y. WCp/Fe metal matrix composites produced by laser melt injection. J. Surface & Coatings Technology. 202(2008).Pp. 1771-1777.

[97] Nascimento, A. M. Docelik, V. Ierardi, M. C. F. Hosson, J. T. M. De: Wear resistance of WCp/Duplex Stainless Steel metal matrix composite layers prepared by laser melt injection. J. Surface & Coatings Technology. 202 (2008). Pp. 4758-4765.

[98] Lima JC, Jerônimo AR, Gomez A, Souza SM, Trichês DM, Campos CEM, Grandi TA, Kycia S. Structural investigation of an amorphous $Si_{24}Nb_{76}$ alloy produced by mechanical alloying using reverse Monte Carlo simulations. J. Non-Cryst. Solids. 354(2008). Pp. 4598-4602.

[99] Lima JC, Almeida TO, Jerônimo AR, Souza SM, Campos CEM, Grandi TA. Reverse montecarlo simulations of an amorphous Cr_25Nb_{75} alloy produced by mechanical alloying. J. Non-Cryst Solids. 352 (2009), Pp. 109-150.

[100] Rock C, Qiu J, Okazaki K. Electro-discharge consolidation of nanocrystalline Nb-Al powders produced by mechanical alloying. J. Mater Sci. 33 (1998). Pp. 241-260.

[101] Wang XL, Zhang KF. Mechanical alloying, microstructure and properties of Nb-16Si alloy. J. Alloys Compd. 490(2010). Pp. 677-683.

[102] M. Krasnowski, T. Kulik, Nanocrystalline Al-Fe intermetallics light weight alloys with high hardness. J. Intermetallics.18 (2010). Pp. 47-50.

[103] M.M. Verdian, Fabrication of supersaturated NiTi(Al) alloys by mechanical alloying. J. Mater. Manuf. Processes. 25 (2010).Pp.1437-1439.

[104] R. Yazdi, S.F. Kashani, Formation of TiN/TiB2/TiAl nanocomposite by mechanical alloying of a powder mixture of Ti-Al-BN, Int. J. Modern Phys.: Confer. Series 5 (2012). Pp. 581-588.

[105] T.T. Sasaki, T. Ohkubo, K. Hono, Microstructure and mechanical properties of bulk nanocrystalline Al-Fe alloy processed by mechanical alloying and spark plasma sintering .J. Acta Mater. 57 (2009).Pp.3529-3538.

[106] K.A. Yazovskikh, S.F. Lomayeva. Mechanosynthesis of Fe-NbC nanocomposite. J. Alloys and Compounds. 586 (2014).Pp. 65-67.

[107] M. Woydt, A. Skopp, I. Dörfel, K. Witke. Wear engineering oxides/anti-wear oxides. J. Wear. 218 (1999). Pp. 84-95.

[108] M. Woydt, H. Mohrbacher. Friction and wear of binderless niobium carbide. J. Wear. 306 (2013).Pp. 126-130.

[109] Bin Kong, Lina Jia, Hu Zhang, Jiangbo Sha, Songxin Shi, Kai Guan. Microstructure, mechanical properties and fracture behavior of Nb with minor Si. addition. Int. J. Refractory Metals and Hard Materials. 58 (2016). Pp. 84-91.

[110] Kao, C. R., J. Woodford, Y. A. Chang. A mechanism for reactive diffusion between Si single crystal and NbC powder compact. Journal of materials research 11. 4 (1996).Pp. 850-854.

[111] S. Kurokawa, J. E. Ruzzante, A. M. Hey & F. Dyment. Diffusion of Nb in Fe and Fe alloys. J. Metal Science. 17 (1983). Pp. 433-438.

[112] Y. S. Tian, C. Z. Chen, S. T. Li, and Q. H. Huo. Research progress on laser surface modification of titanium alloys. J. Appl. Surf. Sci. V 242 (2005). Pp. 177-184.

[113] Koch CC. The synthesis and structure of nanocrystalline materials produced by mechanical attrition: a review. J. Nanostruct. Mater. 2 (1993).Pp.109-129.

[114] J. R. Keough and K. L. Hayrynen. Designing with Austempered Ductile Iron (ADI); Applied Process Inc. Technologies Division, Livonia, MI. AFS Proceedings USA. (2010). Pp. 100-129.

[115] H.O. Pierson. Handbook of Refractory Carbides and Nitrides, Properties Characteristics, Processing and Applications, Noyes Publications, New Jersey, 1996.

[116] S.Y. Zhang. Titanium carbonitride-based cermets: processes and properties. J. Mater. Sci. Eng. A 163 (1993).Pp. 141-148.

[117] S.G. Huang, O. Van der Biest, L. Li, J. Vleugels. Properties of NbC-Co cermets obtained by spark plasma sintering. J. Mater. Lett. 61 (2007).Pp. 574-577.

[118] A.G.P. Da Silva, C.P. De Souza, U.U. Gomes, F.F.P. Medeiros, C. Ciaravino, M. Roubin. A low temperature synthesized NbC as grain growth inhibitor for WC-Co composites. J. Mater. Sci. Eng. A 293 (2000).Pp. 242-246.

[119] Dai-hong XIAO. Yue-hui HE, Wei-hong LUO, Min SONG: Effect of VC and NbC additions on microstructure and properties of ultrafine WC-10Co cemented carbides. J. Transactions of Nonferrous Metals Society of China. V 19, Issue 6, (2009). Pp. 1520-1525

[120] J. Wang, Y. Liu, Y. Feng, J. Ye, M.J. Tu. Effect of NbC on the microstructure and sinterability of Ti(C0.7, N0.3)-based cermets. Int. J. Refract. Met. Hard Mater. 27 (2009).Pp. 549-551.

[121] H. Mohrbacher, Q. Zhai. Niobium alloying in grey cast iron for vehicle brake discs, in: Proceedings of Materials Science&Technology Conference, October 16-20, 2011, Columbus, OHIO, ASMInt. Pp. 434-445.

[122] M. Woydt, H. Mohrbacher: The tribological and mechanical properties of niobium carbides (NbC) bonded with cobalt or Fe_3Al. J. Wear. 321(2014).Pp. 1-7

[123] J.P. Guha, D. Kolar. Systems of niobium monocarbide with transition metals. J. Less-Common Met. 29 (1972).Pp. 33-40.

[124] M. Woydt, H. Mohrbacher, J. Vleugels, S. Huang.Niobium carbide for wear protection - tailoring its properties by processing and stoichiometry. Int. J. Metal Powder Report. 71. (2016).Pp. 265-272.

[125] J.K Rath. Low temperature polycrystalline silicon: a review on deposition, physical properties and solar cell applications. J. Solar Energy Materials and Solar Cells.76 (2003). Pp. 431-487.

[126] X.L. Wang, G.F. Wang, K.F. Zhang, Effect of mechanical alloying on microstructure and mechanical properties of hot-pressed Nb-16Si alloys. J. Materials Science and Engineering A 527 (2010). Pp. 3253-3258.

[127] A. Kwade, J. Schwedes: Handbook of Powder Technology 12, Chapter 6 Wet Grinding in Stirred Media Mills. (2007). Pp. 253-254.

[128] T.L. Kirk, A review of scanning electron microscopy in near-field emission mode. J. Advances in imaging and electron Physics. (2016). Pp. 247-326.

[129] Juhász A. Z, Opoczky L.: Mechanichemistry and agglomeration (Mechanokémia és agglomeráció). Építőanyag, 55-3, Szilikátipari Tudományos Egyesület, Budapest, 2003.(In Hungarian).

[130] D.Z. Zhang, M.L. Qin, Rafi-ud-din, L. Zhang, X.H. Qu: Fabrication and characterization of nanocrystalline Nb-W-Mo-Zr alloy powder by ball milling. Int. Journal of Refractory Metals and Hard Materials. 32 (2012).Pp. 45-50.

[131] Benjamin JS, Volin TE: The mechanism of mechanical alloying. J. Metall Trans (1974).Pp. 34.

[132] Suryanarayana C, Klassen T, Ivanov E.: Synthesis of nanocomposites and amorphous alloys by mechanical alloying. J. Mater Sci. (2011).Pp. 15.

[133] Li Lu, M.O. Lai: Formation of new materials in the solid state by mechanical alloying. J. Mater Des (1995).Pp. 33-39.

[134] Weeber AW, Bakker H. Amorphization by ball milling. A review. J. Physica B (1988). Pp. 93-135.

[135] Razavi Tousi SS, Yazdani Rad R, Salahi E, Mobasherpour I, Razavi M. Production of Al-20 wt.% Al_2O_3 composite powder using high energy milling. J. Powder Technol. 192 (2009).Pp. 346-351.

[136] Fogagnolo JB, Robert MH, Ruiz-Navas EM, Torralba JM. 6061 Al reinforced with zirconium diboride particles processed by conventional powder metallurgy and mechanical alloying. J. Mater Sci, 39(2004).Pp.127-132.

[137] Leon L. Shaw. Processing nanostructured materials: An overview. Journal of The Minerals, Metals& Materials Society (TMS). V 52 (2000).Pp. 41-45

[138] N. Al-Aqeeli, N. Saheb, T. Laoui, and K. Mohammad. The Synthesis of Nanostructured WC-Based Hardmetals Using Mechanical Alloying and Their Direct Consolidation. Journal of Nanomaterials. (2014).Pp. 16.

[139] K.S. Chan.A computational approach to designing ductile Nb-Ti-Cr-Al solid-solution alloys. J. Metall. Mater. Trans. A 32 (10) (2001).Pp. 2475.

[140] S.G. Huang, J. Vleugels, H.Mohrbacher: Stainless steel bonded NbC matrix cermets using a submicron NbC starting powder. Int. Journal of Refractory Metals and Hard Materials. 63 (2017). Pp. 26-31.

[141] X.B. Liu, X.J. Meng, H.Q. Liu, G.L. Shi, S.H. Wu, C.F. Sun, M.D. Wang, L.H. Qi: Development and characterization of laser clad high temperature self-lubricating wear resistance composite coatings on Ti-6Al-4V alloy. J. Mater. Des. 55 (2014).Pp. 404-409.

[142] M.S. Yang, X.B. Liu, J.W. Fan: Microstructure and wear behaviors of laser clad Ni/ Cr3C2-WS2 high temperature self-lubricant wear-resistance composite coating. J. Appl. Surf. Sci. 258 (2012).Pp.3757-3762.

[143] John R. Keough, PE, Kathy L. Hayrynen, Ph.D. Automotive Applications of Austempered Ductile Iron (ADI): A Critical Review: Applied Process Inc. Technologies Div.- Livonia, Michigan, USA. (2000) .Pp. 1-12.

[144] Ping Shen, Lifeng Zhang, Hao Zhou, Ying Ren, Yi Wang.Wettability between Fe-Al alloy and sintered MgO.Journal of Ceramics International.Volume 43, Issue 10, (2017).Pp. 7674-7681.

[145] S. Panneerselvam, S. K. Putatundaa, R. Gundlach, J. Boileau. Influence of intercritical austempering on the microstructure and mechanical properties of austempered ductile cast iron (ADI), J. Materials Science & Engineering A 694 (2017).Pp.72-80.

[146] C. Suryanarayana, T. Klassen, E. Ivanov. Synthesis of nanocomposites and amorphous alloys by mechanical alloying. J. Materials Science. 46(2011).Pp 6301-6315.

[147] G. Kaptay: On the size and shape dependence of the solubility of nanoparticles in solutions. Int. J. Pharmaceutics. 430 (2012). Pp. 253-257.

[148] S. Huang, D. Sun, W. Wang, H. Xu: Microstructures and properties of in-situ TiC particles reinforced Ni-based composite coatings prepared by plasma spray welding. J. Ceram.Int.41 (2015). Pp. 12202-21221.

[149] Sarka Houdkova, E. Smazalova, M. Vostrak, J. Schubert: Properties of NiCrBSi coating, as sprayed and remelted by different technologies. J. Surf. Coat. Technol. 253 (2014).Pp. 14-26.

[150] A. Khalili, M. Goodarzi, M. Mojtahedi, M.J. Torkamany: Solidification microstructure of in-situ laser-synthesized Fe-TiC hard coating. J. Surf. Coat.Technol. 307 (2016). Pp. 747-775.

[151] Agarwal, Akash, and Mani Bhushan. Synthesis of Iron Oxide Pigment by Planetary Milling. PhD. diss., 2015.

[152] Gábor Mucsi, Ádám Rácz, Viktor Mádai: Mechanical activation of cement in a stirred media mill. J. Powder Technology. 235 (2013).Pp. 163-172.

10 APPENDIX

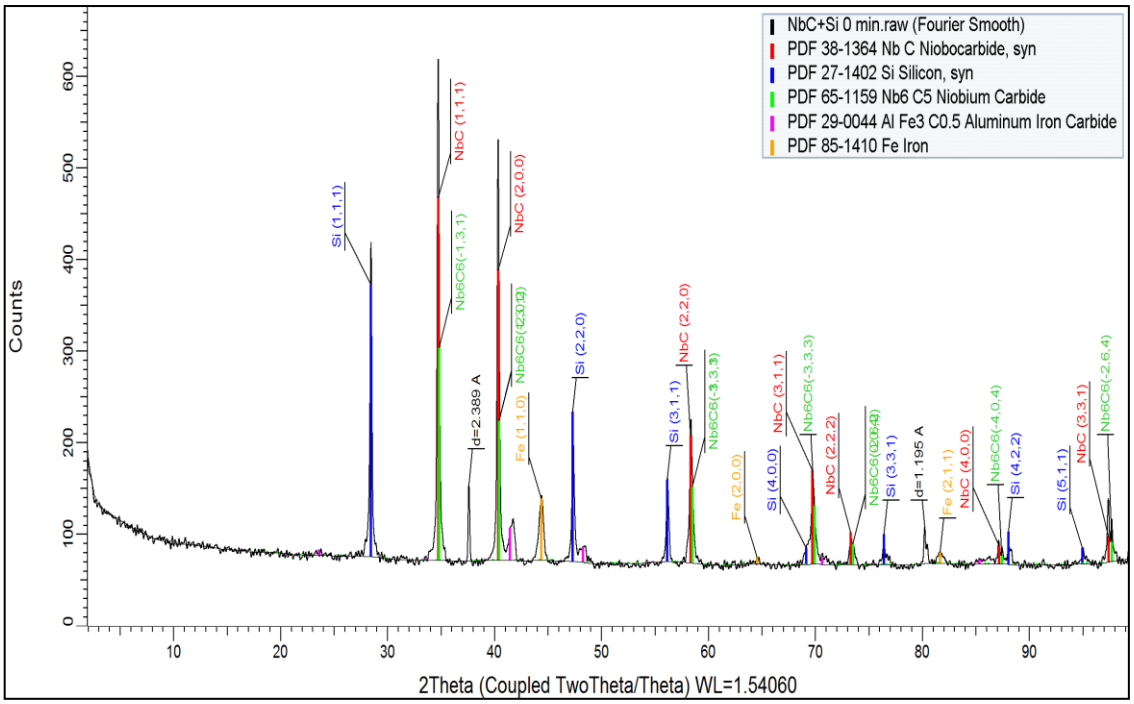

Figure 49. XRD image of iron coated NbC+Si powder before mechanical alloying

Table 9. Components intensity of XRD image in Figure 49

(NbC+Si) Powder before MA	Left Angle	Right Angle	Net Height	Net Area
Si (111)	27.251	29.505	18.70	3.673
NbC (111)	33.429	36.062	30.30	6.746
Nb_5C_6 (-131)				
NbC (200)	39.658	41.221	28.10	5.086
Nb_5C_6 (202)				
Fe (110)	43.525	45.409	4.95	1.469
Si (220)	46.536	47.878	8.89	1.737
Si (311)	55.291	57.010	7.59	1.457
NbC (220)	57.446	59.322	12.50	2.183

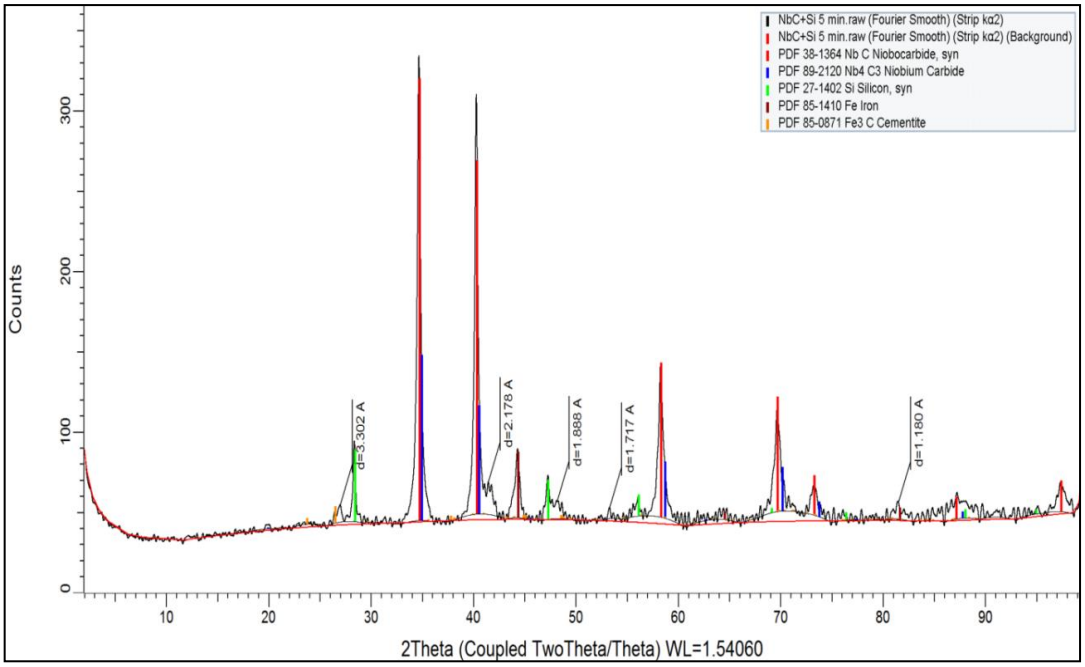

Figure 50. XRD image of iron coated NbC+Si powder after MA for 5 min

Table 10. Components intensity of XRD image in Figure 50

(NbC+Si) 5 min	Left Angle	Right Angle	Net Height	Net Area
Si (111)	27.251	29.505	6.63	1.733
NbC (111)	33.479	36.062	20.70	10.520
Nb_4C_3 (111)				
NbC (200)	39.173	41.107	18.60	6.751
Nb_4C_3 (200)				
Fe (110)	43.525	45.409	5.48	1.968
Si (220)	46.536	47.878	3.42	0.8351
NbC (220)	57.446	59.322	10.30	5.305
Nb_4C_3 (220)				

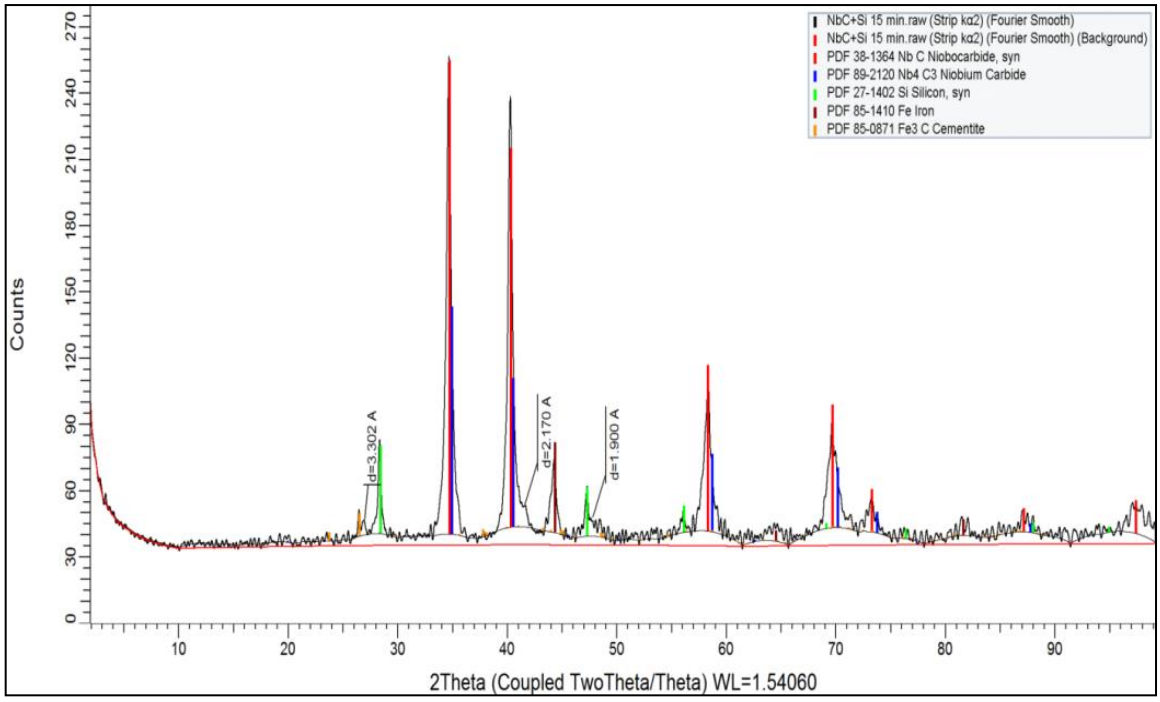

Figure 51. XRD image of iron coated NbC+Si powder after MA for 15 min

Table 11. Components intensity of XRD image in Figure 51

(NbC+Si) 15 min	Left Angle	Right Angle	Net Height	Net Area
Si (111)	27.251	29.505	5.17	2.523
NbC (111)	33.479	36.062	22.70	13.240
Nb_4C_3 (111)				
NbC (200)	39.173	41.164	14.10	6.978
Nb_4C_3 (200)				
Fe (110)	43.418	45.409	3.38	1.540
Si (220)	46.536	47.878	2.90	0.274
Si (311)	55.291	57.010	2.04	0.270
NbC (220)	57.331	59.322	6.43	3.269
Nb_4C_3 (220)				

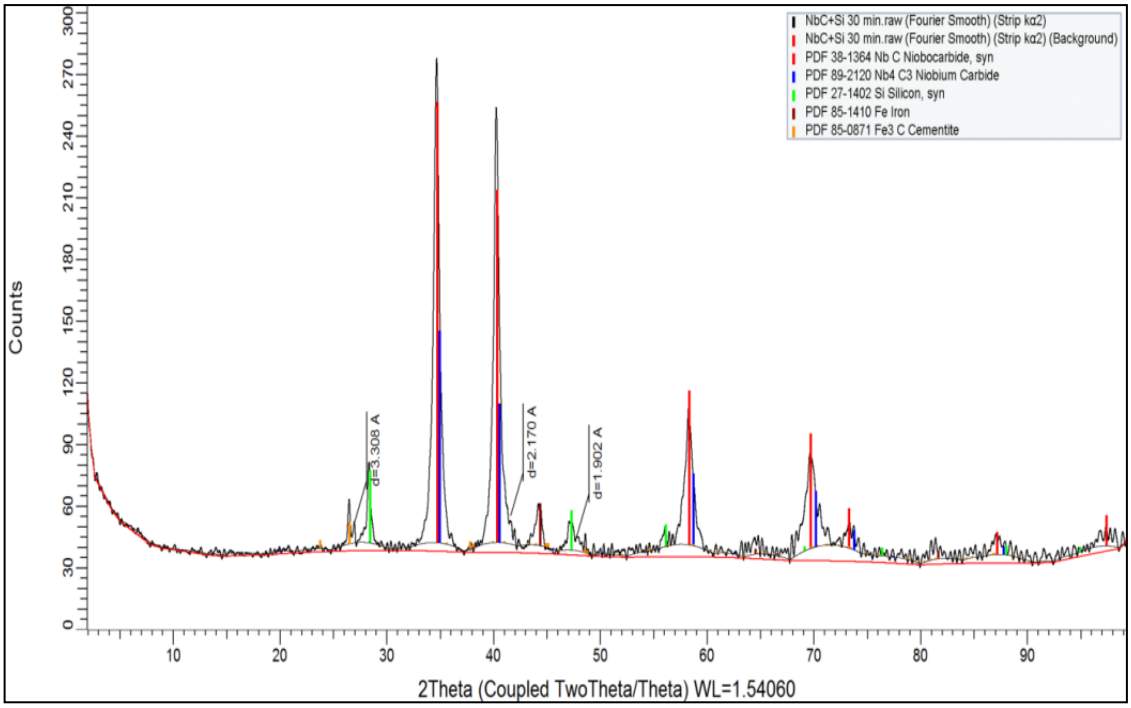

Figure 52. XRD image of iron coated NbC+Si powder after MA for 30 min

Table 12. Components intensity of XRD image in Figure 52.

(NbC+Si) 30 min	Left Angle	Right Angle	Net Height	Net Area
Si (111)	27.786	29.505	5.96	1.093
NbC (111)	33.429	36.062	25.10	17.870
Nb_4C_3 (111)				
NbC (200)	39.173	41.542	20.90	14.330
Nb_4C_3 (200)				
Fe (110)	43.368	45.409	3.76	1.730
Si (220)	46.536	47.878	2.52	0.806
Si (311)	55.291	57.01	2.22	0.443
NbC (220)	57.224	59.322	6.37	4.889
Nb_4C_3 (220)				

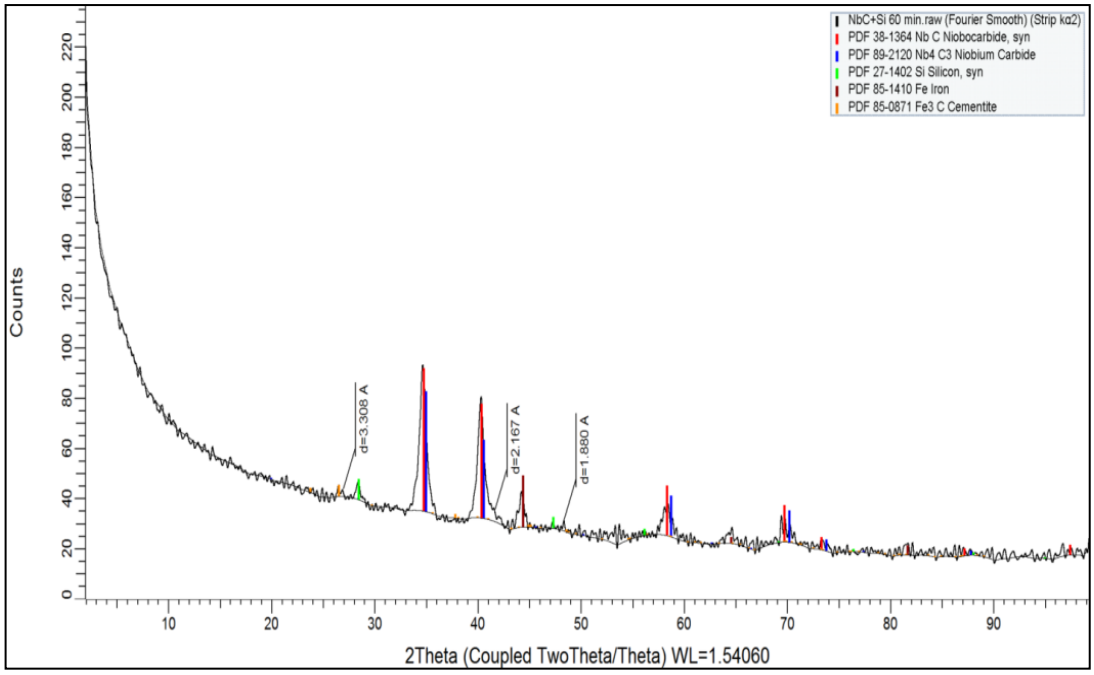

Figure 53. XRD image of iron coated NbC+Si powder after MA for 60 min

Table 13. Components intensity of XRD image in Figure 53

(NbC+Si) 60 min	Left Angle	Right Angle	Net Height	Net Area
Si (111)	27.786	29.505	2.13	0.723
NbC (111)	33.265	35.841	5.85	3.280
Nb_4C_3 (111)				
NbC (200)	39.173	41.428	4.42	2.467
Nb_4C_3 (200)				
Fe (110)	43.311	45.409	2.30	0.831
Si (220)	46.536	47.878	1.44	0.132
Si (311)	55.291	57.010	1.29	0.150
NbC (220)	57.224	59.001	2.08	0.529
Nb_4C_3 (220)				

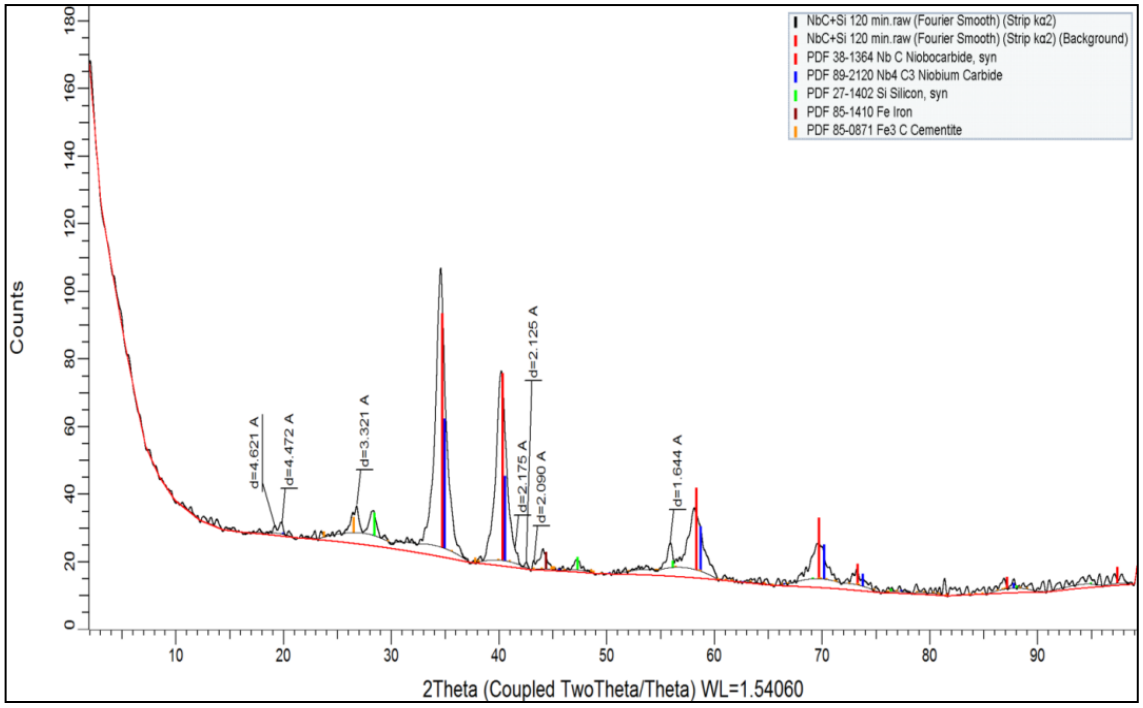

Figure 54. XRD image of iron coated NbC+Si powder after MA for 120 min

Table 14. Components intensity of XRD image in Figure 54

(NbC+Si) 120 min	Left Angle	Right Angle	Net Height	Net Area
Si (111)	27.736	29.505	1.65	0.572
NbC (111)	33.051	36.326	9.62	9.157
Nb_4C_3 (111)				
NbC (200)	39.066	41.428	6.36	5.130
Nb_4C_3 (200)				
Fe (110)	43.311	45.409	1.47	0.393
Si (220)	46.536	47.985	1.16	0.218
Si (311)	55.291	57.010	1.35	0.314
NbC (220)	57.224	59.265	2.56	1.670
Nb_4C_3 (220)				

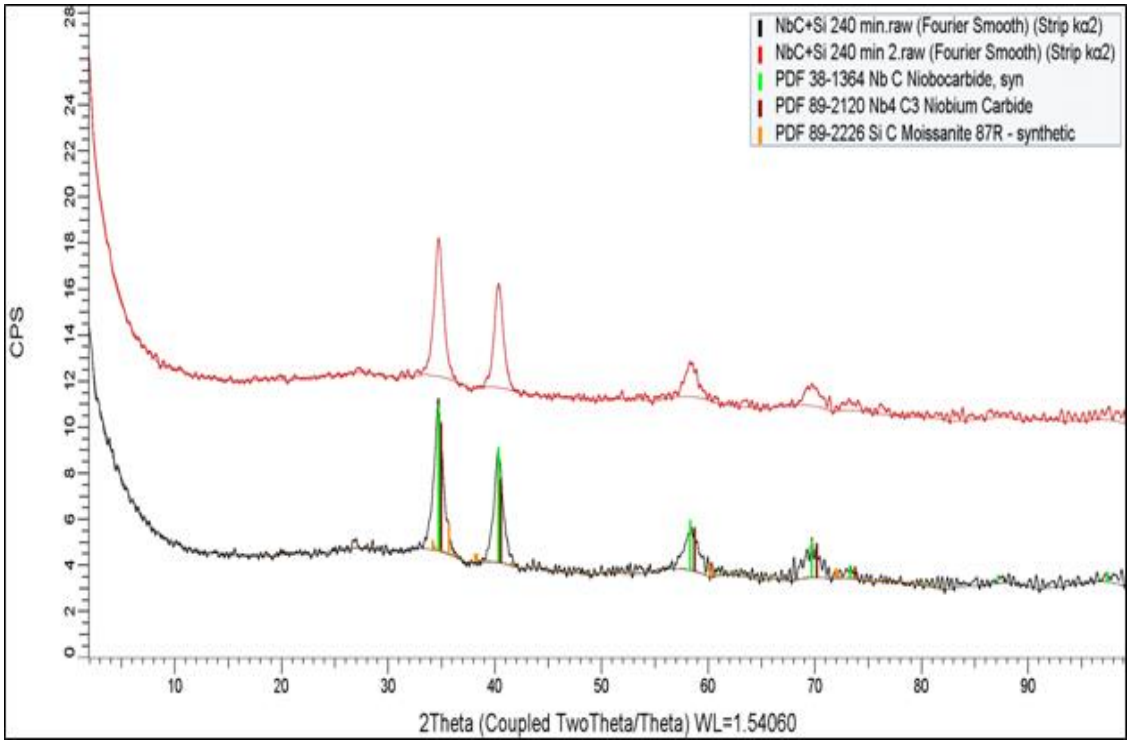

Figure 55. XRD image of iron coated NbC+Si powder after MA for 240 min

Table 15. Components intensity of XRD image in Figure 55

(NbC+Si) 240 min	Left Angle	Right Angle	Net Height	Net Area
NbC (111)	33.158	36.868	7.71	6.646
Nb_4C_3 (111)				
NbC (200)	38.802	42.020	6.93	4.901
Nb_4C_3 (200)				
----------	56.418	60.285	4.19	2.251
----------	68.455	71.516	3.14	2.030

Table 16. Peak parameter of Si(111) in the XRD image with different milling time

Milling Time	Left Angle	Right Angle	Net Height	Net Area
0	27.251	29.505	18.7	3.673
5	27.251	29.505	6.63	1.733
15	27.251	29.505	5.17	2.523
30	27.786	29.505	5.96	1.093
60	27.786	29.505	2.13	0.723
120	27.736	29.505	1.65	0.572

Table 17. Peak parameter of NbC(111) + Nb_5C_6(-131) in the XRD image with different milling time

Milling Time	Left Angle	Right Angle	Net Height	Net Area
0	27.251	29.505	18.70	3.673
5	33.479	36.062	20.70	10.520
15	33.479	36.062	22.70	13.240
30	33.429	36.062	25.10	17.870
60	33.265	35.841	5.85	3.280
120	33.051	36.326	9.62	9.157

Table 18. Peak parameter of NbC(200) + Nb_5C_6(-202) in the XRD image with different milling time

Milling Time	Left Angle	Right Angle	Net Height	Net Area
0	39.658	41.221	28.10	5.086
5	39.173	41.107	18.60	6.751
15	39.173	41.164	14.10	6.978
30	39.173	41.542	20.90	14.330
60	39.173	41.428	4.42	2.467
120	39.066	41.428	6.36	5.130

Figure 56. Friction coefficient as a function for a wear test time of sample 5 min MA

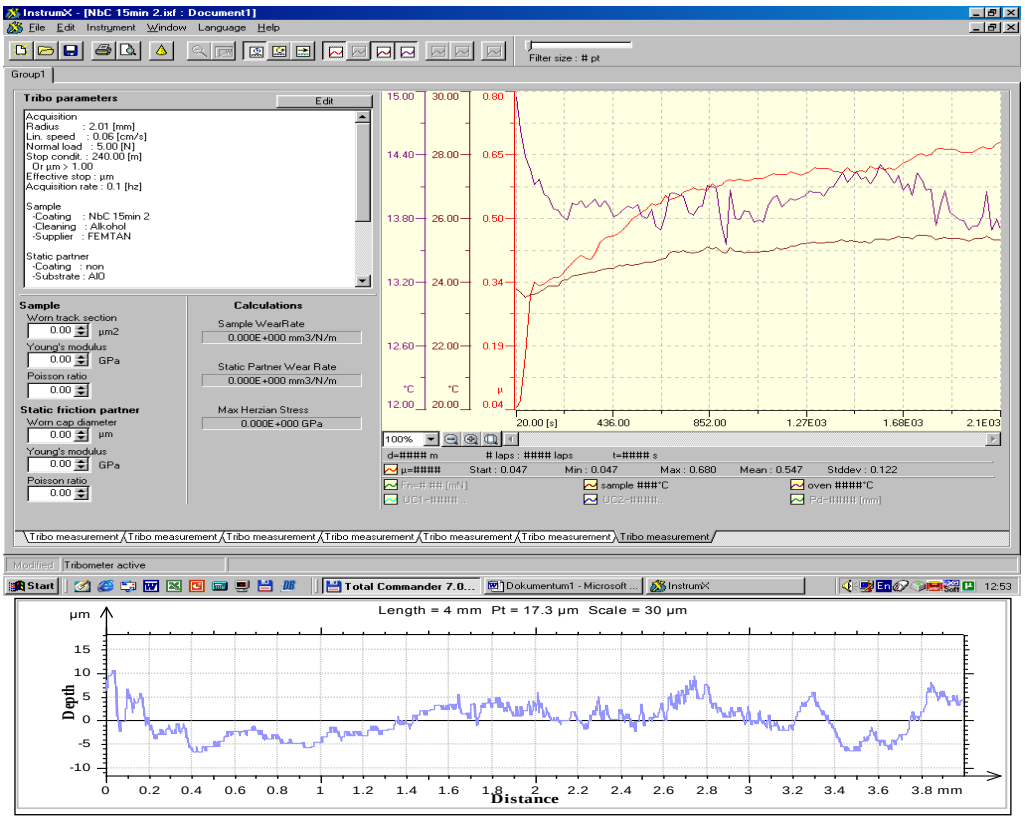

Figure 57. Friction coefficient as a function for a wear test time of sample 15 min MA

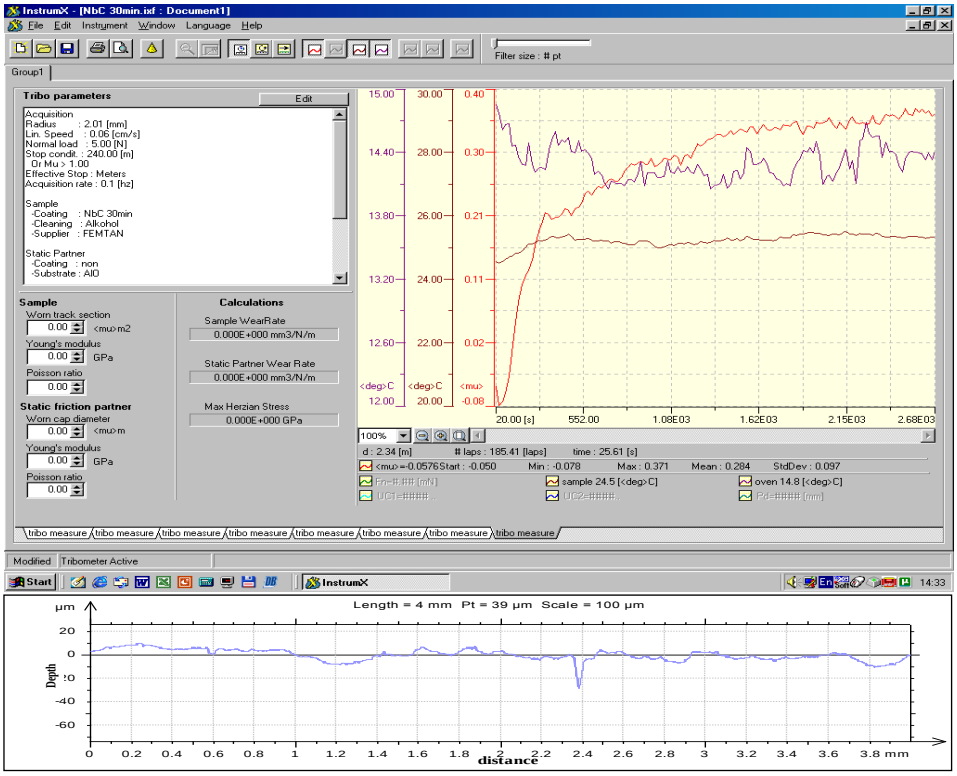

Figure 58. Friction coefficient as a function for a wear test time of sample 30 min MA

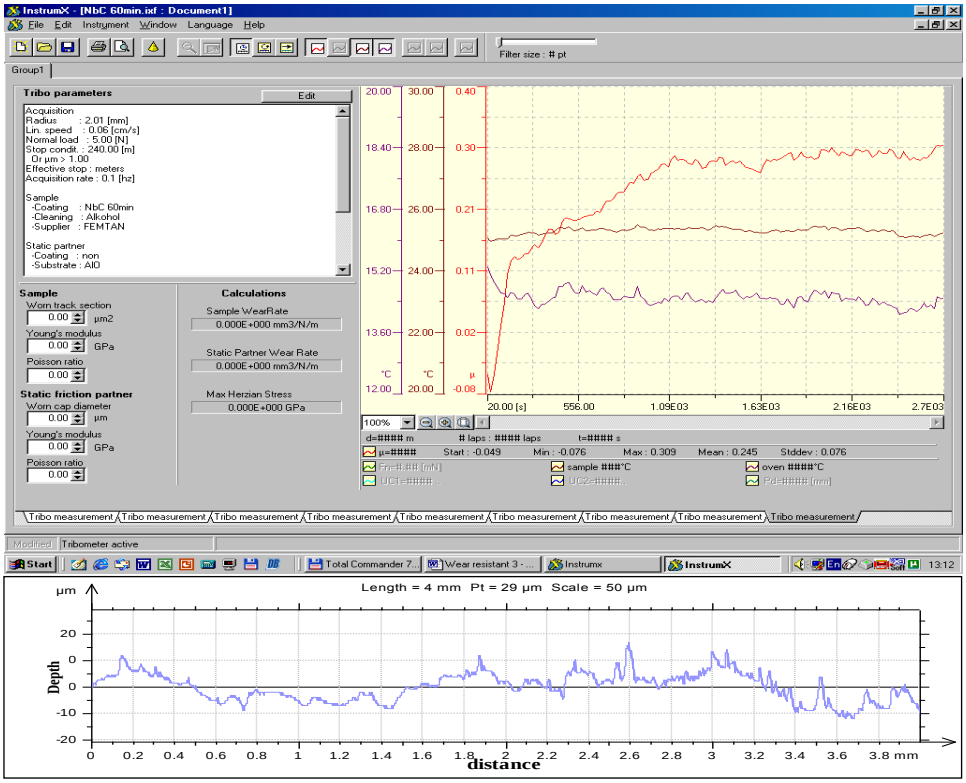

Figure 59. Friction coefficient as a function for a wear test time of sample 60 min MA

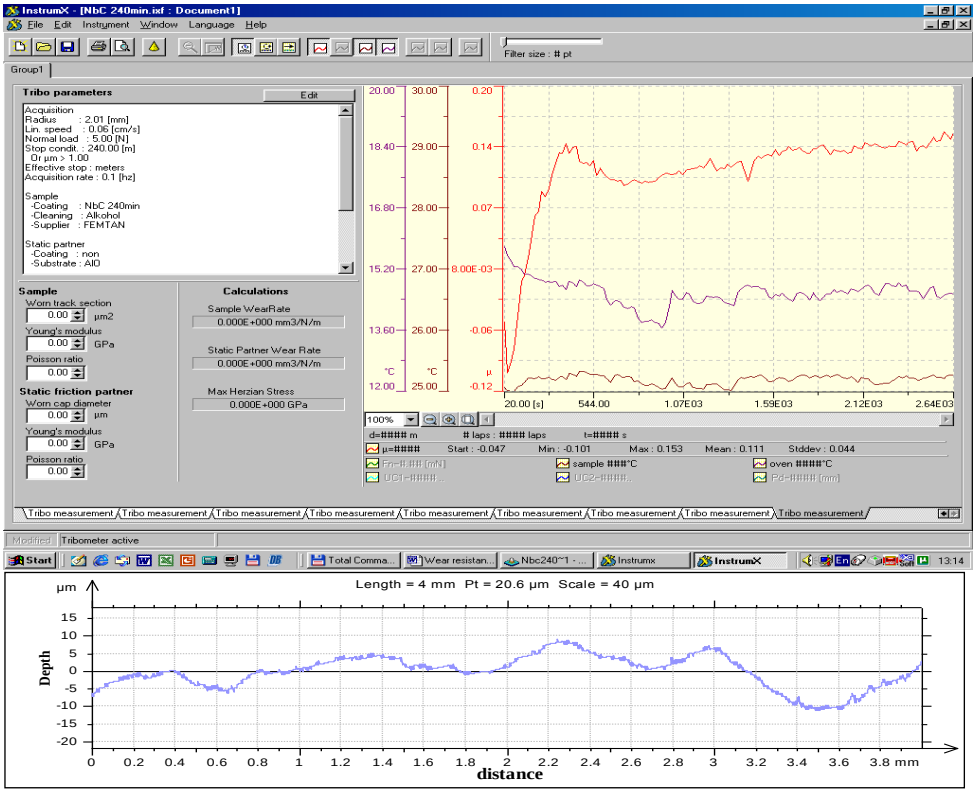

Figure 60. Friction coefficient as a function for a wear test time of sample 240 min MA